APPLICATIONS OF MARANGONI FORCES IN ACTUATING SOLID PHASE OBJECTS

by

Erwin Hendarto

A dissertation submitted in partial fulfillment
of the requirements for the degree of
Doctor of Philosophy
(Electrical Engineering)
in the University of Michigan
2013

Doctoral Committee:

Professor Yogesh B. Gianchandani, Chair
Assistant Professor Anastasios John Hart
Assistant Research Scientist Tao Li
Assistant Professor Sunitha Nagrath
Professor Euisik Yoon

To my parents,

my wife, and my daughters

ACKNOWLEDGMENTS

It is truly a great privilege to acknowledge the contributions of the many people around me who have played a part in my quest for a Ph.D. This work certainly would not have been possible without their help and support.

It is with immense gratitude that, first and foremost, I acknowledge the teachings and guidance of my research advisor, Professor Yogesh Gianchandani, who presented me with the numerous opportunities and challenges that broadened my expertise and research proficiency beyond all boundaries. I appreciated the frequent one-on-one technical discussions I had with him. But the only exchanges I cherish the most were the ones where he constantly advised me to prioritize my family above anything else. Despite his busy schedule, he would never fail to allocate a few minutes of his time whenever I needed to have a discussion with him, and I sincerely thank him for that. Along with him, I would also like to thank the dissertation committee for being very supportive in shaping the outcome of this work.

I would not have embarked on this eventful journey had it not been for the persistent encouragement of my undergraduate research advisors, the late Professor Jacob Phang of the National University of Singapore, and Professor Ludwig Balk of the University of Wuppertal. Although getting an advanced degree was something I had been considering, I was not really working toward it after my undergraduate degree.

Both of them persisted and instilled the confidence in me to pursue a doctorate degree even though I had already been out in the industry for several years. For that, I will always be indebted to them. I am also extremely grateful to my parents who wholeheartedly supported my decision to pursue this Ph.D, just as they have supported me in all of my decisions in life so far. I hope I have made them proud.

I had the pleasure to work with many wonderful colleagues within the Gianchandani group at UM. Past and present members have been instrumental in creating a collaborative atmosphere in which learning is fun and relaxing. In particular, I would like to thank Professor Amar Basu and Dr. Karthik Visvanathan for their mentorship and assistance during the initial phase of this work on Marangoni actuation. This work was also made possible by the numerous intellectually stimulating discussions with members of the group, including Dr. Tao Li, Dr. Scott Green, Dr. Christine Eun, Jun, Seungdo, Xin, Venkat, Anup, Ravish, and Yutao. I thank them for their patience and generosity in sharing their knowledge.

Finally, I would like to end by dedicating this thesis to the love of my life, Wiwy, and my beautiful daughters, Audrey and Ashley. With two young children, this thesis would have been impossible but for the constant and enduring support of my wife. I want to express my deepest gratitude to her for always being there for me. While I had to be away from them on several occasions the last few years, I will always treasure every minute we spent together; they made my Ph.D life colorful, and my life meaningful. My daughters are truly a joy to be with, and I hope that this thesis will serve as an inspiration to them as they embark on the pursuit of their own knowledge.

TABLE OF CONTENTS

DEDICATION	ii
ACKNOWLEDGMENTS	iii
LIST OF FIGURES	viii
LIST OF TABLES	xiii
LIST OF SYMBOLS	xiv
LIST OF PUBLICATIONS	xvi
LIST OF APPENDICES	xvii
ABSTRACT	xviii

CHAPTER

1. Introduction	**1**
1.1 Thermal Marangoni effect	4
1.2 Thermocapillary convection and its applications	6
1.3 Other fluidic manipulation techniques	13
1.4 Structure of this work	16
2. Theoretical equations	**19**
2.1 Effect of temperature on surface tension	19
2.2 Dimensionless fluidic numbers	22
2.3 Governing equations and boundary conditions	25

3. A non-contact method for spatially localized sedimentation of particles from liquid suspensions using Marangoni forces **27**

3.1 Introduction 28

3.2 Theoretical modeling 30

3.3 Experimental results 33

3.4 Discussion and conclusion 40

4. Thermocapillary actuation of millimeter-scale rotary structures **44**

4.1 Introduction 44

4.2 Theory and modeling 47

4.3 Fabrication and experimental results 53

4.4 Conclusions 58

5. Size sorting of floating spheres based on Marangoni forces in evaporating droplets **59**

5.1 Introduction 60

5.2 Experimental procedure and results 64

5.2.1 Procedure 64

5.2.2 Results 66

5.3 Discussion and conclusion 70

6. Investigation of wine glass mode resonance in 200-μm-diameter cenosphere-derived borosilicate hemispherical shells **77**

6.1 Introduction 77

6.2 Theoretical analysis and modeling 81

6.3 Device structure and fabrication 84

6.4 Experimental evaluation 85

6.5 Discussion and conclusions 88

7. Conclusions and future work **90**

7.1 Major contributions to the field 90

7.2 Suggested future work 93

APPENDIX A 97

APPENDIX B 100

REFERENCES 113

LIST OF FIGURES

Figure 1.1: (a) Isothermal heating of a liquid layer from below. Warm, low density liquid rises and cools; higher density liquid sinks. (b) Bénard convection cells at high magnification [Ben00]. The liquid moves upwards in the center of the cell, spreads out and sinks at the edges of the cell. (c) Low magnification view of steady patterned convection [Ben00]. **2**

Figure 1.2: 2D schematic of Marangoni flow generated by a suspended point heat source. Localized heating results in a region of low surface tension below the heater (higher temperature), while a region of high surface tension develops at the lower temperature areas. **5**

Figure 1.3: (a) Liquid flow patterns in an evaporating droplet on a heated substrate. A stable Marangoni flow forms in the droplet. (b) Liquid flow patterns in an evaporating droplet on an unheated substrate. Evaporation induced radial flow is dominant. **6**

Figure 1.4: (a) Transporting a droplet by activating the parallel thermal elements of a microfluidic device in a sequence [Far04]. (b) Sequential operation of embedded resistive elements and patterning of substrate with hydrophobic/hydrophilic regions to actuate droplets [Dar03a]. (c) Droplet displacement and switching in a bifurcating microfluidic channel [Sel10]. **8**

Figure 1.5: (a) Merging of droplets by laser [Bar07a]. (b) Optical valve realized by laser [Bar07b]. (c) Separation of silicone oil (SO) and glycerol droplets (GI) by laser [Far06]. **9**

Figure 1.6: Heat sources of various geometries to generate Marangoni flows [Bas08]: (a) Point heat source for particle collection, mixing and rotation; (b) Linear heat sources as virtual channels for size filtering; (c) Tapered heat source as guidewire droplet pump. **10**

Figure 1.7: Programmable heater array for thermocapillary actuation [Bas09]: (a) Push-mode actuation for transporting droplets; (b) Pull-mode actuation for merging droplets. **11**

Figure 1.8: SEM images of stripe patterns obtained by retreating liquid in "cylinder-on-flat" geometry [Han11]. The larger 500 nm particles are separated from the 50 nm particles in each stripe. **13**

Figure 1.9: Comparison of passive and active particle manipulation techniques. **16**

Figure 2.1: Linear dependence of surface tension and temperature. **20**

Figure 3.1: (a) Cross-sectional view of 3D schematic diagram of the experimental setup. (b) Simulation result (COMSOL Multiphysics® 3.5a) showing temperature distribution profile and generated Marangoni flow cells in silicone oil DC-704. **30**

Figure 3.2: Temperature of a heater surface at various heater powers measured by thermocouple and infrared (IR) thermometer, and the resultant liquid surface temperature rise directly below the heater in silicone oil DC-704 obtained by simulation. **35**

Figure 3.3: (a) No accumulation is observed in silicone oil DC-704 with an estimated liquid surface temperature of 28.5°C directly below the active heater. All the particles have settled onto the glass substrate after about 3 minutes 30 seconds. Before taking the image, the suspended heater is raised but the liquid is not removed. (b) Number of particles below the left, center and right heaters per 200 × 200 μm^2 in the first 4 minutes of the experiment. **35**

Figure 3.4: Sedimentation in silicone oil DC-704. The estimated liquid surface temperature is 34.0°C. (a) Initial random distribution of particles immersed throughout the liquid 1 minute into the experiment. (b) Particle sedimentation after 2 minutes showing a small amount of accumulation on the glass substrate below the active heater. (c) Particle sedimentation after 10 minutes. (d) Particle sedimentation after 20 minutes. (e) Number of particles accumulated below the center active heater, left inactive heater and right inactive heater per 200 × 200 μm^2. **38**

Figure 3.5: Formation of different patterns and amount of sedimentation in silicone oil DC-704 after approximately 15 minutes by: (a) two active heaters; (b) four active heaters. The liquid is not removed. The yellow rectangles identify the locations of the active heaters before they are raised. **38**

Figure 3.6: Particle sedimentation in three different liquids. (a) Sedimentation in silicone oil DC-550. Particle collection is limited to a small area below the heater. (b) Sedimentation in silicone oil DC-704. More particles are collected from a larger area to form a larger accumulation. (c) No accumulation occurs in electronic liquid FC-3283. The suspended heater is not raised before taking the image. **39**

Figure 4.1: (a) 3D schematic of the experimental setup. The rotary structure made of stainless steel is mounted on a hub and completely immersed in silicone oil. The four square blades bend downwards in the liquid at an angle φ of 34°. The length of each side of the square blade s is 1.2 mm. The air gap between the heater and the liquid surface is

≈500 μm. Only 9 of the 128 heaters are shown, and four heaters are active. An inverted camera is used to record the rotation. (b) 2D schematic of Marangoni flows generated by the activation of a single heater. **46**

Figure 4.2: Modeling results showing the velocity magnitude in silicone oil DC-704 when the blade arm (a) is directly below a heater (rotation angle θ of 0°); (b) has rotated through an angle of 30° anticlockwise as viewed from above. The air gap is 500 μm, and the surface temperature of the two heaters is 446.5 K. Marangoni flow patterns are generated inside the liquid layer. **49**

Figure 4.3: Driving torque calculations based on modeling results. (a) (Top view) Forces F_x and F_y acting on the top and bottom surfaces of the blade when the blade arm is directly below a heater (rotation angle θ of 0°). The driving torque on the blade is ≈435 pN.m, rotating the structure in an anticlockwise direction. (b) (Top view) Forces F_x and F_y acting on the top and bottom surfaces of the blade when the blade arm has rotated through an angle of 30° anticlockwise in the liquid as viewed from above. The driving torque on the blade is ≈325 pN.m, also producing an anticlockwise rotation. The x- and y-coordinates in the figures are in mm. The torque due to forces acting on the sides of the blades is omitted for clarity. **51**

Figure 4.4: (a) Optical micrograph of the micromachined rotary structure made of stainless steel with thickness 125 μm. The length and width of the blade arm are 4.1 mm and 500 μm, respectively. Each square blade measures 1.2 × 1.2 mm^2. The thinned portion of the blades is 40 μm thick. A depression of diameter 300 μm and depth of 80 μm is made at the center of the rotary structure for mounting on the hub. (b) SEM micrograph showing a rotary structure with blade angle φ of 34°. **54**

Figure 4.5: (a) Experimentally observed rotation of the rotary structure in silicone oil DC-704 through a rotation angle of 90° when the maximum liquid surface temperature gradient is 30.6 K/mm, showing regions of acceleration and deceleration in a period of 12 s. (b) Acceleration and deceleration of the rotary structure through a 90° rotation. **55**

Figure 4.6: Time taken to make one complete rotation in silicone oil DC-704 and DC-200 at different maximum temperature gradients generated at the liquid surface. **56**

Figure 4.7: The 360° rotation of a rotary structure in silicone oil DC-200. The rectangles in dashed lines indicate the heaters that are activated. The generated maximum temperature gradient at the liquid surface is 36.6 K/mm. The time taken to make one complete rotation is 28 s. A dot is drawn on one of the blades for identification purposes. **57**

Figure 5.1: 3D schematic of high throughput sorting, showing an array of IPA droplets with cenospheres of various sizes on a heated glass substrate, as well as a schematic diagram of the evaporation process and the final pattern of deposited cenospheres. The cenospheres are sorted according to size, with the larger spheres at the center and the

smaller spheres at the perimeter. The droplet volume ranges from 0.5-8 μL, and the temperature of the glass substrate is 55°C to 85°C. **63**

Figure 5.2: (a) Optical micrograph of the original cenospheres of various sizes. The shell thickness is 1-3 μm. (b) SEM micrograph of the cenospheres. **65**

Figure 5.3: (a) Liquid flow patterns in an evaporating droplet on a heated substrate. A stable Marangoni flow forms in the droplet. (b) Liquid flow patterns in an evaporating droplet on an unheated substrate. Evaporation induced radial flow is the dominant flow. **66**

Figure 5.4: Number of cenospheres in an area of 500 × 500 μm^2 deposited along the radius from the center (r = 0) to the edge (r = R) of the circular droplet area when the temperature of the glass substrate is (a) 55°C, and (b) 65°C. The volume of the droplet used is 0.5 μL, and the droplet radius is about 2.5 mm. **67**

Figure 5.4: Number of cenospheres in an area of 500 × 500 μm^2 deposited along the radius from the center (r = 0) to the edge (r = R) of the circular droplet area when the temperature of the glass substrate is (c) 75°C, and (d) 85°C. The volume of the droplet used is 0.5 μL, and the droplet radius is about 2.5 mm. **69**

Figure 5.5: Number of cenospheres in an area of 500 × 500 μm^2 deposited along the radius from the center (r = 0) to the edge (r = R) of the circular droplet area when the droplet volume is 8 μL. The temperature of the glass substrate is 85°C. **69**

Figure 5.6: (a) Size sorting achieved by placing the droplet on a heated glass substrate without using a perforated metal plate. (b) Placing a droplet on a perforated metal plate in contact with the glass substrate. The radius of the hole is ≈1 mm. (c) Physical removal of most of the small spheres <50 μm by lifting off the perforated metal plate in (b). In each experiment, the droplet volume is 5 μL and the glass substrate temperature is 85°C. **72**

Figure 5.7: (a) Modeling result showing the flow velocities inside the liquid droplet. The substrate temperature is 85°C. The smaller spheres make larger circulation path than the larger spheres inside the droplet. (b) The flow direction is reversed when the substrate is cooled. Here, the substrate temperature is 2 K lower than the room temperature of 300 K. **73**

Figure 5.8: Relationship between the substrate temperature and the ratio of number of 150-200 μm spheres to number of <50 μm spheres at the center of the droplet. The droplet volume is 0.5 μL. **75**

Figure 6.1: (a) Optical micrograph of cenospheres on a US penny. (b) High magnification optical image of cenospheres of varying sizes. **79**

Figure 6.2: (a) SEM micrograph of the original cenosphere with radius R, showing the rectangular mill pattern during FIB milling process. (b) Perspective view of the fabricated micro-hemisphere. (c) Side view of device D214H146 with diameter D of 214 μm and height H of 146 μm. This micro-hemisphere is coated with 50 nm Au on the outer surface to improve optical reflectivity during measurement with the vibrometer. (d) Side view of device D184H144 having diameter D of 184 μm and height H of 144 μm. It is coated with 50 nm Pt on the outer surface. **81**

Figure 6.3: (a) Coordinate system and hemispherical shell model. (b) Original shape and actuated shape of the wine glass resonance mode shape of a micro-hemisphere as obtained by COMSOL Multiphysics 4.2. Simulations show that the wine glass resonance frequency of micro-hemisphere D214H146 is 331.5 kHz, while that of D184H144 is 599.0 kHz. Laser spot size of ≈30 μm from the vibrometer is also drawn. **84**

Figure 6.4: (a) Normalized variation in simulated amplitude and measured velocity in the fundamental wine glass resonance mode of device D214H146 at 332.5 kHz. The dashed line is a fit of simulated points to the function $|A_i \sin(2(\theta + \theta_i))|$. (b) Experimentally-obtained plot of the wine glass mode resonance peak measured at rotation angle of 40°. The measurements are performed in air at atmospheric pressure. **87**

Figure 6.5: Experimentally measured response of micro-hemisphere D184H144 in wine glass mode at 590 kHz. The (red) dashed line is fitted to the data using function $|A_i \sin(2(\theta + \theta_i))|$. The response at 580 kHz represents a structural non-ideality. **88**

Figure A1: A quadrant of the setup is created to perform the simulation using COMSOL Multiphysics® 4.3. **97**

LIST OF TABLES

Table 2.1: Values of surface tension and surface tension temperature coefficient of liquids used in this work [3M01, Dow98a, Dow98b, Xia09]. Water is included for reference. **22**

Table 2.2: Material properties and calculated dynamic Bond numbers of the liquids used in this work. **24**

Table 3.1: Material properties of the liquids used in particle sedimentation: silicone oil DC-550 [Dow98b], silicone oil DC-704 [Dow98a], and electronic liquid FC-3283 [3M01]. **32**

Table 4.1: Properties of silicone oil DC-704 [Dow98a] and DC-200 [Xia09]. **48**

Table 6.1: Device parameters and material properties used in modeling. **83**

LIST OF SYMBOLS

c – concentration (mol/dm^3)

C_p – specific heat capacity (J/kg.K)

E – Young's Modulus (Pa)

$\left|\vec{E}\right|$ – electric field (V/m)

f – force vector per unit volume (N/m^3)

F_i – force component in the i-direction (N)

f_n – natural frequency of the nth mode (Hz)

g – gravitational acceleration (m/s^2)

I – moment of inertia (kg.m^2)

k – thermal conductivity (W/m.K)

k_γ – Eötvös constant (2.1×10^{-7} J/K.mol$^{2/3}$ for most liquids)

L – characteristic length scale (m)

M – molar mass

$\vec{N}$ – surface normal vector

p – pressure (Pa)

Q – rate of heat transfer per unit volume (W/m^3)

T – temperature (K)

t – time (s)

T_c – crictical temperature (K)

ΔT – temperature difference (K)

V_m – molar volume (m^3/mol)

u – velocity vector (m/s)

$\vec{u_s}$ – tangential surface velocity vector (m/s)

α – thermal expansion coefficient (K^{-1})

κ – thermal diffusivity (m^2/s)

μ – dynamic/absolute viscosity (kg/m.s)

μ_k – kinematic viscosity (cSt)

ν – Poisson's ratio

ρ – density (kg/m^3)

σ – surface tension (N/m)

σ_T – surface tension temperature coefficient (N/m.K)

τ_s – thermocapillary shear stress (N/m^2)

Bo_D – dynamic Bond number

Ma – Marangoni number

Pr – Prandtl number

Ra – Rayleight number

LIST OF PUBLICATIONS

REFEREED JOURNAL PUBLICATIONS

E. Hendarto, Y.B. Gianchandani, "A non-contact method for spatially localized sedimentation of particles from liquid suspensions using Marangoni forces," *Journal of Micromechanics and Microengineering*, vol. 21, no. 11, pp. 115028 (7 pages), Nov. 2011.

E. Hendarto, Y.B. Gianchandani, "Thermocapillary actuation of millimeter-scale rotary structures," *Journal of Microelectromechanical Systems* (under review).

E. Hendarto, T. Li, Y.B. Gianchandani, "Investigation of wine glass mode resonance in 200-μm-diameter cenosphere-derived borosilicate hemispherical shells," *Journal of Micromechanics and Microengineering*, vol. 23, no. 5, pp. 055013 (6 pages), Apr. 2013.

E. Hendarto, Y.B. Gianchandani, "Size sorting of floating spheres based on Marangoni forces in evaporating droplets," *Journal of Micromechanics and Microengineering* (under review).

REFEREED CONFERENCE PROCEEDINGS

E. Hendarto, Y.B. Gianchandani, "Directed precipitation of suspension particles onto blank substrates using Marangoni cells," in *the 14th International Conference on Miniaturized Systems for Chemistry and Life Sciences (MicroTAS 2010),* Groningen, The Netherlands, Oct. 2010, pp. 1100-1102.

E. Hendarto, Y.B. Gianchandani, "Marangoni-driven micromotor in liquid medium," in *16th International Conference on Solid-State Sensors, Actuators and Microsystems (Transducers 2011)*, Beijing, China, Jun. 2011, pp. 246-249.

LIST OF APPENDICES

Appendix A: Boundary conditions to simulate thermocapillary actuation of rotary structures **97**

Appendix B: EDM code for machining rotary structures **100**

ABSTRACT

The Marangoni effect develops due to surface tension variations at the liquid/gas interface caused by temperature gradient in the liquid. Spatially localized temperature rise reduces the localized surface tension, resulting in surface flows away from the heat source and subsurface flows in opposite direction. This phenomenon shows potential in droplet/particle manipulation for microfluidic applications. In this work, a series of experiments is performed to address several important questions to further evaluate the utility of this effect. The questions address how to spatially localize suspension particles on blank substrates, sort floating particles according to size, and actuate millimeter-sized solid objects.

Using a heater array suspended ≈500 μm above the liquid, Marangoni flows are shown to spatially localize sedimentations of microscale suspended particles. The sedimentation patterns and accumulation levels depend on the temperature gradient at the liquid surface, number of active heaters and type of liquid used. For example, a single active heater is used to generate a temperature elevation of 6.9°C at the surface of silicone oil DC-704, resulting in the localized sedimentation of suspended 25 μm pollen over a region of 2.9 mm^2 beneath the active heater.

Marangoni flows in evaporating liquid droplets can be utilized to sort cenospheres with sizes in a continuous spectrum from 5–200 μm. By heating the droplets from below,

larger spheres (100–200 μm) are deposited at the center and smaller spheres (<50 μm) at the droplet periphery. The physical separation of large and small spheres is possible by using perforated metal plates. Cenospheres ≈200 μm in diameter are subsequently modified by a focused ion beam to form hemispherical shells, and the fundamental wine glass mode resonance is investigated.

Activating the suspended heater array in a certain configuration rotates a millimeter-scale rotary structure mounted on a hub and completely immersed in the liquid. With a maximum temperature gradient of 36.6 K/mm at the surface of a liquid with viscosity 5 cSt, the structure takes 28 s to make a 360° rotation. The angular velocity of the structure depends on the temperature gradient and viscosity of the liquid.

In summary, the experiments demonstrate the utility of micro-scale Marangoni flows in controlled manipulation and positioning of particles and millimeter-sized structures without the need for embedded actuating elements.

CHAPTER 1

Introduction

The term "Marangoni effect" generally refers to surface tension driven flow phenomena. It is named after C. Marangoni who first made an observation and explanation on flows driven by surface tension gradient in 1865 [Mar65]. It was however first identified by physicist J. Thomson, who observed "tears of wine" in 1855 [Tho55]. Marangoni's work was later followed by the work of Henri Bénard, who observed regular hexagon-shaped convection flow patterns by heating a ≈1 mm deep liquid layer from below as shown by Figure 1.1 [Ben00]. This method of heating creates temperature fluctuations at the liquid surface; surface tension decreases at warmer regions, and increases at cooler regions. Aluminum flakes were added to the liquid, and the image was taken under a long exposure time so it becomes evident that the liquid moves upwards in the center of the cell, spreads out and sinks at the edges of the cell. The Bénard convection cell was originally thought to be caused by natural convection by Rayleigh [Ray16], but it was later confirmed by Block [Blo56] and Pearson [Pea58] that the flow pattern is a type of convection dominated by surface tension gradient. Today this flow is known as Bénard-Marangoni convection.

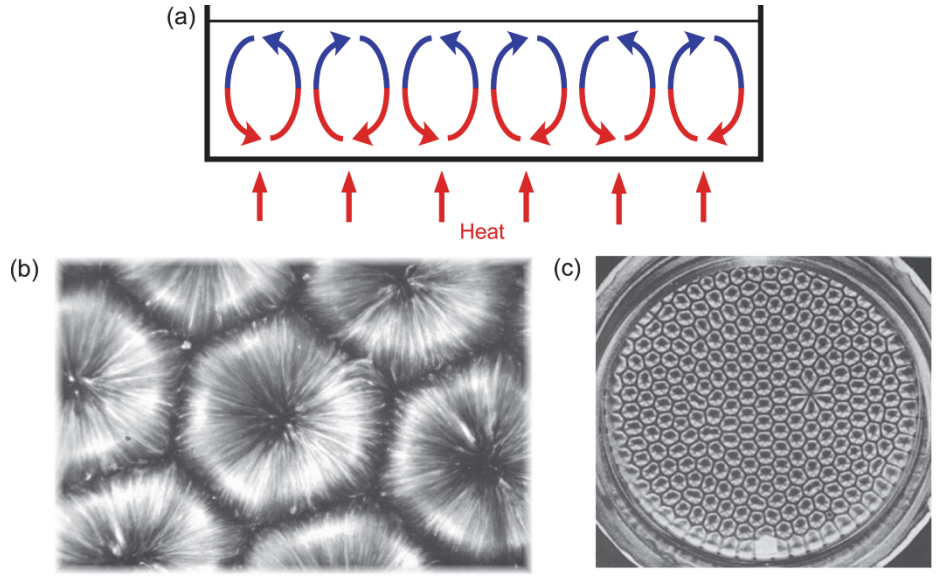

Figure 1.1: (a) Isothermal heating of a liquid layer from below. Warm, low density liquid rises and cools; higher density liquid sinks. (b) Bénard convection cells at high magnification [Ben00]. The liquid moves upwards in the center of the cell, spreads out and sinks at the edges of the cell. (c) Low magnification view of steady patterned convection [Ben00].

Surface forces such as surface tension are well known to be dominant forces at small length scales. The Marangoni effect is an example of a surface phenomenon. At larger length scales, the Marangoni effect is negligible and masked by bulk phenomena such as buoyancy and other inertial forces. Without using equations and dimensionless numbers of liquids, a simple explanation is often given by the scaling law in microfluidics [Bru08, Li08]. Based on this law, when all factors such as time, pressure, temperature, etc. are kept constant, reducing the size of the system, L, would decrease volume phenomena (such as gravity and inertia) much faster than surface phenomena (such as surface tension and viscosity). This is because surface phenomena decrease with L^2, while volume phenomena decrease with L^3. As the length scale L decreases, bulk phenomena diminish much more quickly than surface phenomena. Therefore, surface tension forces become the dominant forces in the microscale domains.

The Marangoni effect is responsible for many everyday occurrences. As such, the Marangoni effect has been studied extensively in recent times. The familiar coffee-ring stains left behind when a droplet of coffee dries up, and the ring patterns left on a dried dish are both attributed to Marangoni effect [Dee97, Hu02]. The deposition of particles in a ring-like pattern during evaporation is influenced by Marangoni stresses [Bha09]. The superspreading of SURFace ACTive AgeNTS (surfactants) is also due to the Marangoni effect [Nik02]. Marangoni effect also plays a critical role in several industrial processes such as thin film coating, the floating-zone process for crystal growth [Chu80, Li93] and separation processes such as distillation and absorption [Rup89]. Control of crystal growth process is achievable by careful regulation of convective heat and mass transfer, and a more comprehensive study of liquid flow phenomena is warranted. Chun *et al.* first observed that Marangoni convection is present in a liquid of a floating zone at reduced gravity condition. The resulting temperature oscillations lead to formations of striations in monocrystals [Chu79]; this was also confirmed by Eyer *et al.* [Eye85]. Methods to suppress such oscillations by rotating the liquid flows had been proposed [Chu81]. "Marangoni drying", a drying process based on Marangoni effect, produces dry, clean wafers free of contaminants, making these wafers desirable for the manufacture of integrated circuits [Lee90]. Schatz et al. provides a good review of the numerical analysis and experimental works of thermocapillary effect [Sch01].

Although surface tension gradient can be created by several methods such as chemical, electrical and thermal, the thermal method is considered the most versatile because no chemical treatment of the liquid surface is necessary [Far04]. The various forms of Marangoni effects include thermal Marangoni effect (temperature gradient

induced), solutal Marangoni effect (concentration gradient induced) and electric field induced Marangoni effect. Section 1.1 explains thermal Marangoni effect (also known as thermocapillarity or Bénard-Marangoni effect), which is the emphasis of this work. Section 1.2 focuses the discussion on past applications of thermal Marangoni effect. The Marangoni technique may potentially serve as a complementary technique to other fluidic manipulation methods, which are discussed in Section 1.3. Finally, Section 1.4 presents the focus and structure of this work.

1.1 Thermal Marangoni Effect

Interfacial phenomena such as surface tension, σ, develop at the interface of two immiscible fluids, and play important roles in microfluidic systems. A common example of such interface is that of liquid and gas; in this case, the liquid is considered to have a free top surface, a condition necessary for Marangoni convection to occur. The Marangoni effect develops as a result of surface tension variations at the liquid/gas interface caused by temperature gradient in the liquid [Scr60]. When thermally induced, this phenomenon is also referred to as the thermocapillary effect. Surface tension depends on temperature, and typically decreases linearly with increase in temperature for many liquids. Instead of isothermally heating the liquid from below, heating can be provided by a suspended point heat source in close proximity to the liquid surface. Local heating at the liquid surface by micrometer scale heat sources leads to spatially localized temperature increase, which in turn reduces the surface tension at the heated area. A gradient of surface tension develops, and this results in thermocapillary shear stress at the interface which directs surface flow from a region of low surface tension (high

temperature) to that of high surface tension (low temperature). To maintain fluid continuity, this interface flow is accompanied by subsurface flows of opposite direction in the bulk liquid. Both the surface and subsurface flows constitute the Marangoni flow. This is schematically summarized in Figure 1.2.

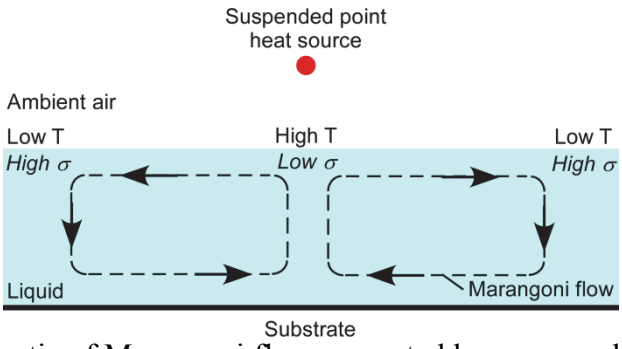

Figure 1.2: 2D schematic of Marangoni flow generated by a suspended point heat source. Localized heating results in a region of low surface tension below the heater (higher temperature), while a region of high surface tension develops at the lower temperature areas.

The thermocapillary shear stress is directly proportional to the temperature gradient of the liquid surface, not the absolute temperature values. If the length scale over which temperature variation occurs is small enough, a small change in temperature can potentially lead to a large temperature gradient and hence large thermocapillary stress. In general, the strength of the convective motion can also be determined by the Marangoni number.

A stable Marangoni flow also develops inside an evaporating liquid droplet on a *heated* substrate [Mar89, Rui02, Gir06]. The higher the substrate temperature, the larger the surface tension gradient that is generated along the droplet surface and the more dominant the Marangoni flow becomes. In the proximity of the pinned perimeter (contact line) of the droplet on the substrate is a region of low surface tension, while the apex, which is at a lower temperature, is a region of high surface tension. The direction

of the shear stress and liquid flow are from a region of low surface tension to that of a high surface tension; therefore, the resultant surface tension gradient leads to a tangential flow upwards from the contact line toward the apex along the curvature of the droplet surface, as shown in Figure 1.3(a). The recirculating flow in the droplet is in the opposite direction: downward in the center of the droplet, and radially outward beneath the surface.

When a droplet evaporates on an *unheated* substrate, the droplet contact line experiences a higher evaporation rate compared with the rest of the droplet surface. The induced Marangoni flow due to different evaporation rates at the surface is negligible in this case. A radial flow predominantly transports the liquid from the center of the droplet to the edge to replenish the lost liquid (Figure 1.3(b)).

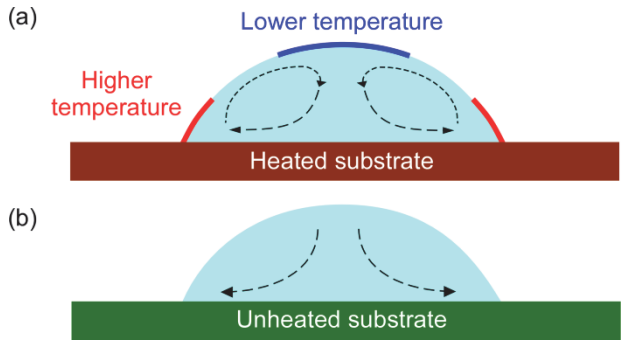

Figure 1.3: (a) Liquid flow patterns in an evaporating droplet on a heated substrate. A stable Marangoni flow forms in the droplet. (b) Liquid flow patterns in an evaporating droplet on an unheated substrate. Evaporation induced radial flow is dominant.

1.2 Thermocapillary Convection and its Applications

Many techniques are continuously developed and optimized to manipulate micrometer-sized particles, bubbles or droplets in microfluidic systems. These techniques transport, rotate, merge, divide, mix or sort particles to realize the functions of the microfluidic systems such as DNA analysis and environmental monitoring. The

study and application of thermocapillary effect have also been performed by several groups. Marangoni force has been utilized for transporting nano-liter amounts of liquids over a large area by activating the parallel thermal elements of a microfluidic device in a sequence, creating localized temperature rise and hence surface tension gradient that displaces the droplets [Far04]. This is shown by Figure 1.4(a). The thermal lines are pulsed to create a huge temperature gradient and avoid overall increase in liquid temperature. By integrating resistive elements in the substrate and patterning some parts of the substrate to be hydrophilic/hydrophobic, splitting and transporting of liquid drops can be achieved as shown by Figure 1.4(b) [Dar03a]. This work also involves the sequential operation of embedded resistive elements to transport the droplets. The hydrophilic regions serve as virtual paths for the droplets to travel along. The work is later extended to division of droplets from a reservoir onto a wettable strip [Dar10]. Another work that utilizes patterned resistive elements on substrate to impose Marangoni stresses is the droplet displacement and switching in a bifurcating microfluidic channel [Sel10]. The microfluidic channel is placed above the resistors. The left channel is designed such that it has a lower hydrodynamic resistance, and bubbles flow preferentially toward that channel as shown in Figure 1.4(c). With actuation, the bubbles switch to flowing to the channel on the right. Another example of thermocapillary actuation by activating thermal elements in a substrate is the actuation of a micromirror resting on a liquid drop [Dhu11]. Marangoni flows are created within the droplet by the microheaters in a silicon substrate, causing the droplet to deform because of non-uniform temperature distribution established within the droplet. This causes the micromirror to

tilt. The angle of tilt of the micromirror depends linearly on the applied voltage to the microheaters.

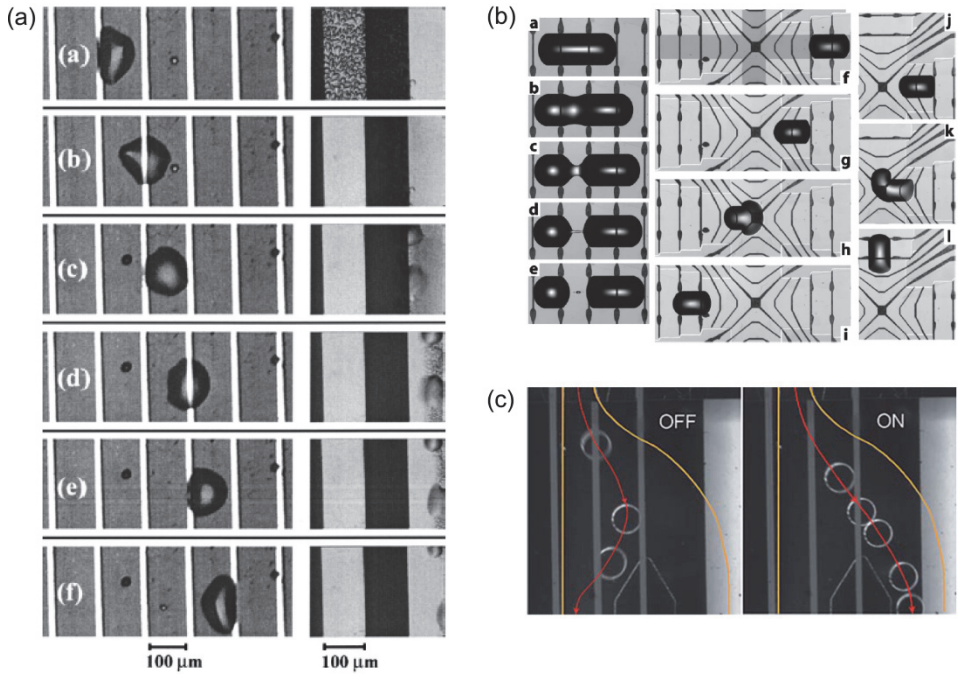

Figure 1.4: (a) Transporting a droplet by activating the parallel thermal elements of a microfluidic device in a sequence [Far04]. (b) Sequential operation of embedded resistive elements and patterning of substrate with hydrophobic/hydrophilic regions to actuate droplets [Dar03a]. (c) Droplet displacement and switching in a bifurcating microfluidic channel [Sel10].

Marangoni convection may also be induced by laser radiation, and it was found that the surface tension driven flows are dependent on beam size, temperature increase in liquid, etc among several factors [Lon99]. The use of laser to create localized heating for the purpose of merging droplets or altering their paths in channels is shown by Baroud et al. [Bar07a, Bar07b]. In Figure 1.5(a), droplets from the lower channel can be temporarily held in place by a laser illumination (represented by the small white circle). The laser exerts a thermocapillary force on the liquid interface to prevent the droplet from moving forward. When a droplet from the upper channel arrives, merging of the two

droplets takes place when the interface of the two droplets reaches the laser. The laser can also serve as an optical valve as shown in Figure 1.5(b). With the laser inactivated, drops split to form two equal parts at a bifurcation. When the laser is applied at the right-side channel, that path is blocked, and the entire droplet flows to the left side. Figure 1.5(c) shows sorting of silicone oil and glycerol droplets by using laser [Far06]. The laser power is adjusted to create temperature gradient sufficient to move silicone oil but not glycerol. Therefore silicone oil droplets are displaced to a new location, while the glycerol droplets remain at the original location on the substrate.

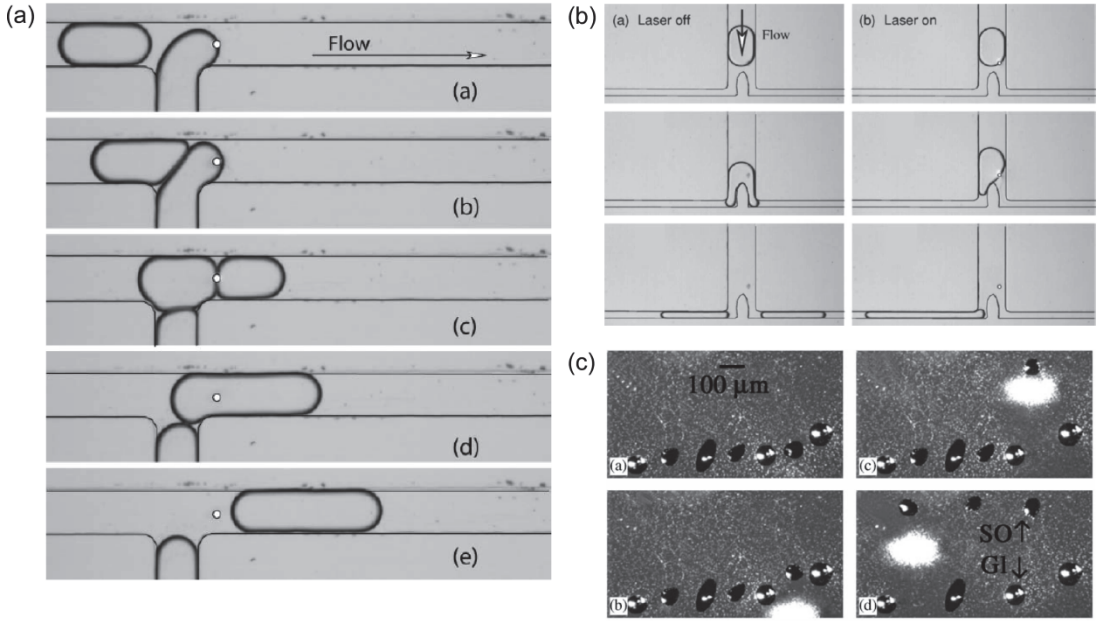

Figure 1.5: (a) Merging of droplets by laser [Bar07a]. (b) Optical valve realized by laser [Bar07b]. (c) Separation of silicone oil (SO) and glycerol droplets (GI) by laser [Far06].

Another method to generate Marangoni flow is to subject a liquid surface to a micrometer scale temperature source suspended above the liquid. This method takes advantage of the low thermal conductivity of air to create localized high temperature gradient at the top surface of the liquid, and may eliminate the need and complexity of patterning substrates with resistive elements. Different shapes of heat sources in the

micrometer range can be utilized to generate Marangoni flows capable of manipulating immersed micro particles and droplets on featureless substrates [Bas08a]. This includes point heat source (Figure 1.6(a)), linear heat sources (Figure 1.6(b)), annular heat source and tapered heat source (Figure 1.6(c)). The point heat source can be used for droplet collection, mixing and rotation. The linear heat sources act as virtual channels; they filter particles by size and pull in target-sized droplets, demonstrating 100% selectivity for droplets 300 μm – 1000 μm in diameter. The annular heat source is a droplet trap, and translating it causes the trapped droplet to move with it. The tapered heat source can function as a droplet pump. Unlike the annular heat source, the tapered heat source remains stationary when it transports droplets.

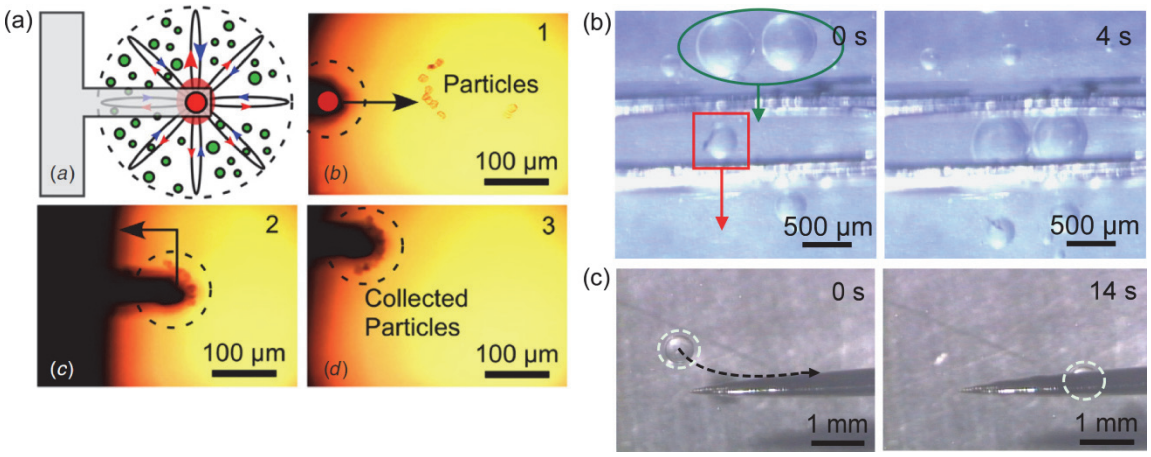

Figure 1.6: Heat sources of various geometries to generate Marangoni flows [Bas08a]: (a) Point heat source for particle collection, mixing and rotation; (b) Linear heat sources as virtual channels for size filtering; (c) Tapered heat source as guidewire droplet pump.

Instead of heat sources of definite shapes, the actuation of immersed particles and droplets can be accomplished by thermocapillary flow generated by a programmable heater array. The 16 × 8 pixel heater array is suspended above the liquid surface and by sequential activation of these heaters, motion of droplets can be controlled in two

dimensions by two modes: the push-mode actuation (Figure 1.7(a)) and pull-mode actuation (Figure 1.7(b)) [Bas09]. Droplets can be instructed to move in a certain path, make a 90° turn, or merge with other droplets. If a higher droplet velocity is desired, a liquid with a higher figure of merit can be chosen. This suspended heater array is used in some of this work to demonstrate the capabilities of Marangoni flows in actuating solid phase objects.

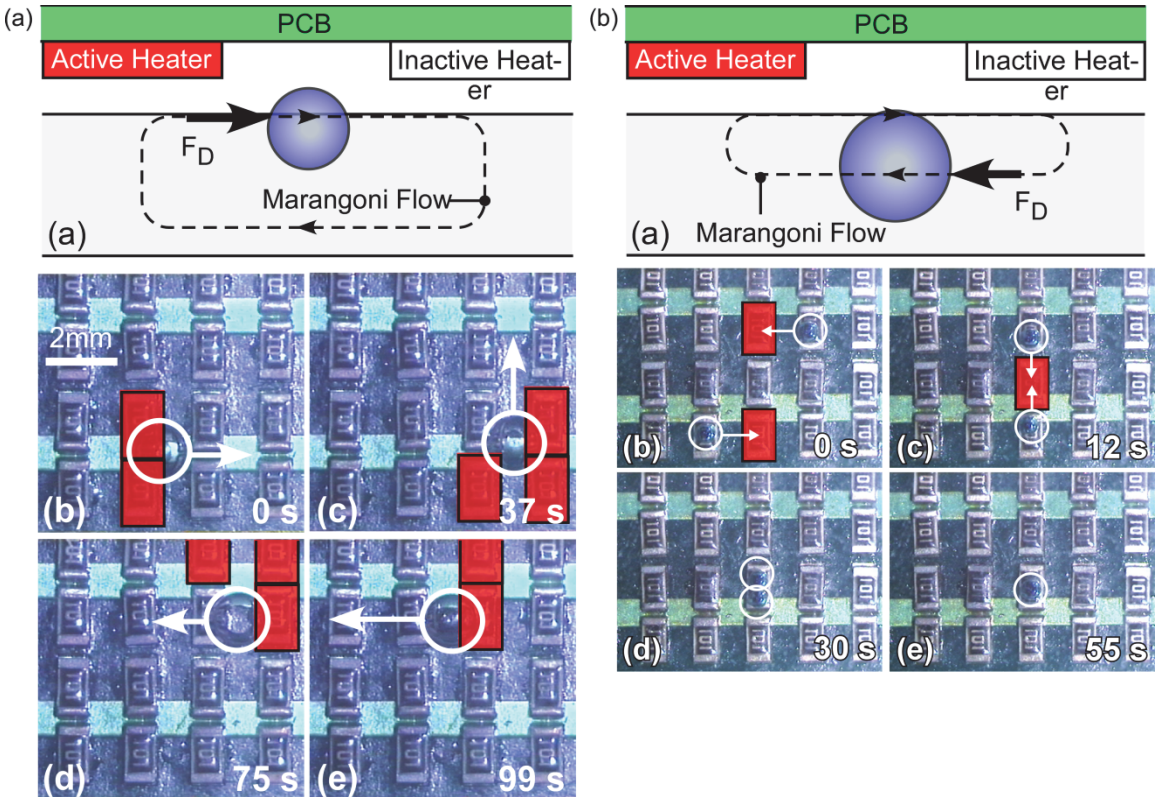

Figure 1.7: Programmable heater array for thermocapillary actuation [Bas09]: (a) Push-mode actuation for transporting droplets; (b) Pull-mode actuation for merging droplets.

One other application of Marangoni flow is in organizing suspended particles on a substrate from evaporating liquid droplets. The main reason why the evaporation of liquid droplets has become an important research area is that it plays a significant role in many new applications such as DNA mapping [Jin98], self-assembly [Big06, Lou10], etc.

As mentioned in Section 1.1, the higher evaporation rate at the droplet perimeter pulls more liquid and the particles in it toward the edges. This results in formation of "coffee-ring" patterns on the substrates [Dee00a, Dee00b]. One way to avoid the "coffee-ring" patterns is making the Marangoni effect in the liquid dominant [Hu06]. This can be done, for example, by heating the substrate, and the result is a more homogeneous distribution of particles placed on the substrate when all liquid evaporates. The role of surfactants in altering the patterns of deposited particles has also been investigated [Ngu02]. Surfactants decrease the surface tension at the interface, and a condition may be created to favor or suppress the formation of Marangoni cells which dictate the final distribution of deposited solute. The environment in which the liquid droplet evaporates can be altered to manipulate the flows inside the droplet [Maj12]. It is also found that the shape of the particles can also determine the deposition patterns. For example, under the same experimental conditions, spherical particles tend to form a ring after evaporation, whereas ellipsoids tend to be uniformly deposited [Yun11]. Controlled evaporation to separate particles of two different diameters into regularly arranged striped patterns is achieved by using the "cylinder-on-flat" geometry [Han11]. The scanning electron microscope (SEM) images of the stripe patterns are shown in Figure 1.8. The cylindrical lens on the heated substrate suppresses the Marangoni flow in the evaporating liquid, and it also allows the pinning and depinning of contact lines to occur several times during evaporation, forming the stripe patterns with separation of the different particles. Other methods to control the drying process are summarized by Han *et al.* [Han12]. A natural progression following the sorting and separation of particles of two different sizes is the separation of three or more particles of different sizes as well as particles which have diameters in a continuous

spectrum. With sorting according to particle size accomplished, it is not difficult to envision physical separation of the bigger and smaller particles.

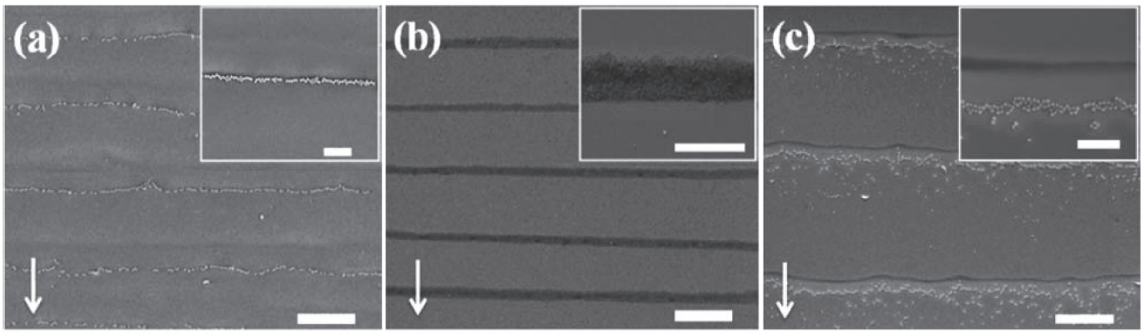

Figure 1.8: SEM images of stripe patterns obtained by retreating liquid in "cylinder-on-flat" geometry [Han11]. The larger 500 nm particles are separated from the 50 nm particles in each stripe.

1.3 Other Fluidic Manipulation Techniques

Other than thermocapillary actuation, several other microfluidics actuation techniques involving the modulation of surface tension are also widely used. One such technique is electrowetting, a technique based on the theory of electrocapillarity developed by Lippmann [Lip75]. In microanalytical chips, a common implementation is the sandwich configuration with a polarizable and conductive liquid droplet confined between two parallel substrates [Pol00, Pol02]. The applied voltage alters the contact angle of the droplet. Transporting, merging and splitting of droplets can be accomplished by electrowetting-on-dielectric (EWOD). Electrowetting is also used to control the flow of water in a microfluidic channel [Huh03]. Activating the array of electrodes below the channel alters the hydrophilicity of the channel floor surface, causing the water to shift and flow along the sidewall. Electrowetting can be categorized as a kind of digital microfluidics; its applications in life science have generated much interest among researchers worldwide. One application of EWOD is in DNA amplification by using

polymerase chain reaction (PCR), and an integrated EWOD/PCR chip has been proposed [Cha06]. Optoelectrowetting (SCOEW) uses light beams to alter the contact angle of the droplets and control the movement of these droplets, eliminating the need for fabricating complex bottom electrode arrays [Par10]. By altering the projected light pattern, SCOEW enables droplets of a wide range of sizes to be manipulated. Patterned hydrophobic/hydrophilic surfaces create "virtual paths" to control liquid displacement [Zha01, Fan04]. Other methods that utilize surface or capillary forces include electroosmosis [Che02] and electrohydrodynamic [Ahn98] to name a few, and will not be discussed in detail here.

Another popular technique is dielectrophoresis (DEP). This method uses non-uniform electric fields applied to polarizable particles that are immersed in non-conductive liquid having polarization characteristics different from the particles [Zha10]. There are two types of DEP: positive DEP (in which particles are more polarizable than its surroundings and are pulled toward higher field region) and negative DEP (in which particles are less polarizable than its surrounding and are repelled toward weak field region). Simulants of biological warfare agents can be separated from blood by DEP [Hua03], and bacteria can be separated from airborne particles such as dust using curved electrodes [Moo09]. By creative geometry designs of electrodes, DEP can also be used to handle biological cells [Wan97, Vol06]. Dielectrophoresis is a technique that is widely used to manipulate cells in biomedical applications because of the advantages it offers, which include the ability to separate cells without biologically damaging them, as well as without the need of biochemical alteration done on the cells.

Other than applying electric field, surface acoustic wave (acoustophoresis), magnetic field (magnetophoresis) and optical fields may also be used to achieve fluid manipulation. Acoustophoresis utilizes surface acoustic waves (SAWs) generated by applying AC signals to the interdigitated transducers to separate particles [Shi09]. The SAWs generate pressure fluctuations in the liquid. Lateral acoustic radiation forces on suspended particles result, and the particles are driven to the pressure nodes or antinodes depending on the density and compressibility. Particles of different magnetic susceptibilities can be separated by magnetophoresis [Pam06]. Non-magnetic particles remain undeflected in the separation chamber, and particles with larger magnetic susceptibility are deflected the most, therefore separating them. An optical technique using laser separates particles based on size and refractive index [Hoi09]. Different particles experience different scattering forces and gradient forces; larger particles possess higher refractive index, and are readily deflected by the optical field. Two or more of the aforementioned sorting techniques are often combined. For example, DEP and magnetophoresis have been utilized in a microfluidic device to separate superparamagnetic microbeads of varying sizes [Kri09].

In general, the different manipulation techniques require patterned substrates. Some manipulation techniques require electrodes to be patterned on the substrate as well. This adds to cost and complexity of substrate design. Figure 1.9 compares the different techniques with respect to substrate complexity for the various particle manipulation techniques. Number of materials, components and complexity in fabrication steps are used to evaluate substrate complexity. The Marangoni technique using suspended heat sources does not require substrates to be patterned; instead the heat sources of various

designs have to be fabricated. Because the heat sources are separate from the substrate on which particle manipulation occurs, these heaters can be reused and easily applied on any other substrates or techniques. Hence the Marangoni technique offers not only a low-cost option for fluidic manipulation, but also flexibility as a result of the physical separation between the powered element and the liquid.

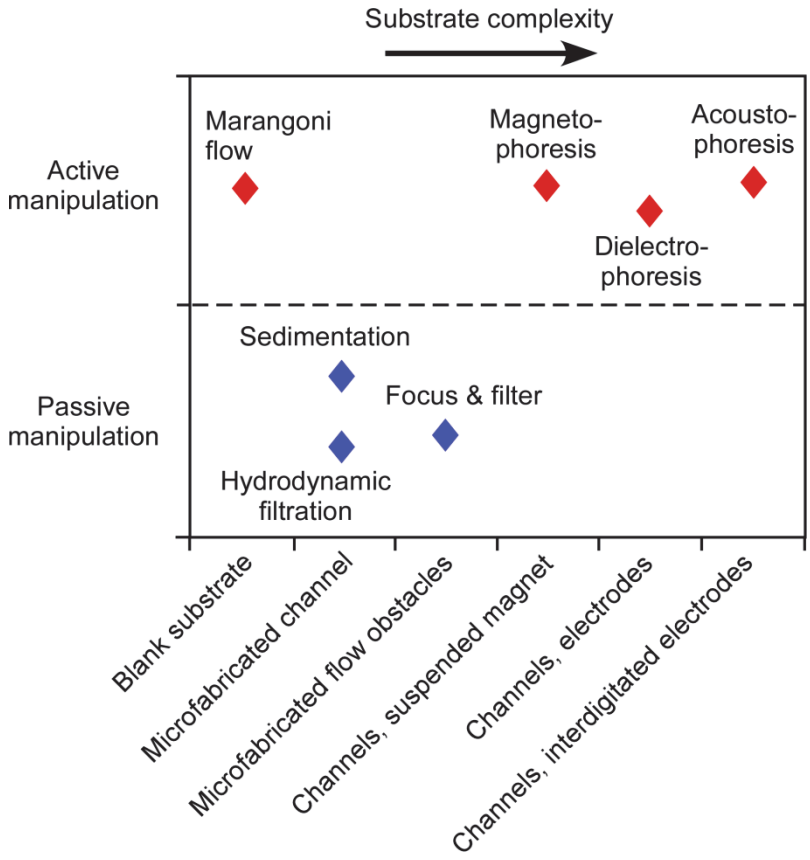

Figure 1.9: Comparison of passive and active particle manipulation techniques.

1.4 Structure of This Work

The Marangoni actuation technique is a suitable method in microfluidic systems, and can complement other fluidic manipulation techniques mentioned in Section 1.3 to achieve desired outcomes in such applications as environmental monitoring, biochemistry

etc. As described in Section 1.2, numerous past efforts of thermal Marangoni actuation are focused on manipulating liquid droplets. The Marangoni flows are generated by either heaters patterned on the substrate, suspended heaters or lasers to transport, split and merge these droplets which are μL in volume and micrometer in size. Several research groups have also focused on the manipulation of solid particles. This is accomplished by using point heat sources, or evaporating liquid droplets in the μL range having particles in them with or without heating from below.

To date, almost all published works pertain to transport of droplets, and transport of nanoscale and microscale particles. There are a number of interesting questions that remain to be addressed:

1. Can thermocapillary flows spatially localize the sedimentation of suspension particles on blank substrates?
2. Can the thermal Marangoni effect be exploited to actuate larger solid objects, such as those that are millimeter in size?
3. Is the Marangoni effect also a useful phenomenon for sorting, based on size, of low density solid particles that float on liquid?
4. Will the sorting method work for particles having a continuous distribution of sizes?
5. What are the conditions necessary to achieve the outcomes in points 1-4 above, and what are the potential utilities?

This work contemplates to address these questions by further investigating the applications of thermocapillary effect in actuating solid phase objects of various geometries and properties. Chapter 2 summarizes the theoretical background of

Marangoni effect and surface tension. Chapters 3, 4 and 5 describe the utilization of Marangoni convection in actuation of solid phase objects. Chapter 3 begins by showing the utilization of Marangoni forces, generated by millimeter-sized suspended heaters, in transporting and localizing sedimentations of micrometer-sized weed pollens on a blank glass substrate. There is no physical contact between the powered elements and the liquid suspensions, therefore this contactless method prevents sample contaminations. The heater array can be reused; therefore this technique also eliminates the need for costly fabrication processes and allows spatially localized sedimentations to be performed on any substrate. Using the same heater array, another application of Marangoni convection – actuation of millimeter-sized rotary structures completely submerged in liquid – is described in Chapter 4. The rotary structure is placed on a hub, and an optimum heating configuration is set up to achieve 360° rotations of the structure. The third application of Marangoni convection is in sorting of micrometer-sized floating spheres according to size. In particular, cenospheres with sizes of a continuous spectrum from 5 μm – 200 μm are sorted by evaporating liquid droplets for the purpose of studying their mechanical resonance.

Chapter 6 shifts the focus to the mechanical resonance characterizations of the cenospheres that are sorted according to size. The wine glass mode resonance is investigated to determine the practicality and suitability of cenospheres as resonators. Finally, Chapter 7 presents a summary of contributions of this work, and possible design improvements and future investigations.

CHAPTER 2

Theoretical equations

This chapter presents the theoretical equations used throughout this work. Some dimensionless fluidic numbers that are applicable in this work are also discussed.

2.1. Effect of Temperature on Surface Tension

In general, the gradient in surface tension, σ, may be caused by gradient in temperature, T, concentration of surfactants, c, or electric field, $\left|\vec{E}\right|$. This relationship can be summarized as [Ber08]:

$$d\sigma = \frac{\partial \sigma}{\partial T} dT + \frac{\partial \sigma}{\partial c} dc + \frac{\partial \sigma}{\partial \left|\vec{E}\right|} d\left|\vec{E}\right| \tag{2.1}$$

The first term in equation 2.1 is due to temperature variations. Surface tension typically decreases with increasing temperature. Eötvös proposed one of the first empirical relationships of the temperature dependence of surface tension [Eot86]:

$$\sigma = \frac{k_\gamma}{V_m^{2/3}} (T_c - T) \tag{2.2}$$

Here, k_γ is the Eötvös constant, with a value of 2.1×10^{-7} J/K.mol$^{2/3}$ for most liquids. T_c is the critical temperature at which the surface tension goes to zero, and V_m is the molar volume of the liquid:

$$V_m = M / \rho \tag{2.3}$$

where M is the molar mass of the liquid and ρ is the density of the liquid. Equation 2.2 was later improved by Katayama and Guggenheim to become [Gug45]:

$$\sigma = \sigma^* \left(1 - \frac{T}{T_c}\right)^n \tag{2.4}$$

where σ^* is a unique constant for each liquid, and n is an empirical factor whose value depends on the liquid. A linear approximation of the Guggenheim-Katayama formula is obtained by letting n =1:

$$\sigma = \sigma^* \left(1 + \beta T\right) \tag{2.5}$$

with β = -1/T_c. A graphical representation of the linear relationship between surface tension, σ, and temperature, T, is given in Figure 2.1. The value σ_o is a measured surface tension value at a certain temperature, T_o.

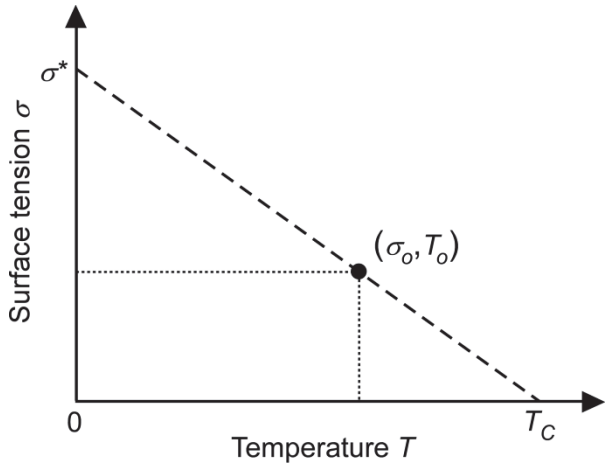

Figure 2.1: Linear dependence of surface tension and temperature.

As temperature increases, surface tension decreases for most liquids. Local heating of liquid surface results in reduction of surface tension at the heated area, and this is the origin of Marangoni convection in liquid layers of millimeter scale or less. The

cooler interfaces away from the heated area are regions of high surface tension, and surface tension gradient develops. This results in thermocapillary shear stress at the interface given by [Bas09, Hig00]:

$$\tau_s = \mu \frac{d\vec{u_s}}{d\vec{N}} = \sigma_T \nabla T_s \tag{2.6}$$

In this equation, μ is the dynamic viscosity of the liquid, $\vec{u_s}$ is the tangential surface velocity vector, $\vec{N}$ is the surface normal vector and σ_T is the surface tension temperature coefficient of the liquid obtained by differentiating equation (2.2):

$$\sigma_T = \frac{d\sigma}{dT} = -\frac{k_\gamma}{V_m^{2/3}} \tag{2.7}$$

Equation (2.7) is also referred as the Eötvös equation. σ_T is typically negative for most liquids (implying surface tension decreases with increasing temperature), and is assumed to be constant in this work.

As liquid moves from a region of low surface tension to that of high surface tension, a surface flow directed away from the high temperature region forms. To ensure fluid continuity, a subsurface flow in the opposite direction is developed. The surface and subsurface flows constitute the Marangoni flows shown by Figure 1.2. Note that when the heat source is removed, liquid motion homogenizes the temperature of the liquid. Absence of temperature gradient means absence of surface tension gradient and Marangoni flows cease to exist in the liquid.

Table 2.1 provides values of surface tension and surface tension temperature coefficients of the liquids used in this work; water is included for reference. Surface tension temperature coefficients are very small in magnitude. This implies that the change in surface tension is minimal even when there is a huge temperature variation,

making it difficult to create sufficient surface tension gradient at the liquid surface to induce Marangoni flows. Marangoni convection is thus often masked by volume forces such as buoyancy in large-scale systems. Equation 2.6 shows that the thermocapillary shear stress is directly proportional to the temperature gradient of the liquid. When the size of the system is reduced to a few millimeters or less, thermocapillary convection becomes the dominant effect. This is because at small length scales of a few millimeter, a small temperature change results in a large temperature gradient and hence large thermocapillary stress.

Table 2.1: Values of surface tension and surface tension temperature coefficient of liquids used in this work [3M01, Dow98a, Dow98b, Xia09]. Water is included for reference.

Liquid	**Surface tension (at 25^{o}C), σ (mN/m)**	**Surface tension temperature coefficient, σ_T (10^{-5} N/m.K)**
Silicone oil DC-200	19.7	-2.4*
Silicone oil DC-550	24.5	-6.9*
Silicone oil DC-704	37.3	-3.6
Fluorinert FC-3283	16.0	-4.8*
Water	72.9	-13.8

* Data not available; value estimated from other similar liquids.

2.2. Dimensionless Fluidic Numbers

When Benard observed cellular flow patterns in 1900, Rayleigh attributed it to buoyancy [Ray16]. It was not until 1958 that Pearson provided the right explanation – Marangoni effect [Pea58]. Often times, both thermocapillary convection and other volume effects such as buoyancy are present at the same time, and the former may be easily masked by the latter which manifests as natural convection. The dimensionless analysis presents a way to determine the more dominant effect when two competing phenomena are involved.

The dimensionless numbers which are helpful in determining which type of convection dominates are Marangoni number, Ma, and Rayleigh number, Ra [Vel09]. The strength of thermocapillary convection is characterized by Marangoni number given by:

$$\mathrm{Ma} = \frac{\text{Surface tension}}{\text{Viscous forces}} = \frac{|\sigma_T|\Delta TL}{\mu\kappa} \tag{2.8}$$

where L is the liquid layer depth, ΔT is the temperature difference, and κ is the thermal diffusivity. It gives the ratio between surface tension and viscous forces. The Rayleigh number, the ratio between buoyancy forces and viscous forces, is given by:

$$\mathrm{Ra} = \frac{\text{Buoyancy forces}}{\text{Viscous forces}} = \frac{\alpha g \Delta T L^3}{\mu_k \kappa} \tag{2.9}$$

Here, α is the thermal expansion coefficient of the liquid, g is the gravitational acceleration, and $\mu_k = \mu / \rho$ is the kinematic viscosity of the liquid where ρ is the density of the liquid. The ratio Ma/Ra characterizes the strength of the surface tension compared to buoyancy forces. The inverse, Ra/Ma, is the dynamic Bond number, Bo_D:

$$\mathrm{Bo}_D = \frac{\mathrm{Ra}}{\mathrm{Ma}} = \frac{\rho \alpha g L^2}{|\sigma_T|} \tag{2.10}$$

The dynamic Bond number (Bo_D) gives the ratio between buoyancy and surface-tension gradient forces, and determines whether the Marangoni effect is the dominant phenomenon. As $\mathrm{Bo}_D \propto L^2$, L has to be sufficiently small for thermocapillarity to be the dominant effect. Alternatively, buoyancy can be virtually eliminated by conducting the experiments under microgravity conditions, e.g. in space, where g approaches zero. Assuming that the characteristic length L is a conservative 1 mm and taking $g = 9.81$ m/s^2, Table 2.2 gives the calculations of the dynamic Bond numbers of various liquids used in

this work. When L decreases, the dynamic Bond numbers decrease. In the chapters that follow, we assume that Marangoni convection is the dominant mechanism in the manipulation of solid phase objects.

Table 2.2: Material properties and calculated dynamic Bond numbers of the liquids used in this work.

	Liquid			
Parameter at 25°C	**DC-200**	**DC-550**	**DC-704**	**FC-3283**
Density, ρ (kg/m^3)	913	1068	1070	1820
Thermal expansion coefficient, α (10^{-6} K^{-1})	1050	750	950	1400
Surface tension temperature coefficient, σ_T (10^{-6} N/m.K)	-24*	-69*	-35.6	-48.3
Dynamic viscosity, μ (10^{-3} kg/m.s)	4.6	134	42	1.4
Kinematic viscosity, μ_k (cSt)	5	125	39	0.75
Thermal conductivity, k (W/m.K)	0.13*	0.13	0.16*	0.066
Specific heat capacity, C_p (J/kg.K)	1600*	1500	1542	1100
Prandtl number, Pr	55	1.5×10^3	4×10^2	25
Dynamic Bond number, Bo_D	0.39	0.11	0.28	0.52

* Data not available; value estimated from other similar liquids.

Marangoni flows are generally weak in aqueous solutions and water. This has been confirmed by particle-tracing technique [Hu06]. The main reason is that the surface of water is easily contaminated by surfactants, chemically-active agents which are capable of easily altering the properties of Marangoni convection [Sav02, Hu06]. For that reason, silicone oil is the most preferred liquid in many experiments involving the study of Marangoni effect [Ril98, Sch01]. Silicone oil is transparent, and any instability can be easily observed under the optical microscope. These oils also have a very low surface tension. They are therefore not easily altered by surfactants [Ber65]. Furthermore, silicone oils are available in a wide range of Prandtl numbers ($50 < Pr < 1500$), making it versatile to alter experimental conditions. The Prandtl number is given by:

$$\mathrm{Pr} = \frac{\mu_k}{\kappa} \tag{2.11}$$

Viscous effects dominate the flow in liquids with a high Prandtl number, while heat diffusivity is high and inertial effects dominate the flow in liquids with low Prandtl number. The Prandtl numbers of the silicone oils used in this work are also given in Table 2.2.

2.3. Governing Equations and Boundary Conditions

In microfluidics, flow velocities are small enough to treat the liquid as incompressible. The density of the liquid is therefore constant, and the continuity equation becomes:

$$\nabla \cdot \mathbf{u} = 0 \tag{2.12}$$

where **u** is the velocity vector. In modeling with COMSOL Multiphysics®, the temperature field that induces the liquid flow due to Marangoni effect is obtained by solving the energy equation [Com11]:

$$\nabla \cdot \left(-k\nabla T + \rho C_p T\mathbf{u}\right) = Q \tag{2.13}$$

where k is the thermal conductivity, T is the temperature, ρ is the liquid density, C_p is the specific heat capacity of the liquid, **u** is the velocity vector, and Q is the rate of heat transfer per unit volume. When modeling of the heater array is done in this work, the heater surfaces are at fixed temperatures. The air gap between the heater element and the liquid surface is small, typically in the range of 500 μm – 1000 μm, and heat transfer in this domain is assumed to be by conduction only. This temperature distribution is then used to calculate the forces that the Marangoni effect induces on the liquid/air interface using equation (2.6), and the flow velocities in the liquid are calculated using the Navier-

Stokes equation for incompressible fluid:

$$\rho\left(\frac{\partial \mathbf{u}}{\partial t}+\mathbf{u}\cdot\nabla\mathbf{u}\right)=-\nabla p+\mu\nabla^2\mathbf{u}+\mathbf{f} \tag{2.14}$$

Here, p is the pressure that the liquid experiences from the surroundings, and $\mathbf{f}$ represents other external body forces such as gravitational force acting on the liquid per unit volume. In this work, effects of gravity and other external forces can be neglected, hence $\mathbf{f} = \mathbf{0}$. The sides of the liquid layer are assigned *no slip* boundary condition, while the liquid/air interface has a *slip* boundary layer.

CHAPTER 3

A non-contact method for spatially localized sedimentation of particles from liquid suspensions using Marangoni forces

This chapter presents the directed sedimentation of suspension particles in a thin layer of liquid (≤ 1 mm) onto a featureless glass substrate by Marangoni flows. A programmable 16 × 8 array of surface mount resistors suspended 0.1 mm – 2 mm above the liquid provides dynamic millimeter-sized heat sources to locally heat the liquid surface to temperatures from approximately 28.5°C to 36.5°C. The heaters in this array can be activated independently by a graphical user interface, creating surface tension gradients along the liquid surface. The resulting Marangoni flows direct spatially localized particle sedimentation on the substrate. The resultant sedimentation patterns and accumulation levels depend on factors such as the temperature gradient at the liquid surface, number of active heaters and type of liquid used. For example, when a single heater is activated, a liquid surface temperature elevation of 6.9°C results in a localized sedimentation of suspended weed pollen *Kochia scoparia* (Φ = 25 μm) in silicone oil DC-704 over a region of 2.9 mm^2 that is centered directly beneath the active heater. This sedimentation method is a contactless technique, which reduces the likelihood of sample contamination.

3.1. Introduction

Low cost diagnostic systems that offer high sensitivity and quick response are increasingly important for healthcare monitoring [Yag06, Pol11] and environmental monitoring [Moo09]. Such systems utilize microfluidic technologies to manipulate particles or liquids. Often, particle trapping, separation and deposition are necessary to increase the concentration level of the particles so that detection and accurate analysis are possible. As these systems progressively decrease in size, surface phenomena become more dominant and play important roles in microfluidic applications, influencing particle transport, trapping, mixing, reaction and separation. The Marangoni effect develops as a result of surface tension variations at the liquid/gas interface caused either by temperature gradient or concentration gradient in the liquid, and is an example of a surface phenomenon. This phenomenon is known to be responsible for many common occurrences, such as the "tears of wine" [Scr60] and superspreading of solution [Nik02]. In several industrial processes such as the floating-zone process for crystal growth, Marangoni effect also plays a critical role [Lap05]. As a result, the Marangoni effect has been studied extensively [Lai86, Lu96, Aub05, Hu05a, Hu06, Tad09, Bha09]. Factors which influence Marangoni flow such as presence of turbulence [Kam98] and liquid depth [Ron07] have also been investigated.

The Marangoni effect, when induced by a temperature gradient, is also known as thermocapillarity. It is considered as a form of thermophoresis when the liquid flow and corresponding particle movement are induced by such a temperature gradient [And89, Wur07]. When temperature variation is imposed on a liquid surface, surface tension gradient develops at the liquid surface. This results in liquid motion along the liquid/gas

interface, and flow in the opposite direction in the bulk liquid. Such liquid motion is referred to as Marangoni flow. Marangoni force has been utilized for transporting nano-liter amounts of liquids over a large area [Far04], and droplet displacement and switching in a bifurcating microfluidic channel [Sel10]. One method to generate Marangoni flow is to subject a liquid surface to a micrometer scale temperature source suspended above the liquid. Different shapes of heat sources in the micrometer range have been utilized to generate flows capable of manipulating micro particles and droplets [Bas08a]. Marangoni flow has also been employed to perform droplet actuation by programmable manipulation using a 128-pixel heater array suspended 0.1 mm – 2 mm above the liquid surface [Bas09]. This chapter describes the investigation of the directed sedimentation of suspension particles in a liquid onto a featureless glass substrate by Marangoni flows using this 128-pixel heater array [Hen10, Hen11a]. Figure 3.1(a) shows the cross-section of a 3D schematic diagram of particle sedimentation by Marangoni cells and part of the heater array suspended above the liquid. By activating a particular heater in the heater array, a temperature gradient is created on the surface of a thin liquid layer directly below the heater. This results in surface tension gradient, which generates Marangoni flows capable of directing particles to accumulate at desired locations on a blank glass substrate in a contactless manner. The Marangoni sedimentation technique reduces the need for costly fabrication processes and allows spatially localized particle sedimentation to be performed on any substrate.

Section 3.2 presents the theoretical and simulation modeling of Marangoni flow in a bulk liquid induced by a millimeter sized heat source in close proximity to the liquid surface. Section 3.3 describes the experimental results, showing the various

sedimentation patterns formed by different conditions. The discussion and conclusion are presented in Section 3.4.

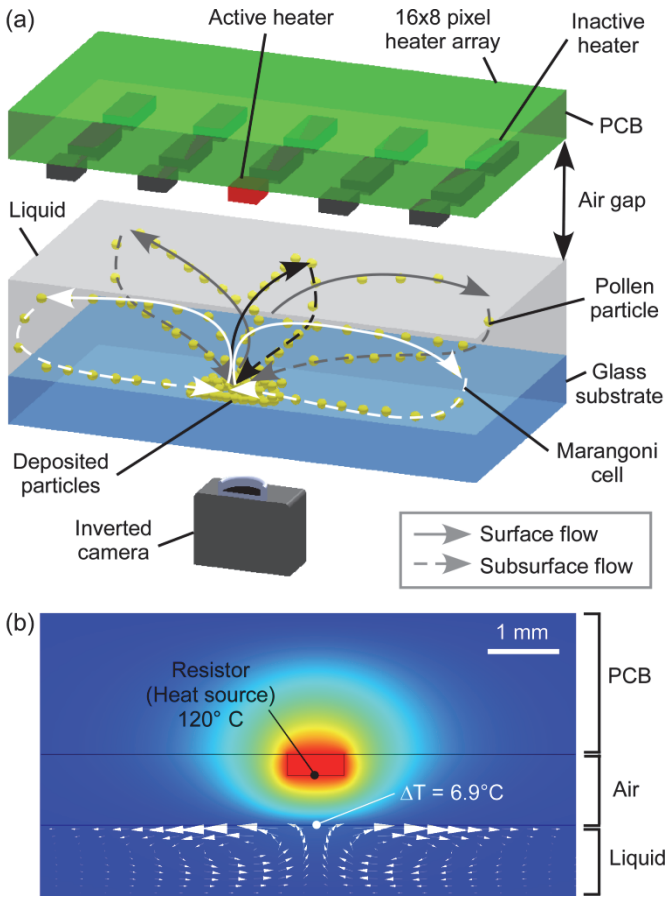

Figure 3.1: (a) Cross-sectional view of 3D schematic diagram of the experimental setup. (b) Simulation result (COMSOL Multiphysics® 3.5a) showing temperature distribution profile and generated Marangoni flow cells in silicone oil DC-704.

3.2. Theoretical Modeling

The heat generated from the heat source travels through the air gap and increases the liquid surface temperature directly below the heat source in a spatially localized manner. A temperature gradient is created at the liquid surface, resulting in a surface tension gradient. The corresponding thermocapillary shear stress, τ_s, is proportional to the temperature gradient, ∇T_s according to equation (2.6). As the direction of the shear

stress and liquid flow are from a region of low surface tension (high temperature) to that of a high surface tension (low temperature), Marangoni flow at the surface of the liquid is directed away from the heat source. This produces subsurface flows towards the heat source in the bulk liquid. The surface and subsurface flows together form the Marangoni cell, transporting suspended particles in a toroidal pattern. This phenomenon is depicted by Figure 3.1(a).

A 3D simulation model is created using COMSOL Multiphysics® 3.5a; it includes the heater array and its supporting printed circuit board (PCB), the air gap, and the liquid on the glass substrate as shown in Figure 3.1(b). Power is supplied to the heater to achieve localized temperature elevation of ≈7°C on the liquid surface. The liquid is assumed to be 1 mm deep silicone oil DC-704 (Dow Corning Corporation, Midland, MI) with properties summarized in Table 3.1 [Dow98a]. Air is a relatively poor conductor of heat, with a low thermal conductivity of 0.025 W/m.K. When the air gap between the heater and the liquid surface is 700 μm, the liquid surface temperature increase of 6.9°C is obtained for a power level of 600 mW, which elevates the surface of the resistor to 120°C (This has been experimentally verified by measurements with a thermocouple as well as an infrared (IR) thermometer). Such temperature elevation can be achieved with a power of 150 mW and 80 mW when the air gap is reduced to 100 μm and 10 μm, respectively. Assuming that the sides of the liquid are at ambient temperature of 27°C, a temperature gradient and surface tension gradient develop at the surface. In thin layers of liquids, the dominant driving force is the Marangoni effect, while buoyancy force and other bulk phenomena are smaller. In Figure 3.1(b), the arrows show the resulting Marangoni surface and subsurface flows in silicone oil DC-704. Simulation results also

show that the surface temperature of the liquid immediately below the resistor rises proportionately as the heater temperature is increased or the air gap is decreased.

Table 3.1: Material properties of the liquids used in particle sedimentation: silicone oil DC-550 [Dow98b], silicone oil DC-704 [Dow98a], and electronic liquid FC-3283 [3M01].

	Liquid		
Parameter at 25°C	**DC-550**	**DC-704**	**FC-3283**
Density, ρ (kg/m^3)	1068	1070	1820
Heat capacity, C_p (J/kg.K)	1418	1542	1100
Thermal conductivity, k (W/m.K)	0.13	0.16	0.066
Absolute viscosity, μ (10^{-3} kg/m.s)	134	42	1.4
Kinematic viscosity, μ_k (cSt)	125	39	0.75
Surface tension temperature coefficient, σ_T (10^{-6} N/m.K)	-69	-35.6	-48.3
Thermal expansion coefficient, α (10^{-6} K^{-1})	750	950	1400

The particle velocity is the greatest at the liquid/gas interface, and drops towards the sides and bottom of the liquid. The subsurface flows of the Marangoni cells are able to create sweeping actions on the substrate which result in particles close to the glass substrate being transported across the substrate, localizing the sedimentation below the heat source where the subsurface radial flow converges and rises to the surface. This final location of the particles is independent of whether the sedimentation of the particles upon the substrate is caused by gravitational forces or particle-substrate interaction.

The type of liquid used in the experiment can also affect the resultant particle velocity, and hence the particle collection. Three kinds of liquids are used in this work, namely silicone oil DC-550 [Dow98b], silicone oil DC-704 [Dow98a] and electronic liquid Fluorinert^{TM} FC-3283 (3M Specialty Materials, St. Paul, MN) [3M01] with some

of the properties listed in Table 3.1. Thermal conductivity values are generally available, but this value is not available for DC-704, so its value is estimated from a similar liquid. The surface tension temperature coefficients are calculated from the Eötvös equation according to equation (2.7) [Eot86]. The molar volume of silicone oil DC-550 is not known, and its surface tension temperature coefficient is estimated from a similar liquid.

The particles used in this work are Φ = 25 μm weed pollen from *Kochia scoparia* (Sigma-Aldrich, St. Louis, MO) [Ald10]. Small, spherical particles reach a terminal or settling velocity due to gravitational force. The settling velocity, V_t, is given by Stokes' equation:

$$V_t = \frac{2r^2 g(\rho_s - \rho_f)}{9\mu} \tag{3.1}$$

where r is the radius of the particle, g is the gravitational acceleration, ρ_s is the density of a particle and ρ_f is the density of the liquid. Even though every pollen particle is not perfectly spherical, this equation provides a reasonably accurate approximation of the settling rate [Gio95]. Because of pollen grouping, natural differences among pollen particles, the existence of air molecules, and variations in the water retention within the pollen, settling velocities of weed pollen vary widely [Gio95, Sos09].

3.3. Experimental Results

A 16 × 8 heater array is used to generate Marangoni flows in a thin layer of liquid, typically less than a millimeter deep. The heater array consists of 100 Ω #0603 surface-mount resistors, each of size 1 × 0.8 × 0.35 mm^3 placed at 1.9 mm pitch on a PCB. Each resistor can be switched on and off independently via a user interface written in LabView (National Instruments, Austin, TX). The range of the heater power used is usually less

than 1.3 W. A complete description of the design, fabrication and electrical circuitry of the heater array is given by Basu *et. al* [Bas09].

Figure 3.1(a) shows the 3D schematic diagram of the experimental setup. The weed pollen particles are mixed homogeneously in a carrier liquid. The experiments are performed on 100 μl samples. The depth of the liquid mixture is in the range of 500 μm – 1000 μm; the heater array with the resistors is suspended 700 μm ±100 μm above the liquid surface. The heating is initiated immediately after the introduction of the suspension onto the substrate, so that most of the particles are still in suspension within the liquid and do not have sufficient time to settle onto the glass substrate. The results are visualized by an inverted camera located under the glass substrate. The programmable heater array produces various sedimentation patterns.

Experimentally measured temperatures of a single active heater at different powers are shown in Figure 3.2. Power is supplied to a resistor for about 1 minute before temperature measurement so that the resistor has sufficient time to reach thermal equilibrium. The range of the power applied to the heater is 0.15 W – 0.6 W. Based on simulation results, this provides liquid surface temperatures of 28.5°C to 34.0°C below the heater at the 700 μm separation in silicone oil DC-704. To ensure accuracy, the temperature of the suspended heaters is measured by two methods – a thermocouple (Omega Engineering Inc, Stamford, CT) and an IR thermometer (Optris LS, Micro-Epsilon Optris, Berlin, Germany). The temperature readings obtained by the two instruments are consistent, and the measured temperatures vary linearly with power within this range. The simulated liquid surface temperature rise directly below the active heater is also shown.

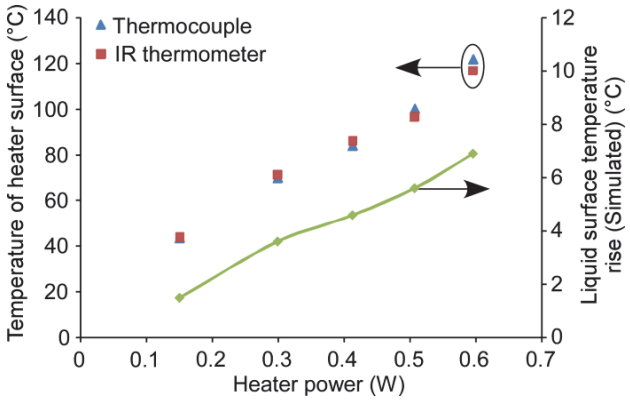

Figure 3.2: Temperature of a heater surface at various heater powers measured by thermocouple and infrared (IR) thermometer, and the resultant liquid surface temperature rise directly below the heater in silicone oil DC-704 obtained by simulation.

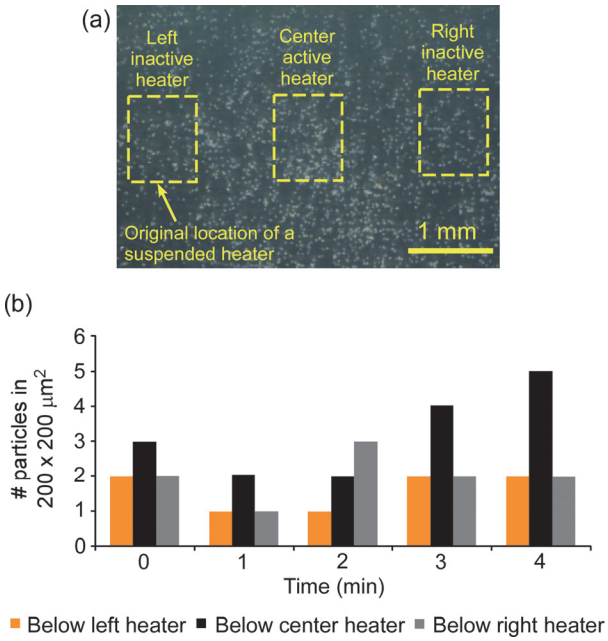

Figure 3.3: (a) No accumulation is observed in silicone oil DC-704 with an estimated liquid surface temperature of 28.5°C directly below the active heater. All the particles have settled onto the glass substrate after about 3 minutes 30 seconds. Before taking the image, the suspended heater is raised but the liquid is not removed. (b) Number of particles below the left, center and right heaters per 200 × 200 μm^2 in the first 4 minutes of the experiment.

Figure 3.3 shows the sedimentation pattern resulting from an estimated liquid surface temperature of 28.5°C directly below the heater. The sample was prepared with 5 mg of weed pollen homogeneously mixed into 1 ml of silicone oil DC-704. The weed

pollen was randomly distributed in the liquid at the start of the experiment. When the center heater is initially activated, particle velocities are low, and particles distant from the central axis of the active heater tend to settle on the substrate according to the settling rate in equation (3.1). There is insignificant change in the distribution of particles during the first 3 minutes of the experiment. After about 3 minutes 30 seconds, particle movement is no longer observed. All the particles have settled onto the glass substrate, and despite the presence of the heat source, the particles remain stationary. No accumulation occurs as shown in Figure 3.3(a). At the end of the experiment, the suspended heater array is raised but the liquid is not removed. The estimated number of particles below the left inactive heater, center active heater and right inactive heater per $200 \times 200\ \mu m^2$ in the first 4 minutes is shown in the graph of Figure 3.3(b). It shows that the number of particles fluctuates and remains roughly constant over the time period despite temperature gradient developed at the liquid surface.

Figure 3.4 shows the temporal sequence of particle sedimentation starting with random distribution of weed pollen immersed in silicone oil DC-704 in Figure 3.4(a). The same sample as that in Figure 3.3 is used, with an estimated liquid surface temperature of 34.0°C. The accumulation begins to form 2 minutes after the start of the experiment. The deposit below the active heater after 2 minutes is shown in Figure 3.4(b). Continued sedimentation in the next 8 minutes results in a pattern as seen in Figure 3.4(c). The size of accumulation grows over time. The power was supplied for approximately 20 minutes until all particles that could be transported are localized to a region directly below the heat source. The final pattern is shown in Figure 3.4(d). The deposit is largely concentrated in a region of approximately 2.2 mm wide on its longer

side, covering an area of 2.9 mm^2 centered directly below the active heater. Some particles that randomly settle onto the glass substrate are not moved by the Marangoni cells.

The estimated pollen count directly under the center of the active heater and adjacent left and right inactive heaters per 200 × 200 μm^2 is plotted for the initial 90 s of the experiment in Figure 3.4(e). The high rate of sedimentation beneath the active heater is evident. The count was terminated at 90 s because manual counting became impractical. The numbers of particles below the left and right inactive heaters fluctuate depending on whether the random particles moving toward and away from the heat source come into the specified region where the count is taken. It can be observed from the graph that these numbers are generally constant and do not increase with time, showing that accumulation occurs only in the liquid region directly under an active heater.

The sedimentation pattern and accumulation level can be easily controlled. By activating different number of heaters simultaneously, different patterns and amount of collected particles can be attained, as shown in Figure 3.5. Each heater is supplied with 0.6 W, resulting in an estimated liquid surface temperature of 34.2°C or 36.4°C beneath the centroid when two or four heaters are activated, respectively. The test sample is of the same as for Figures 3.3 and 3.4. The yellow rectangles in Figure 3.5 identify the locations of the active heaters. More particles are collected when more heaters are active with the same initial concentration of suspension particles, and the accumulation covers a larger area. In Figure 3.5(b), the deposit is concentrated in a region of about 4 mm wide on its longer side, covering an approximate area of 7.9 mm^2 centered between the four heaters.

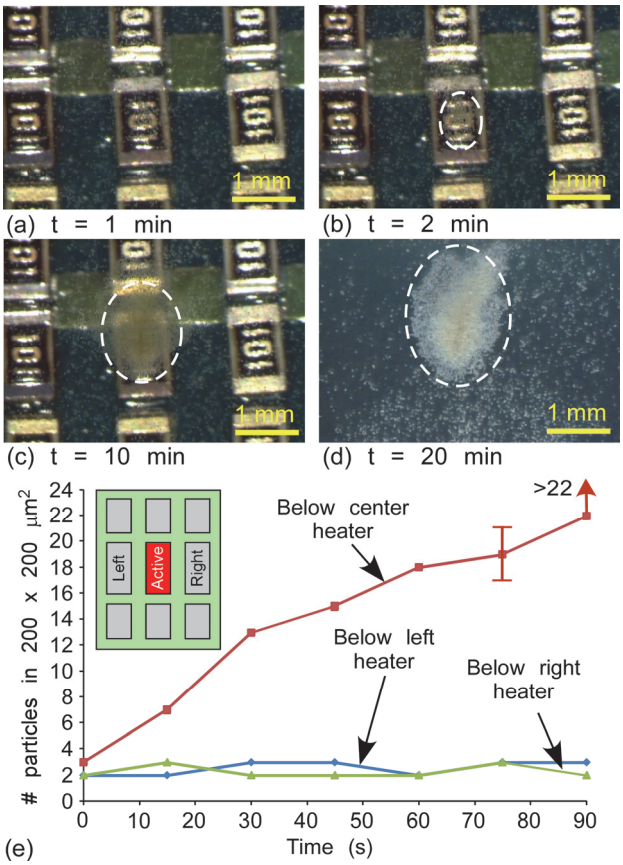

Figure 3.4: Sedimentation in silicone oil DC-704. The estimated liquid surface temperature is 34.0°C. (a) Initial random distribution of particles immersed throughout the liquid 1 minute into the experiment. (b) Particle sedimentation after 2 minutes showing a small amount of accumulation on the glass substrate below the active heater. (c) Particle sedimentation after 10 minutes. (d) Particle sedimentation after 20 minutes. (e) Number of particles accumulated below the center active heater, left inactive heater and right inactive heater per 200 × 200 μm^2.

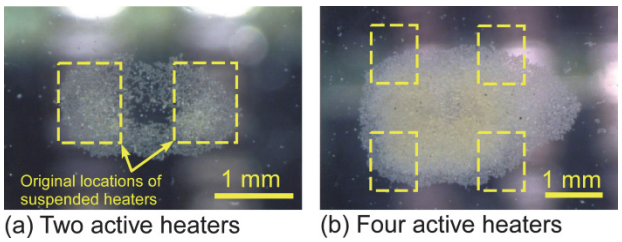

Figure 3.5: Formation of different patterns and amount of sedimentation in silicone oil DC-704 after approximately 15 minutes by: (a) two active heaters; (b) four active heaters. The liquid is not removed. The yellow rectangles identify the locations of the active heaters before they are raised.

The type of liquid used also affects sedimentation. Surface and subsurface flow velocities vary in different liquids such as silicone oil DC-550, silicone oil DC-704 and electronic liquid FC-3283. In this set of experiments, the three different liquids are used, and the concentration of the particles in each liquid is kept constant. Each experiment is run for about 20 minutes except that involving electronic liquid FC-3283. One heater is activated at a power of 0.6 W. Figure 3.6(a) shows the resultant sedimentation in silicone oil DC-550. In this liquid, the liquid surface temperature below the heater is estimated to be 35.5°C. Particle collection is limited to a small area of 1.3 mm^2 below the heater, and the final pattern seems scattered. Figure 3.6(b) shows particle sedimentation in silicone oil DC-704. In this liquid, more particles are collected from a larger area and form a more focused pattern. In electronic liquid FC-3283, the liquid surface temperature is estimated to be 29.7°C. Particles easily settle onto the glass substrate, and those that remain suspended move at a very high speed away from the heat source. No accumulation occurs as shown in Figure 3.6(c).

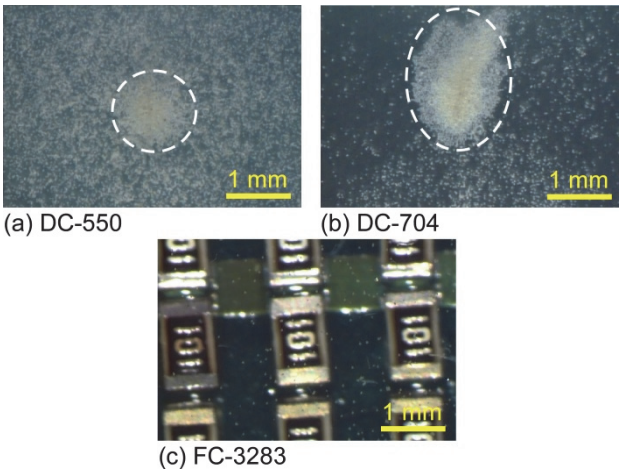

Figure 3.6: Particle sedimentation in three different liquids. (a) Sedimentation in silicone oil DC-550. Particle collection is limited to a small area below the heater. (b) Sedimentation in silicone oil DC-704. More particles are collected from a larger area to form a larger accumulation. (c) No accumulation occurs in electronic liquid FC-3283. The suspended heater is not raised before taking the image.

3.4. Discussion and Conclusion

In order to spatially localize a sedimentation, sufficient temperature gradient at the liquid surface must be achieved to generate Marangoni flows. This can be done by activating a single heater or multiple heaters to create temperature elevations at the liquid surface. A collection with a larger area and higher concentration of particles is formed when a greater amount of particles are accumulated by the Marangoni cells. From equation (2.6), it is evident that higher temperature gradients at the liquid surface and lower viscosities produce higher flow velocities. Marangoni cells with high enough surface and subsurface velocities have the ability to transport particles from a larger area to form a bigger accumulation directly below the active heater(s). Comparing the two silicone oils, silicone oil DC-550 has surface tension temperature coefficient approximately twice that of silicone oil DC-704, and viscosity about three times that of silicone oil DC-704. The lower particle velocities in silicone oil DC-550 cause some particles transported by Marangoni cells to settle on the glass substrate before they come to a region below the active heater, so that the final pattern is not as focused as that obtained by silicone oil DC-704. The electronic liquid FC-3283 has absolute viscosity two to three orders of magnitude lower; its thermal conductivity is also one order of magnitude lower than those of silicone oils. This favors the formation of a higher temperature gradient (the peak temperature gradient is 37 K/mm on the surface, about twice that of the silicone oils) and flow velocities in this liquid. When suspended particles move at high velocities away from the heat source and come in contact with the boundaries used to contain the liquid, some of these particles remain at the boundaries and are not recirculated by the subsurface flows to a region below the active heater.

Different liquids also have different vapor pressures and thus evaporation rates, which may influence the final patterns of sedimentation. Although the vapor pressure of the electronic liquid FC-3283 is much higher than those of the silicone oils, the evaporative effects of the fluorinated liquid on sedimentation are not evident. The volume fraction of evaporation in the duration of one experiment is < 10%. Effects of evaporation become apparent when a liquid having higher vapor pressure is used. Acetone, for example, has a vapor pressure one order higher than that of FC-3283. The high evaporation rate of acetone limits the formation of Marangoni cells as the experiment progresses, and particles are randomly deposited on the glass substrate as the liquid evaporates.

The use of the 16 × 8 heater array allows different configurations of active heaters to be used for different sedimentation patterns. When four corner heaters of a 3 × 3 pixel array are activated, the final sedimentation on the glass substrate covers an area of approximately 28 mm^2 in silicone oil DC-704. The sedimentation is not as focused as that obtained by the 2 × 2 pixel configuration shown in Figure 3.5(b), because the deposited particles are now spread over a larger area. Activating four corner heaters of a 4 × 3 pixel array produces an even more scattered rectangular-shaped sedimentation covering an area of about 32 mm^2 in silicone oil DC-704, with higher counts of particles at the four corners of the rectangular pattern.

It is worthwhile to compare the Marangoni forces that were utilized for particle collection in this effort, with some of the other approaches that have been reported. For example, thermophoresis is a method that uses temperature gradient to move particles. This method has been reported to form two-dimensional colloidal crystals [Duh05]. Although it is conceivable that thermophoretic forces may contribute to some extent to

particle arrangements in the experiments described in the preceding section, the contribution is likely to be minor. Based on the particle transportation velocity, the Marangoni forces are on the order of 10^{-8} N, whereas thermophoretic forces are on the order of 10^{-10} N. This estimate uses Stokes' drag equation; particle velocities for Marangoni flow and thermophoresis are on the order of 1 mm/s and 10 μm/s [Duh04], respectively.

One of the most widely explored methods for particle manipulation in microfluidic systems is dielectrophoresis (DEP) [Gas02, Zha10, Vol06]. This method uses non-uniform electric fields applied to polarizable particles that are immersed in non-conductive liquid having polarization characteristics different from the particles. Typical utilization involves electrical lead transfer to electrodes that are located on the microfluidic chip. Typical forces that have been reported for DEP structures are in the range of 10^{-12} N to 10^{-10} N [Wan97]. Hence, the Marangoni technique is potentially a complementary technique to others that have been explored for use in microanalytical systems.

In summary, this study shows that a millimeter-sized heat source is able to generate Marangoni cells in the liquid films for the purpose of spatially localized sedimentation of small suspension particles such as weed pollen. Various sedimentation patterns can be produced on a blank substrate by a suspended 2D heater array, which is able to impose different temperature profiles on the liquid surface and consequently alter the surface and subsurface flows. Among the three liquids used, silicone oil DC-704 shows to be the best carrier liquid to obtain a focused sedimentation of the weed pollen. A localized sedimentation of area 2.9 mm^2 directly below the heater is obtained when a

single heater is activated to generate a liquid surface temperature rise of 6.9°C in 1 mm deep silicone oil DC-704. When four heaters are activated, the area of the sedimentation obtained is about 7.9 mm^2. Because this is a non-contact technique, the problem of contamination is eliminated. This method of directed deposition may have potential applications in environmental science and biology if temperature elevation is not a critical issue in the sedimentation process. Following the demonstration of thermocapillary forces in manipulating micrometer-sized particles, the next chapter demonstrates the capability of Marangoni convection in manipulating millimeter-sized objects.

CHAPTER 4

Thermocapillary actuation of millimeter-scale rotary structures

In this chapter, we describe the rotary motion, by Marangoni flow, of a millimeter-scale rotary structure immersed in a thin layer of liquid. A 16 × 8 array of 1 × 0.8 × 0.3 mm^3 surface-mount resistors is suspended ≈500 μm above the liquid to serve as a programmable heat source. The continuous operation of resistor elements is used to impose a spatially-defined temperature gradient on the surface of the liquid. With a maximum temperature gradient of 36.6 K/mm at the surface of a 2 mm-thick film of liquid with viscosity 5 cSt, a stainless steel rotary structure with a mass of ≈10 mg, a diameter of 4.1 mm, and blade angle of 34° takes 28 s to make a 360° rotation. In general, the angular velocity of the rotary structure is affected by the temperature gradient of the liquid surface and liquid viscosity among several factors.

4.1. Introduction

In order to dynamically manipulate particles and droplets, several microfluidic technologies have been extensively studied in the past decade. For instance, the theory and technology of dielectrophoresis (DEP), which involves the manipulation of neutral particles by electric field gradients, have become established and investigations on various practical applications are ongoing [Pet10a, Pet10b]. Electrowetting, which

involves the electrical manipulation of the wettability of a surface, is another technique that is being widely explored [Pol02]. This technique has been used mainly to control discrete droplets in digital microfluidics [Pol11]. It has also been used to rotate a millimeter-sized thin plate structure [Tak10]. Like DEP, electrowetting does not require the fabrication of microchannels, making it versatile and easy to reconfigure.

Marangoni forces can also be used to manipulate droplets by altering the surface tension of the liquid [Dar05]. When caused by temperature gradient at the liquid-gas interface, this property is also known as thermocapillarity. The surface tension gradient is generally created by heating elements integrated within the microfluidic systems. It has been shown that droplets can be transported by activating the thermal elements that are embedded within a microfluidic device in a particular sequence, creating localized temperature gradients – and hence surface tension gradients – that displace the droplets [Far04, Dar03b, Sel09, Sel10]. Lasers have also been used to perform the localized heating [Bar07a, Bar07b, Vel09, Kot04]. Another method to realize contactless droplet manipulation by Marangoni flows is to use a programmable 2-dimensional (2D) heater array suspended 100 μm – 500 μm above a liquid layer [Bas09]. The separation of the electronic and fluidic substrates eliminates the need to pattern the substrate and reduces the likelihood of sample contamination and adsorption. This method has been used to direct precipitation of suspension particles in a liquid onto blank glass substrates [Hen11a].

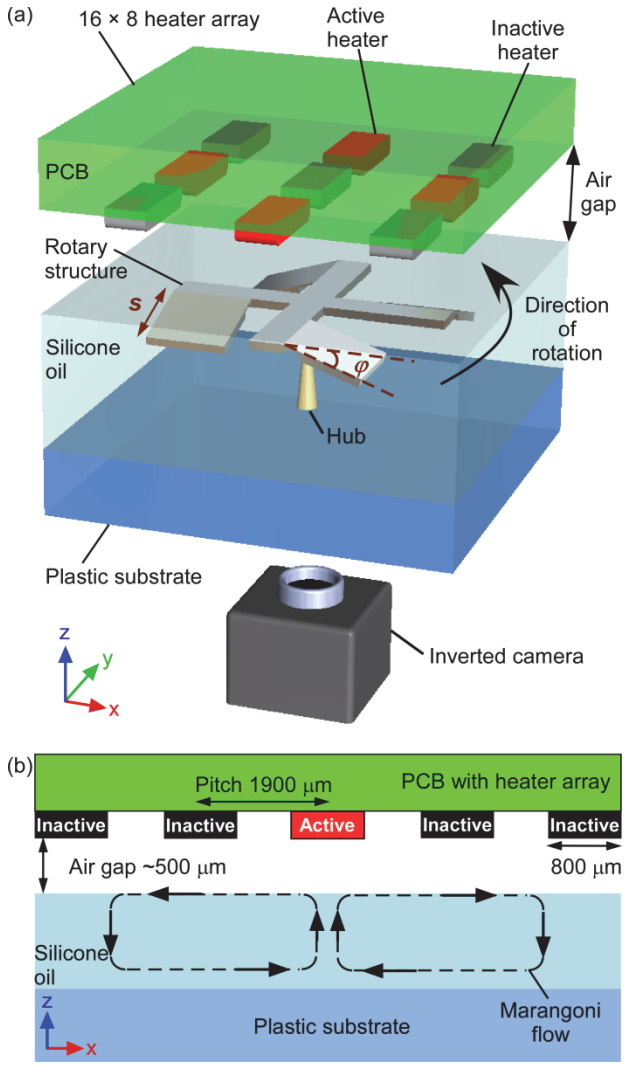

Figure 4.1: (a) 3D schematic of the experimental setup. The rotary structure made of stainless steel is mounted on a hub and completely immersed in silicone oil. The four square blades bend downwards in the liquid at an angle φ of 34°. The length of each side of the square blade s is 1.2 mm. The air gap between the heater and the liquid surface is ≈500 μm. Only 9 of the 128 heaters are shown, and four heaters are active. An inverted camera is used to record the rotation. (b) 2D schematic of Marangoni flows generated by the activation of a single heater.

The interaction of chip-scale thermocapillary flows with movable mechanical structures has not been widely reported. It has been shown that the thermocapillary actuation of a micromirror resting on a liquid droplet is possible through the creation of Marangoni flows within the liquid droplet by microheaters below the droplet [Dhu11]. However, the Marangoni effect permits forces to be applied without physical contact

between the powered element (such as suspended microheaters or laser) and the moving object. This chapter explores the application of Marangoni forces to rotate millimeter-scale structures completely immersed in a thin layer of liquid by the use of suspended heaters [Hen11b, Hen13a]. Surface-mount resistors on a printed circuit board (PCB) are held above the liquid surface as shown in Figure 4.1(a) to serve as heaters and generate the surface tension gradients at the liquid surface. Heaters are activated continuously to actuate the rotary structure by Marangoni flows. Figure 4.1(b) shows the 2D schematic of the Marangoni flows generated by a single active heater. The effects of temperature gradient at the liquid surface and liquid viscosity on the angular velocity of the rotary structures are investigated.

Section 4.2 shows the theory and modeling results of a blade immersed in liquid, showing that the blade is subjected to varying torques at different positions relative to the heaters. Section 4.3 describes the fabrication and experimental results. Section 4.4 presents the conclusions.

4.2. Theory and Modeling

When a heat source of millimeter size is suspended at close proximity above a liquid, temperature variations are created at the liquid surface. The heat that travels through the air gap raises the temperature of the liquid directly below the heater in a spatially localized manner. The lateral temperature gradient leads to surface tension gradient at the liquid-gas interface, and the resultant thermocapillary shear stress, τ_s, at the liquid surface is governed by equation (2.6). The shear stress is proportional to the temperature gradient, ∇T_s, with its direction from a region of low surface tension (high

temperature) to a region of high surface tension (low temperature). The Marangoni flow is thus directed away from the heated regions to colder regions of the liquid surface, and circulates in the opposite direction in the bulk liquid beneath the surface. This flow is schematically shown in Figure 4.1(b). For any pure liquid at all temperatures, the Eötvös equation can be used to estimate the surface tension temperature coefficient, σ_T, according to equation (2.7) [Eot86].

Table 4.1: Properties of silicone oil DC-704 [Dow98a] and DC-200 [Xia09].

Properties at 25°C	**DC-704**	**DC-200**
Density, ρ (kg/m^3)	1070	913
Thermal conductivity, k (W/m.K)	0.16	0.13*
Dynamic viscosity, μ (10^{-3} kg/m.s)	42	4.6
Kinematic viscosity, μ_k (cSt)	39	5
Surface tension temperature coefficient, σ_T (10^{-5} N/m.K)	-3.6	-2.4*
Specific heat capacity, C_p (J/kg.K)	1542	1600*

* Data not available; value estimated from other similar liquids.

Figure 4.2 shows the 3D simulation results using COMSOL Multiphysics® 4.3. The problem is modeled in a 3D geometry; a quadrant of the setup is drawn. The complete rotary structure has four blades each measuring 1.2 × 1.2 mm^2, and the length of the blade arm is 4.1 mm. The blades bend downwards at an angle φ of 34° as shown in Figures 4.1 and 4.2. The thickness of the structure is 125 μm. The structure is completely submerged in the liquid; the layer of liquid above the blade arm is 200 μm. The entire liquid has dimensions 20 × 20 × 2 mm^3. The liquid is assumed to be silicone oil DC-704 (Dow Corning, Midland, MI), and the properties of this liquid are listed in Table 4.1. Two of the active heaters, each measuring 1 × 0.8 × 0.3 mm^3, are suspended

500 µm above the liquid surface. Figure 4.2 shows a quadrant of the liquid layer measuring 10 × 10 mm^2 with a height of 2 mm. The thickness of the PCB is 1.6 mm.

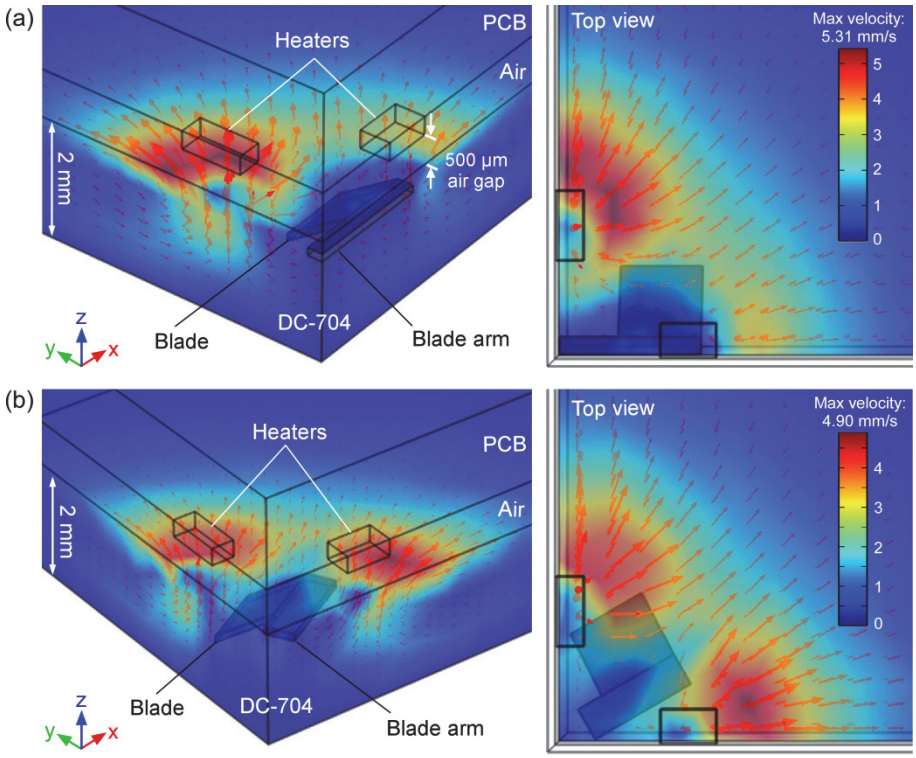

Figure 4.2: Modeling results showing the velocity magnitude in silicone oil DC-704 when the blade arm (a) is directly below a heater (rotation angle θ of 0°); (b) has rotated through an angle of 30° anticlockwise as viewed from above. The air gap is 500 µm, and the surface temperature of the two heaters is 446.5 K. Marangoni flow patterns are generated inside the liquid layer.

The temperature field that induces the liquid flow due to Marangoni effect is obtained by solving the energy equation given by equation (2.13). The air gap is small, and heat transfer in this domain is assumed to be by conduction only. This temperature distribution is then used to calculate the forces that the Marangoni effect induces on the liquid/air interface using equation (2.6), and the flow velocities in the liquid are calculated using the Navier-Stokes equation for incompressible fluid according to equation (2.14). The surfaces of the heaters are assigned fixed temperatures as boundary

conditions; the background is at 300 K. Full details of the boundary conditions used in the modeling are given in Appendix A. Two cases are simulated: (1) the blade arm of the rotary structure is directly below a heater at rotation angle θ of 0° (Figures 4.2(a) and 4.3(a)), and (2) the blade arm has rotated through an angle of 30° anticlockwise as viewed from above (Figures 4.2(b) and 4.3(b)). When the air gap is 500 μm and the surface temperatures of the heaters are 446.5 K, 428 K and 409 K, the maximum temperature gradients generated at the liquid surfaces are 30.6 K/mm, 26.7 K/mm and 22.8 K/mm, respectively. This heater surface temperature can be reduced to ≈355 K and ≈320 K when the air gaps are 100 μm and 10 μm, respectively, to generate the same maximum temperature gradient of 30.6 K/mm at the liquid surface.

The temperature gradient results in shear stress and liquid flow. Modeling results show that the maximum magnitudes of the liquid velocity are at the liquid surface, and that Marangoni flow patterns are generated inside the liquid layer. Figure 4.2(a) shows that when the blade arm is directly below a heater, the maximum liquid flow velocity is about 5.30 mm/s, while a maximum velocity magnitude of 4.90 mm/s is obtained when the blade arm has rotated 30° anticlockwise (as viewed from the top) shown in Figure 4.2(b).

With a liquid depth of 2 mm, the Marangoni effect is the dominant phenomenon in the liquid in comparison to free convection. This can be explained by the dynamic Bond number (Bo_D), which is the ratio between buoyancy and surface tension gradient forces [Vel09]:

$$Bo_D = \frac{Ra}{Ma} \propto L^2 \tag{4.3}$$

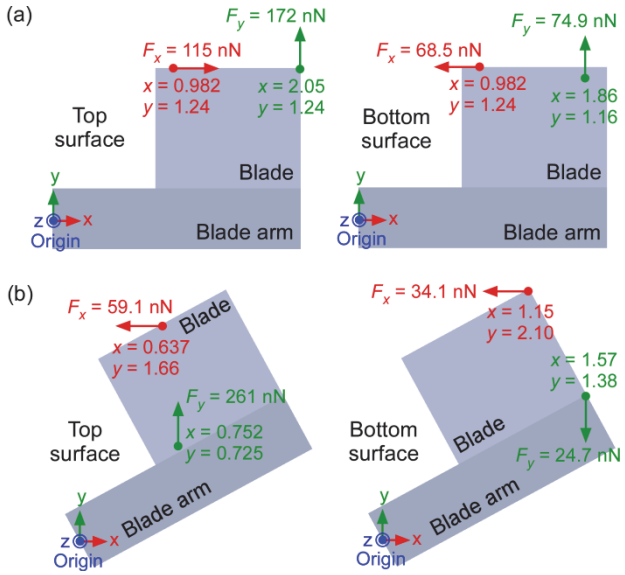

Figure 4.3: Driving torque calculations based on modeling results. (a) (Top view) Forces F_x and F_y acting on the top and bottom surfaces of the blade when the blade arm is directly below a heater (rotation angle θ of 0°). The driving torque on the blade is ≈435 pN.m, rotating the structure in an anticlockwise direction. (b) (Top view) Forces F_x and F_y acting on the top and bottom surfaces of the blade when the blade arm has rotated through an angle of 30° anticlockwise in the liquid as viewed from above. The driving torque on the blade is ≈325 pN.m, also producing an anticlockwise rotation. The x- and y-coordinates in the figures are in mm. The torque due to forces acting on the sides of the blades is omitted for clarity.

Ra and Ma are the Rayleigh number and Marangoni number, respectively. The dynamic Bond number, Bo_D, is directly proportional to L^2, where L is the characteristic length scale of the liquid. Therefore, for L of a few mm or smaller, free convection or buoyancy force becomes negligible.

The liquid motion produces a driving torque acting on the rotary structure. This torque is calculated with the z-axis as the axis of rotation, and the origin is at the center of the end of the blade arm as shown in Figure 4.3. The two force components that generate the torque to rotate the blade are F_x and F_y, and both act on each of the top and bottom surface of the blade. The magnitudes of these force components are obtained by

integrating the total stress over the top or bottom surface area of the blade. To obtain the perpendicular distances for torque calculations, F_x and F_y are assumed to be acting at the locations of maximum stress on the upper and bottom surfaces of the blade separately. There are also forces acting on the sides of the blade; including the effects of these forces reduces the driving torques by only 5-8%. Forces acting on the blade arm are assumed to produce negligible torques.

Figure 4.3 summarizes the results when only force components F_x and F_y acting on the top and bottom surfaces of the blade are considered. When the temperature of the heater surfaces is 446.5 K and the air gap is 500 μm, torque calculations based on simulations indicate that the driving torque on one blade is ≈435 pN.m when the blade arm is directly below the heater; this torque causes the blade to rotate in an anticlockwise direction as viewed from above. When the blade arm has rotated through an angle of 30° in the liquid, such that the blade is in between two heaters as viewed from above, the driving torque acting on the blade is ≈325 pN.m, also producing an anticlockwise rotation. After the effects of the forces acting on the sides of the blade are included, the driving torques are ≈400 pN.m and ≈310 pN.m when the blade arm is directly below a heater and when it has rotated through an angle of 30° anticlockwise, respectively. Direct evaluation of the torques in COMSOL indicates that the driving torques are ≈380 pN.m and ≈340 pN.m at rotation angle θ of 0° and 30°, respectively. Hence the blade is subjected to a varying torque as it makes a complete rotation. The greater torque acting on the blade at rotation angle θ of 0° causes the structure to accelerate, while a reduced torque when the blade is between two heaters causes it to decelerate. The rate of rotation depends on a variety of factors such as temperature gradient of the liquid surface and

liquid viscosity. It can be assumed that the frictional torque is similar to the driving torque because acceleration is small.

4.3. Fabrication and Experimental Results

The heater array is implemented in a 16 × 8 arrangement of #0603 surface-mount resistors (100 Ω, size 1 × 0.8 × 0.3 mm^3) placed at 1.9 mm pitch on a PCB. The position of the heater array above the surface of the liquid is controlled by a micromanipulator with a resolution of 2 μm. A user interface written in LabView (National Instruments, Austin, TX) is used to individually activate each heater.

The rotary structures, which have four square blades, are fabricated from a stainless steel substrate (thickness = 125 μm; density = 7850 kg/m^3) using micro-electro-discharge-machining (μ-EDM) (MG-ED72W, Panasonic, Osaka, Japan) [Tak02, Ric08]. The programming code which is used to create these rotary structures is given in Appendix B. Figure 4.4(a) shows the fabricated rotary structure before the blades are bent. In a typical structure, the total length of the blade arm is 4.1 mm and its width is 500 μm. Each of the four blades measures 1.2 × 1.2 mm^2, and is bent manually at a region of reduced thickness (40 μm) adjacent to the blade arm. A 300-μm-diameter depression of depth 80 μm is made at the center of the rotary structure to mount the structure on a hub. With such dimensions, the mass of the rotary structure is about 10 mg and its moment of inertia I is 2.35 × 10^{-11} $kg.m^2$. The blade angle φ is 34° as shown in Figure 4.4(b). All the blades of the rotary structure bend downward in the liquid when the structure is placed on the hub. The bends enable the structure to rotate and maintain balance during the rotation.

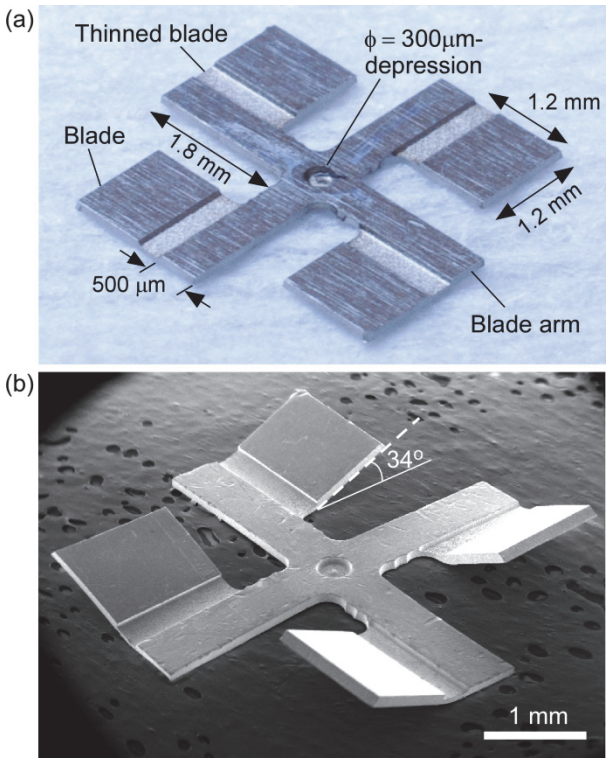

Figure 4.4: (a) Optical micrograph of the micromachined rotary structure made of stainless steel with thickness 125 μm. The length and width of the blade arm are 4.1 mm and 500 μm, respectively. Each square blade measures 1.2 × 1.2 mm^2. The thinned portion of the blades is 40 μm thick. A depression of diameter 300 μm and depth of 80 μm is made at the center of the rotary structure for mounting on the hub. (b) SEM micrograph showing a rotary structure with blade angle φ of 34°.

A micropipette is used to dispense the liquid onto the plastic substrate, and the depth of the liquid is ≈2 mm in order to completely immerse the rotary structure in the liquid. Silicone oil DC-200 and DC-704 are used as the liquid medium with some of their properties summarized in Table 4.1. To observe the rotation, an inverted camera is placed underneath the transparent plastic substrate.

When four heaters suspended 500 μm above the liquid surface are activated with a configuration shown in Figure 4.1(a), the temperature gradient and corresponding surface tension gradient at the liquid surface generate Marangoni flows, which rotate the millimeter-sized rotary structure submerged in liquid.

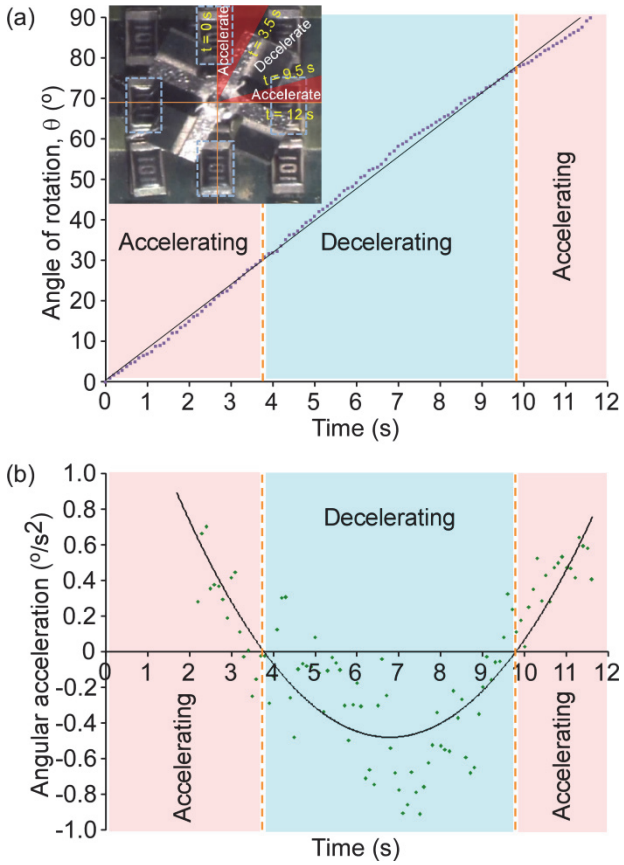

Figure 4.5: (a) Experimentally observed rotation of the rotary structure in silicone oil DC-704 through a rotation angle of 90° when the maximum liquid surface temperature gradient is 30.6 K/mm, showing regions of acceleration and deceleration in a period of 12 s. (b) Acceleration and deceleration of the rotary structure through a 90° rotation.

Figure 4.5(a) shows the experimentally-measured angle of rotation, θ, of the rotary structure submerged in silicone oil DC-704 with respect to time. In this experiment, the heater surface temperature is 446.5 K and the maximum temperature gradient at the liquid surface is estimated at 30.6 K/mm. From this graph, regions of acceleration and deceleration are identified as the rotary structure makes one quarter of a rotation in a time period of 12 s. The inset in Figure 4.5(a) shows an image of a rotation in a clockwise direction as obtained by the inverted camera. The four rectangles in dashed lines highlight the four active heaters suspended above the liquid. It is evident that a varying torque is acting on the rotary structure. The structure accelerates when the

blade arms are located directly below the active heaters and decelerates otherwise. The regions of acceleration correspond to regions of higher driving torques acting on the blades consistent with the simulation results. Figure 4.5(b) shows the graph of the angular acceleration of the rotary structure in this 90° rotation. When the blades of the structure bend upwards in the liquid, the direction of rotation is reversed.

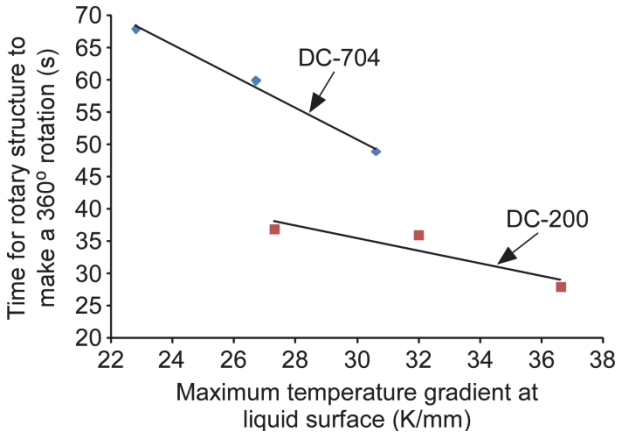

Figure 4.6: Time taken to make one complete rotation in silicone oil DC-704 and DC-200 at different maximum temperature gradients generated at the liquid surface.

The type of the liquid used can significantly affect the speed of rotation. Figure 4.6 shows the time taken by the rotary structure to make a 360° rotation in silicone oil DC-704 and DC-200 for different values of maximum temperature gradient at the liquid surface. When silicone oil DC-704 is used, the rotary structure does not make a complete rotation when the maximum temperature gradient at the liquid surface is less than 22.8 K/mm. The corresponding value is 27.3 K/mm when silicone oil DC-200 is used, and these values are repeatable. The graph depicts a linear dependence between the time taken by the rotary structure to make one complete rotation and the temperature gradient. As observed in Table 4.1, the properties of the two liquids are rather similar, but the dynamic viscosity of DC-704 is one order of magnitude higher than that of DC-200. It is,

therefore, expected that the structure takes more time to make a complete rotation in DC-704. Changing the viscosity of the liquid by one order of magnitude does not necessarily result in a direct increase in rotation rate by one order of magnitude because of the complex interaction between the liquid and the rotary structure, the role of the frictional forces at the hub, etc. At a maximum temperature gradient of 30.6 K/mm, the rotary structure takes 49 s to make a 360° rotation in silicone oil DC-704. Figure 4.7 shows the rotation of the rotary structure in silicone oil DC-200 when the maximum temperature gradient at the liquid surface is 36.6 K/mm. A dot drawn on one blade denotes the orientation of the rotary structure. The four activated heaters are indicated by rectangles in dashed lines. These four heaters are activated continuously, maintaining the temperature gradients and hence surface tension gradients at the liquid surface. The rotary structure takes 28 s to make a complete rotation in this liquid under these conditions.

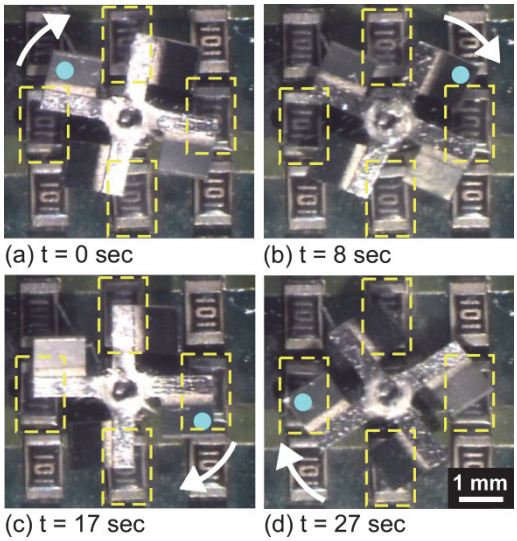

Figure 4.7: The 360° rotation of a rotary structure in silicone oil DC-200. The rectangles in dashed lines indicate the heaters that are activated. The generated maximum temperature gradient at the liquid surface is 36.6 K/mm. The time taken to make one complete rotation is 28 s. A dot is drawn on one of the blades for identification purposes.

4.4. Conclusions

The intent of this effort was to determine whether millimeter-scale rotary structures that are fully submerged in liquid can be actuated by thermocapillary forces without physical contact between the liquid and powered source. Millimeter-scale rotary structures with a blade angle φ of 34°, and mass of ≈10 mg were fabricated and evaluated. As the structure makes a 360° rotation, it experiences varying torque depending on its position relative to the microheaters. When the blade arms of the rotary structure are directly below the heaters, a larger torque acts on the blades and the rotary structure accelerates. A reduced torque acts on the blades otherwise, and the rotary structure decelerates. Frictional forces at the hub and drag forces on the blades also affect the angular velocity and acceleration of the rotary structure. The time needed by the rotary structure to make a complete rotation in silicone oil DC-200 is 28 s when the maximum temperature gradient at the liquid surface is 36.6 K/mm. In the long term, it is possible to envision an active control system in which the activation of heaters is synchronized to the angular position of the rotary structure. It should also be possible to replace the joule heaters by lasers, thereby reducing unnecessary heating.

In Chapters 3 and 4, the Marangoni effect used for fluidic manipulation is developed by localized heating of the liquid surface. As shown by Bénard and other researchers, thermocapillary flows can also be generated in thin layers of liquid heated from below. Marangoni flows are present in evaporating liquid droplets, but these flows are generally weak unless the substrate is heated. In Chapter 5, the utility of Marangoni flows in evaporating liquid droplets to achieve size sorting of solid phase objects is presented.

CHAPTER 5

Size sorting of floating spheres based on Marangoni forces in evaporating droplets

The high throughput size sorting of particles in liquid suspensions is of interest for a variety of microanalytical and micromanufacturing applications. Hollow glass cenospheres of various diameters ranging from 5-200 μm are sorted according to size by evaporation of isopropyl alcohol droplets on an unpatterned glass substrate. By raising the temperature of the glass substrate, a stable Marangoni convection is developed inside the droplet. At a substrate temperature of 55°C, more of the larger spheres (150-200 μm) are deposited near the droplet center, but smaller spheres <50 μm are found everywhere throughout the dried region. Better sorting is observed when the temperature of the substrate is above the boiling point of the liquid. When the substrate temperature is 85°C, higher than the boiling point of IPA, most of the spheres <50 μm are transported close to the droplet edge. In the center of the dried pattern obtained from a 0.5 μL droplet, the spheres with >150 μm diameter outnumber those with <50 μm diameter by 6X. The deposited spheres remain attached to the substrate surface when dry. The self-assembled nature of this drying pattern results in size sorting.

5.1. Introduction

The study of evaporating liquid droplets has been investigated to gain understanding of everyday natural phenomena such as the ring patterns left on a dried dish, and the familiar "coffee-ring" outlines left on the substrate by an evaporated coffee droplet [Dee97, Hu02, Hu05b]. In recent years, the investigation on the mechanisms of liquid evaporation has intensified because new and useful applications have been enabled by such a commonplace phenomenon. For example, under appropriate conditions, droplet drying has been reported to produce uniform monolayer gold films exhibiting long-range ordering [Big06]. This self-assembly method may be useful for the formation of ultra-thin films used in sensors and other devices. Other work has focused on droplet drying for striated, close-packed assemblies of 50-nm diameter and 500-nm diameter particles [Han11]. In general, the desired deposition pattern has been achieved by manipulating the internal droplet flows and kinetics [Fis02]; this may involve heating the droplet [Gir06], adding surfactant [Ngu02], or altering the surrounding in which the droplet evaporates such as letting it dry in a saturated ethanol environment [Maj12]. Another factor that influences the way the particles are distributed when the liquid dries is the shape of the particles. For example, it has been reported that spherical particles form a ring after evaporation, whereas ellipsoids tend to be uniformly distributed [Yun11].

The separation or sorting of particles is an important process that is often necessary to reduce analysis time and increase concentration of the constituent(s) of interest. Several sorting techniques have been proposed by the microfluidic community in the past several years. There are two main modes of particle sorting: the batch mode,

and the continuous mode. The batch mode requires a fixed volume of sample reagent to be processed, whereas the continuous mode typically allows constant flow to be maintained during the sorting [Pam07].

It is well known that liquid flow can result from surface tension gradients in liquid; this is known as the Marangoni effect. Surface tension gradients can be generated by temperature or surfactant concentration. Flow induced by the Marangoni effect due to temperature gradient is also known as thermocapillarity. To generate this temperature gradient on the surface of the liquid, thermal elements may be suspended in close proximity above the liquid surface. The resulting Marangoni flows in the liquid are capable of actuating droplets [Bas09] and directing sedimentations of suspended particles [Hen11a]. Alternatively, these heater elements may also be fabricated on the substrate, and the Marangoni forces may be utilized to transport nano-liter amounts of liquids over a large area [Far04]. A stable Marangoni flow pattern also develops inside an evaporating liquid droplet when the droplet is placed on a heated substrate. The higher temperature at the substrate contact region results in an area of lower surface tension as compared to the apex of the droplet. This results in an upward tangential flow along the curvature of the droplet from the edge to the apex, and a recirculating flow in the opposite direction within the droplet [Gir06].

Cenospheres, which are lightweight, hollow spheres produced as byproducts in coal-burning power plants, were once deemed as difficult waste, but they were later discovered to possess excellent material properties that make them highly useful in certain applications [Wan96]. For example, they have been used as lightweight fillers in building materials such as concrete [McB02], and they can be coated with metal such as

copper to make conducting fillers for electromagnetic interference shielding materials [Shu01]. These cenospheres typically come unsorted in various sizes, yet only cenospheres of a particular size are useful in certain applications. One potential application of cenospheres is inertial sensors because of the radial symmetry and properties – mechanical, electrical and optical – that are afforded by the spherical shape. The mechanical resonance of such structures has been reported recently [Hen13b].

The objective of this chapter is to investigate the possibility of size sorting cenospheres by utilizing the Marangoni convection inside an evaporating liquid droplet [Hen13c]. This is quite different from past efforts directed at the close-packed self-assembly of homogeneous nanometer-sized particles in suspension with the intent to create a film. First, the cenospheres, having a mean diameter of 85 μm, are much larger than the nanoparticles that have been investigated in the past, and they are present in a continuous spectrum from 5 μm to 200 μm, although the technique is not limited to this size range. Second, the low-density of the sealed, gas-filled cenospheres causes them to float on the liquid surface. Third, the goal is to permit the physical separation, and possible removal of smaller spheres, to allow the larger spheres to be harvested for subsequent use. The entire process of drying and segregation takes about 10 s. Other sorting methods such as electrophoresis [Koh08], acoustophoresis [Shi09], magnetophoresis [Pam06] and hydrodynamic filtration [Mat11] may take several minutes, and require the fabrication of electrodes, transducers, magnets and/or microchannels. The evaporation-based technique presented in this work avoids the complexity and costs of microfabrication.

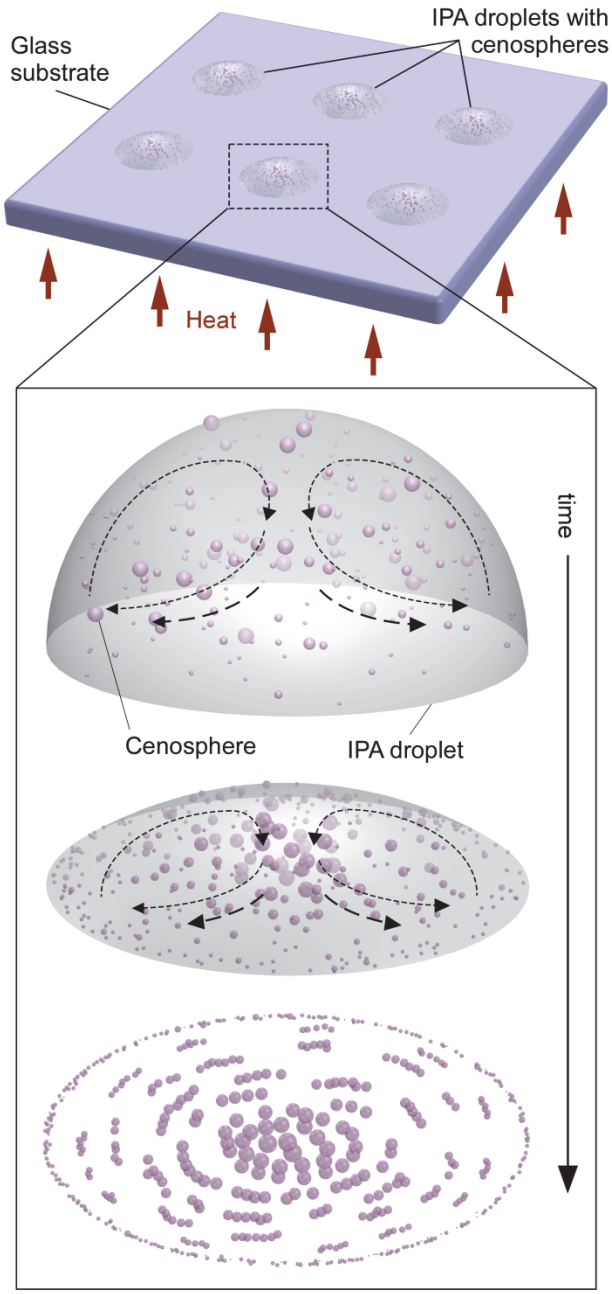

Figure 5.1: 3D schematic of high throughput sorting, showing an array of IPA droplets with cenospheres of various sizes on a heated glass substrate, as well as a schematic diagram of the evaporation process and the final pattern of deposited cenospheres. The cenospheres are sorted according to size, with the larger spheres at the center and the smaller spheres at the perimeter. The droplet volume ranges from 0.5-8 µL, and the temperature of the glass substrate is 55°C to 85°C.

Figure 5.1 shows a 3-D schematic of a concept to achieve high throughput sorting. An array of droplets in µL range, consisting of isopropyl alcohol (IPA) and

cenospheres, is placed on a heated substrate. The perimeter of each droplet is pinned, and the cenospheres are recirculated within the droplet by Marangoni flows until all the liquid evaporates. In the following section, it will be shown that, under appropriate conditions, most of the larger spheres are deposited at the center, while most of the smaller spheres are deposited around the circumference of the original droplet. The spheres of interest may be subsequently removed and processed.

5.2. Experimental Procedure and Results

5.2.1 Procedure

Commercially available cenospheres (Q-CEL 6014, Potters Industries LLC, Valley Forge, PA) made of sodium borosilicate glass are obtained. These cenospheres are made by heating solid glass particles; the gases within the glass act as blowing agents to expand the glass particles [Goe93]. The effective density of these hollow glass spheres is approximately 0.14 g/cm^3, and the sizes range from 5-200 μm. The shell thickness of the cenosphere is 1-3 μm. Figure 5.2 shows the optical and Scanning Electron Microscope (SEM) micrographs of the cenospheres of various sizes. To perform the size sorting experiments, a sample of 0.25 g of cenospheres is placed in 15 mL of IPA and mixed. The mixture is left undisturbed and after some time, the intact cenospheres float on the liquid surface, while the broken cenosphere particles settle to the bottom of the beaker.

To achieve size sorting, a small droplet of the mixture consisting of IPA and cenospheres is placed onto a 500-μm thick glass wafer which is heated by a hot plate below it. The temperature of the surface of the glass wafer is measured using a

thermocouple. A micropipette is used to pipette 0.5-8 µL of the droplet mixture by inserting the disposable pipette tip close to the liquid surface so that only the intact cenospheres are obtained. Once the droplet is placed on the glass wafer, a plastic cover is used to shield the droplet during the evaporation process to prevent ambient air flow from influencing the sorting process of the cenospheres. All the IPA evaporates in about 10 s. Due to the transparent nature of the cenospheres, a dark background is placed below the glass wafer during imaging using the optical microscope.

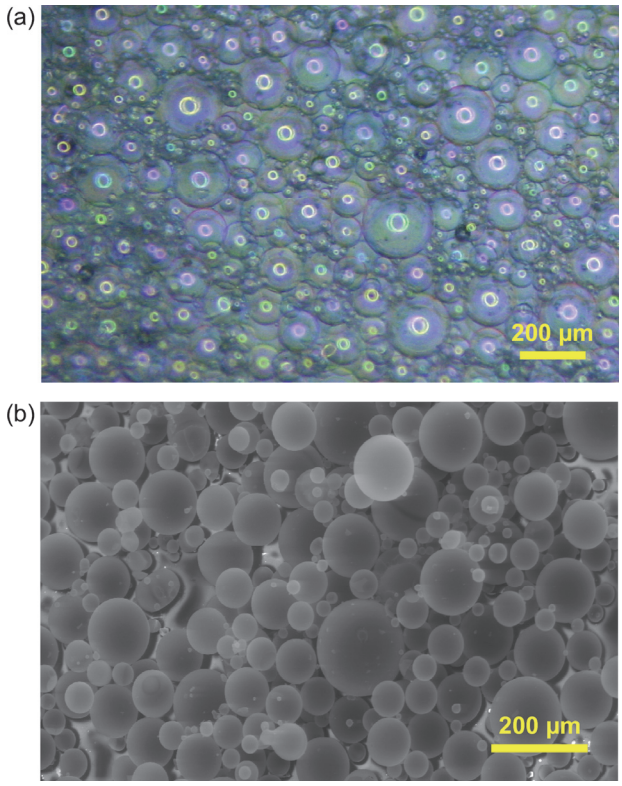

Figure 5.2: (a) Optical micrograph of the original cenospheres of various sizes. The shell thickness is 1–3 µm. (b) SEM micrograph of the cenospheres.

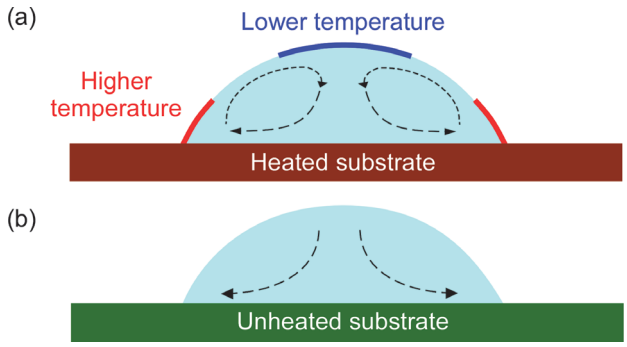

Figure 5.3: (a) Liquid flow patterns in an evaporating droplet on a heated substrate. A stable Marangoni flow forms in the droplet. (b) Liquid flow patterns in an evaporating droplet on an unheated substrate. Evaporation induced radial flow is the dominant flow.

5.2.2 Results

Sorting of these cenospheres according to size can be achieved by evaporating the microliter IPA droplet on a *heated* glass substrate. When the droplet mixture is placed on the heated substrate, the droplet edge is pinned, and the result is a consistent circular droplet shape with radius ranging from about 2 mm to 3 mm. The cenospheres are recirculated in the evaporating droplet by Marangoni flows shown in Figure 5.3(a). Observations reveal that the spheres are subducted by the powerful Marangoni flow, which appears to overcome the buoyancy force. As the liquid evaporates, the majority of the smaller spheres are brought to the edge of the droplet, while the larger spheres are dropped at the center. If the microliter droplet mixture consisting of IPA and cenospheres is evaporated on an *unheated* substrate, the droplet edge is not pinned; the liquid spreads on the substrate randomly, and because the IPA does not evaporate fast enough, the cenospheres float and move on the IPA surface in an arbitrary manner. The result is random deposition of the cenospheres on the substrate when all the liquid dries up, and no sorting is achieved.

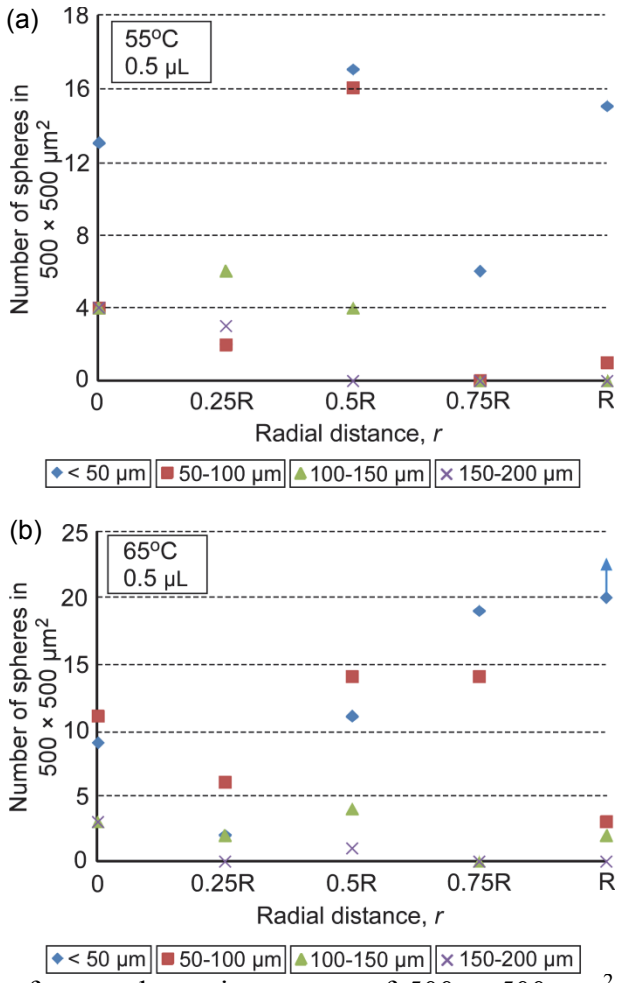

Figure 5.4: Number of cenospheres in an area of 500 × 500 µm^2 deposited along the radius from the center (r = 0) to the edge (r = R) of the circular droplet area when the temperature of the glass substrate is (a) 55°C, and (b) 65°C. The volume of the droplet used is 0.5 µL, and the droplet radius is about 2.5 mm.

The sorting results at different substrate temperatures are shown in Figures 5.4(a)-(d). In each experiment, 0.5 µL of the mixture is pipetted onto the substrate, and the substrate temperature ranges from 55°C to 85°C with increment of 10°C. The droplet radius is ≈2.5 mm. The number of deposited cenospheres on the substrate in a 500 × 500 µm^2 region from the center (radial distance, r = 0) to the edge (radial distance, r = R) of the circular deposited pattern is counted after all the liquid has evaporated. Figure 5.4(a) shows the distribution of the spheres when the substrate temperature is 55°C. Although

more of the larger spheres (150-200 μm) are near the center with the number declining toward the edge, the smaller-sized spheres with diameters <50 μm and 50-100 μm are found everywhere throughout the dried region at this substrate temperature. As the substrate temperature is increased, more spheres with diameter <50 μm are pushed toward the edge of the droplet as shown by Figures 5.4(b)-(c). It is apparent that there is a divergence in the number of spheres with diameter <50 μm and those with diameter 150-200 μm from the center to the edge in these two graphs. When the substrate temperature is 85°C, higher than the boiling point of IPA of 82.5°C, most of the spheres <50 μm are transported close to the edge. The majority of the spheres at the center are 150-200 μm. The result is shown in Figure 5.4(d). The number of 50-100 μm spheres is random with no fixed pattern along the radius of the droplet at any given substrate temperature, but the number of 100-150 μm spheres tends to peak at r = 0.5R when the substrate temperature is 65-85°C.

The experiment is repeated with a higher droplet volume of 8 μL, and it is shown that sorting also takes place. The substrate temperature is fixed at 85°C and the droplet radius is ≈3 mm. The result is shown in Figure 5.5. With a larger volume, more spheres are present in the droplet. It is apparent that the number of spheres <50 μm increases steadily from the center to the edge, while the number of the other spheres decline. The large spheres (100-150 μm) are concentrated at the center.

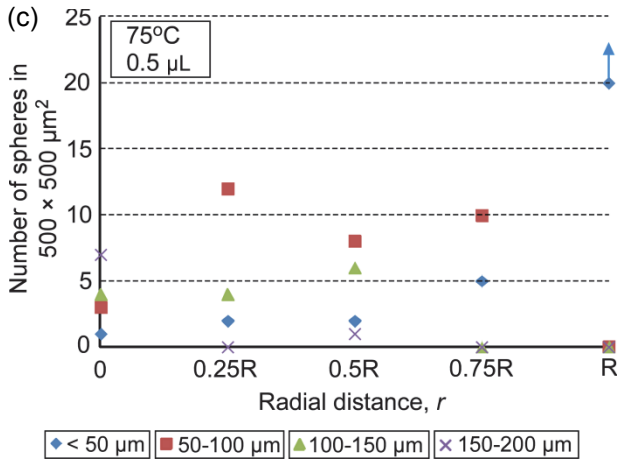

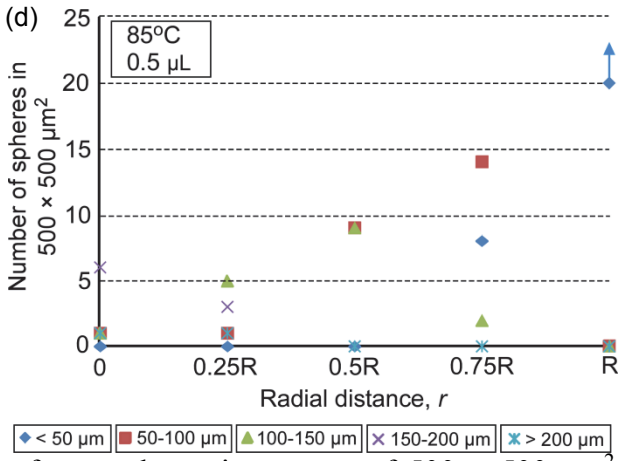

Figure 5.4: Number of cenospheres in an area of 500 × 500 µm^2 deposited along the radius from the center (r = 0) to the edge (r = R) of the circular droplet area when the temperature of the glass substrate is (c) 75°C, and (d) 85°C. The volume of the droplet used is 0.5 µL, and the droplet radius is about 2.5 mm.

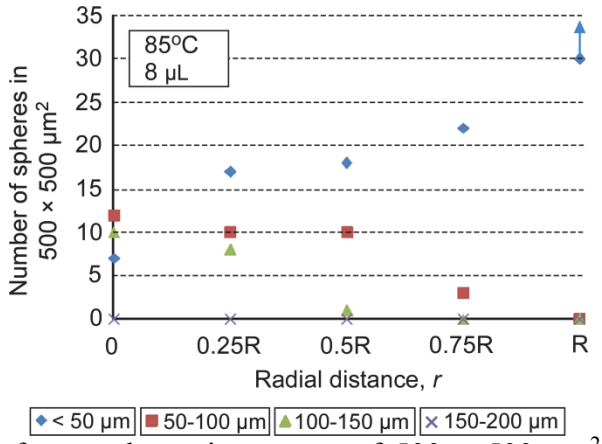

Figure 5.5: Number of cenospheres in an area of 500 × 500 µm^2 deposited along the radius from the center (r = 0) to the edge (r = R) of the circular droplet area when the droplet volume is 8 µL. The temperature of the glass substrate is 85°C.

Physical removal of the smaller spheres is possible by placing a perforated metal plate in contact with the glass substrate prior to the droplets. Figure 5.6 compares the sorting results obtained with and without the use of a perforated metal plate of thickness 25 μm. In each experiment, 5 μL of droplet is pipetted onto a glass substrate at 85°C. As evident in Figure 5.6(a), without the metal plate, the spheres with diameter <50 μm are deposited mainly around the droplet edge, and the larger ones >100 μm are located at the droplet center. With the use of a perforated metal plate having hole radius of ≈1 mm placed in contact with the glass substrate as shown in Figure 5.6(b), most of the spheres <50 μm are deposited on the metal plate. These smaller spheres are removed when the plate is lifted off the glass substrate, leaving the larger spheres on the glass substrate as shown in Figure 5.6(c).

5.3. Discussion and Conclusion

When a liquid droplet evaporates on a *heated* substrate, a temperature gradient develops along the surface of the droplet, resulting in a surface tension gradient. The thermocapillary shear stress, τ_s, is proportional to the temperature gradient, ∇T_s, according to equation (2.6) [Bas07, Hig00]. Marangoni flow develops inside the evaporating droplets [Gir06, Mar89, Rui02]; this flow plays an important role in positioning solid particles on substrates during drying [Hu06].

The higher the substrate temperature, the larger the surface tension gradient that is generated along the droplet surface and the more dominant the Marangoni flow becomes. This can be seen from equation (2.6) and the Marangoni number, which is directly proportional to the temperature gradient in the liquid. Modeling by COMSOL

Multiphysics 4.3 reveals that the highest liquid velocity in the droplet when the substrate temperature is 85°C, 75°C, 65°C and 55°C is 19 mm/s, 15 mm/s, 11 mm/s and 8 mm/s, respectively. Figure 5.7(a) shows the case when the substrate temperature is 85°C. In the proximity of the pinned perimeter (contact line) of the droplet on the substrate is a region of low surface tension, while the apex, which is at a lower temperature, is a region of high surface tension. The direction of the shear stress and liquid flow are from a region of low surface tension to that of high surface tension; therefore, the resultant surface tension gradient leads to a tangential flow upwards from the contact line toward the apex along the curvature of the droplet surface. The recirculating flow in the droplet is in the opposite direction: downward in the center of the droplet, and radially outward beneath the surface. This direction of the Marangoni flow in the droplet also holds true if the size of the heated substrate is larger than the droplet size as confirmed by simulation results [Gir08]. The flow direction inside the droplet is reversed when the substrate is cooled as shown in Figure 5.7(b). Mathematical modeling, numerical analysis and simulations of the evaporation of volatile liquids (such as IPA) on heated surfaces have been reported [And95, Aja05, Sod08]. Lubrication theory, Navier-Stokes and conservation of energy equations were used to perform these investigations. It was reported that the diameter of the droplet and the contact angle remain roughly constant, while the height of the droplet decreases during the initial stage of evaporation. Over time, the contact angle decreases and reaches a minimum value. The droplet diameter then decreases, and the rate of decrease in droplet height reduces.

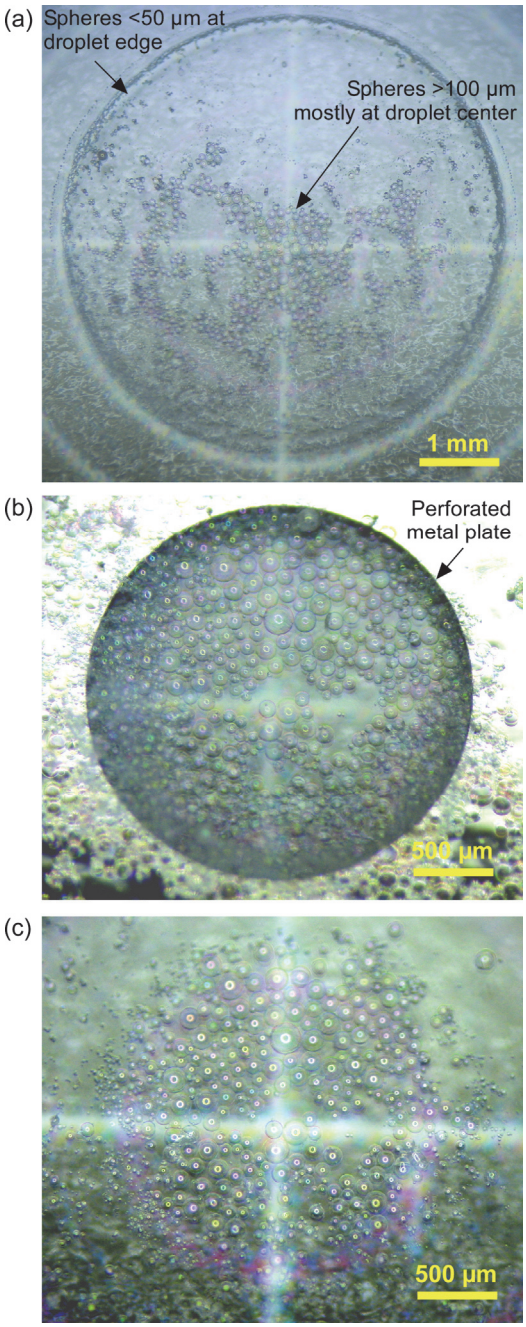

Figure 5.6: (a) Size sorting achieved by placing the droplet on a heated glass substrate without using a perforated metal plate. (b) Placing a droplet on a perforated metal plate in contact with the glass substrate. The radius of the hole is ≈1 mm. (c) Physical removal of most of the small spheres <50 µm by lifting off the perforated metal plate in (b). In each experiment, the droplet volume is 5 µL and the glass substrate temperature is 85°C.

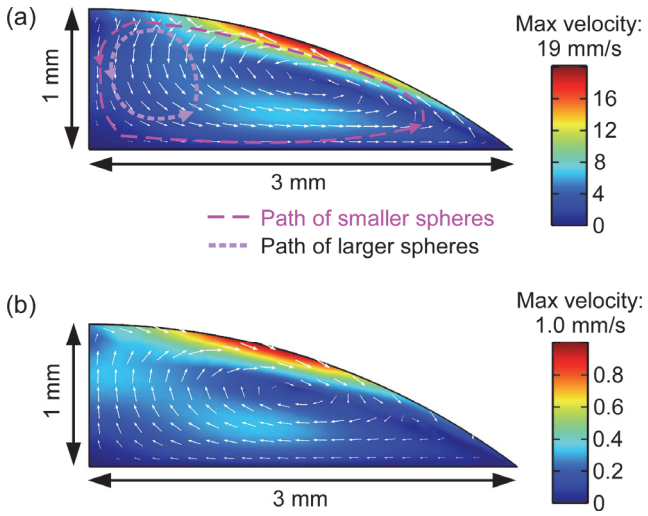

Figure 5.7: (a) Modeling result showing the flow velocities inside the liquid droplet. The substrate temperature is 85°C. The smaller spheres make larger circulation path than the larger spheres inside the droplet. (b) The flow direction is reversed when the substrate is cooled. Here, the substrate temperature is 2°C lower than the room temperature of 27°C.

When a droplet evaporates on an *unheated* substrate, the droplet contact line experiences a higher evaporation rate compared with the rest of the droplet surface. The induced Marangoni flow due to different evaporation rates at the surface is negligible in this case. A radial flow predominantly transports the liquid from the center of the droplet to the edge to replenish the lost liquid (Figure 5.3(b)). When cenospheres float on the droplet, they cannot be transported to the droplet edge. Instead, they float on the liquid surface until all the liquid has evaporated and these spheres subsequently land on the substrate in a random manner.

Better sorting is observed when the temperature of the substrate is above the boiling point of the liquid as evident from Figure 5.8. This could be attributed to the stronger Marangoni flows inside the droplet. It is observed experimentally that the spheres are transported at higher velocities when the substrate temperature is higher. The presence of Marangoni flows results in recirculation and transport of the floating spheres inside the droplet. The flow avoids the random deposition of the floating spheres on the

substrate when all the liquid dries up such as in the case of evaporation on an unheated substrate. The larger spheres experience larger buoyancy force, in the range of $10^{-8} – 10^{-7}$ N; they have greater tendencies to float to the liquid surface, and therefore make smaller circulation loops close to the droplet center as shown in Figure 5.7(a). The smaller spheres experience smaller buoyancy force, in the range of $10^{-12} – 10^{-10}$ N; they make larger circulating paths inside the droplet. The smaller spheres are transported to the pinned perimeter of the droplet mainly by the radially outward flows along the substrate, and the majority is then deposited at the droplet edge as the liquid evaporates. As the height and diameter of the liquid droplet decrease over time, the larger spheres are deposited closer to the center. These spheres remain attached to the substrate and can no longer be transported inside the droplet. At a lower substrate temperature, such as 55°C, the overall evaporation rate of the liquid is lower, and the retreat of the droplet perimeter at the later stage of evaporation, as well as the decrease in droplet height occurs at slower rates; the spheres are deposited in a more arbitrary pattern as the liquid dries up. Interactions between spheres, as well as between the spheres and the substrate during the last stages of evaporation may also determine the final segregation patterns.

Using a higher droplet volume involves the manipulation of even more spheres, and the droplet covers a larger area. However, separation achieved with 8 μL droplets is similar to that with 0.5 μL droplets. Although some <50 μm spheres are found at the center, the majority of the spheres at $r = 0$ are 50-100 μm and 100-150 μm in size. At the edge, only <50 μm spheres are present as the number of spheres larger than 50 μm drops from the center to the edge.

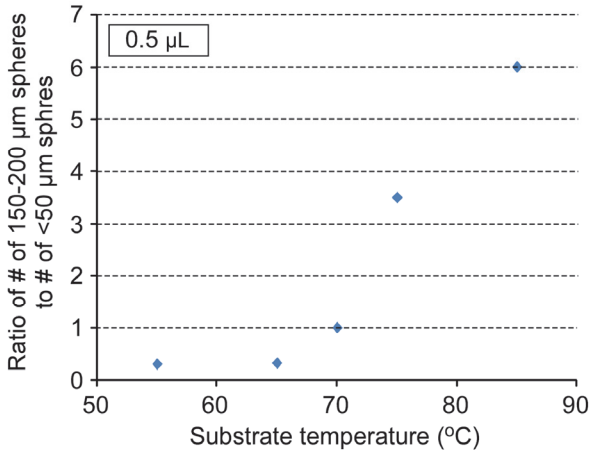

Figure 5.8: Relationship between the substrate temperature and the ratio of number of 150–200 µm spheres to number of <50 µm spheres at the center of the droplet. The droplet volume is 0.5 µL.

The use of a perforated metal plate above the substrate enables the removal of small spheres. The thickness and surface properties of the metal plate may influence the Marangoni flows in the liquid, and determine whether sorting occurs.

With several liquid droplets deposited on a heated substrate simultaneously, as shown in Figure 5.1, high throughput can be achieved through parallelism. In addition, a thin perforated metal plate of thickness in the 10-100 µm range, having holes with appropriate sizes at regular intervals, may be placed in contact with the glass substrate to achieve physical removal of the smaller spheres. This rapid and low-cost separation technique may be applicable to higher-density particles that are suspended in the liquid, as well as particles with sizes other than the 5-200 µm range. By optimizing the nature of the liquid, droplet volume, substrate temperature and evaporating environment, the technique may be extended to biological applications and medical assays. For example, it may be useful in cell sorting based on size or based on other properties that affect how a cell responds to Marangoni flows. The technique may also be useful in high-

throughput sorting of the constituents of blood, which is necessary for a number of medical assays.

The successful sorting and physical separation of larger cenospheres reveal the opportunity to utilize the mechanical resonance of such hollow spheres for sensor applications and signal transducers. The cenospheres used in this work are in the micrometer range, and they can potentially be used to reduce the size of current hemispherical resonant sensors, which are typically in the millimeter range. It is, therefore, necessary to first assess the potential utility of such spheres for the aforementioned uses. Chapter 6 presents the results of the wine glass mode resonance, quality factor and frequency mismatch of hemispherical shell resonators fabricated from the cenospheres using the focused ion beam milling technique.

CHAPTER 6

Investigation of wine glass mode resonance in 200-μm-diameter cenosphere-derived borosilicate hemispherical shells

Following the successful sorting of sodium borosilicate cenospheres according to size described in previous chapter, this chapter presents the study of mechanical resonant characteristics of miniature hollow hemispheres fabricated from these cenospheres. Cenospheres are lightweight, inert hollow spheres which are useful in a large number of applications, particularly as fillers. Potential use of these hollow hemispheres is as sensing elements in inertial sensors, biochemical detectors and other devices. The tested structures are approximately 200 μm, 150 μm and 1.8 μm in diameter, height and thickness, respectively, with the dome anchored and the rim free. The lowest order wine glass modes of these structures are experimentally determined (and confirmed by modeling) to be in the range of 300–600 kHz – in the range of those of planar micro-resonators that have been explored for sensing applications.

6.1. Introduction

Cenospheres are the lightweight, hollow spheres generated in coal-burning power plants as byproducts; these microspheres are the lighter particles in the fly ash. Once considered difficult waste, cenospheres were later discovered to possess excellent

material properties which render them highly suitable in a wide number of applications [Wan96]. In particular, they are used as lightweight fillers in building materials such as concrete [McB02, Bla00]. These microspheres possess high compressive strengths, and are used to replace rock and sand in concrete to produce high quality, low density concrete. When coated with metal such as copper, silver or gold, the hollow spheres become lightweight composites that can be used in manufacturing conductive polymer for electromagnetic interference shielding materials [Shu02]. Figure 6.1 shows the optical images of these three-dimensional microstructures. Because cenospheres are unwanted byproducts produced in huge quantities, they are relatively cheap and offer cost-effective alternatives to other kinds of fillers.

The mechanical resonance of cenospheres is interesting for potential use as sensing elements and signal transducers. Spherical and hemispherical structures, in particular, are attractive because of radial symmetry, and the mechanical, electrical and optical properties afforded by such shapes. One possible application of cenospheres is in inertial sensors. For instance, the centimeter-scale hemispherical shell gyroscope is used for inertial navigation [Roz09]. This bell-like structure can achieve high quality factor and thus long time constant, as well as extended device lifetime because it has no moving parts; its shape also makes it immune to external disturbances [Law98]. One of the future directions of the hemispherical resonator gyroscope is in size reduction of the gyroscopes. Cenospheres, which are largely in the micrometer range, can potentially be utilized to achieve this goal.

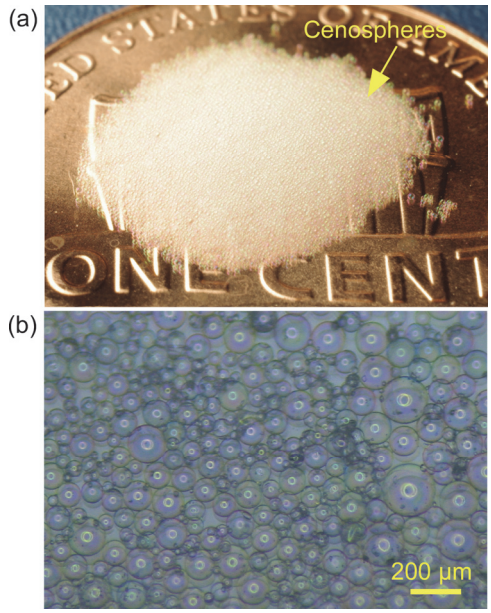

Figure 6.1: (a) Optical micrograph of cenospheres on a US penny. (b) High magnification optical image of cenospheres of varying sizes.

Another promising use of cenospheres is in dielectric resonator antennae. Dielectric resonators come in various shapes such as cylindrical, rectangular or hemispherical [Mon94, Pet10c]. Since Long *et al.* first proposed the hemispherical dielectric resonator antenna design in 1984 and showed that it is attractive due to the simple spherical interface between itself and free space allowing for exact theoretical solution to be obtained [McA84], significant effort has been directed to analyze and improve the design of the hemispherical antenna to achieve wider impedance bandwidth by introducing an air gap [Won93], simplify excitation methods by using a coaxial probe or a parasitic patch [Leu93, Leu05] and so on.

Additionally it is conceivable that cenospheres are suitable as optical detectors for biological and chemical species. Optical biosensors utilizing dielectric micro-spherical structures and optofluidic ring resonator structures have been demonstrated as highly sensitive in detecting label-free biomolecules through shifts in resonance wavelength and

free spectral range measurements, respectively [Vol02, Sch11]. Bio-chemical detectors also come in other forms, including micromachined quartz crystal microbalance array [Kao09], suspended microchannel resonators [God07] and film-bulk acoustic resonator [Xu11], all of which monitor the resonance frequency shifts as a result of biological or chemical specimen adsorption.

While there are many possible applications of cenospheres, it is necessary to proceed in a step-by-step manner, to assess their characteristics for various kinds of transducers. This chapter presents, as a first step, the assessment of the mechanical resonant characteristics of cenosphere-derived hemispheres [Hen13b]. There have been several reported efforts to fabricate spherical structures by methods such as wafer-scale glassblowing [Pri11, Zot12], ultrasonic machining [Vis11], and isotropic etching of silicon molds [Sor12, Cha12] for resonator applications, but their sizes are in the millimeter range. In contrast, cenospheres are about 200 μm or smaller. Although the technology for large-scale assembly and micromachining of cenospheres is not the subject of this investigation, a preliminary assessment can be made of the potential utility of cenospheres by using focused ion beam (FIB) milling to obtain a limited number of samples. Here, we evaluate sub-millimeter hemispherical shell resonators that are about 200 μm in diameter, 150 μm in height, and 1.8 μm in thickness and are made from sodium borosilicate cenospheres. In particular, the fundamental wine glass resonance mode is investigated while *the dome is anchored and the rim is free* (Figure 6.2). The symmetry of this vibration mode is attractive for sensing applications.

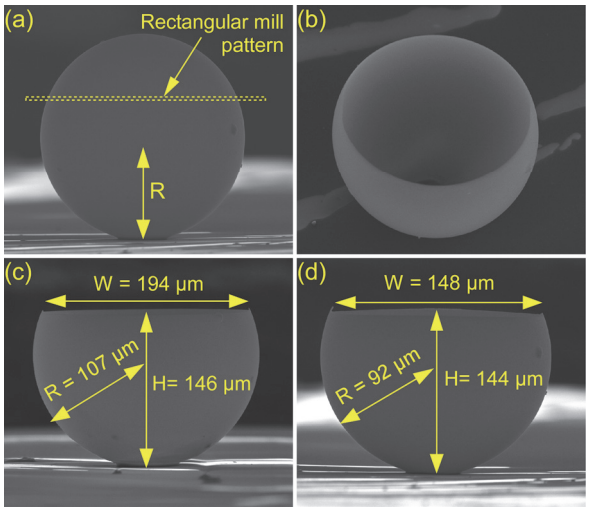

Figure 6.2: (a) SEM micrograph of the original cenosphere with radius R, showing the rectangular mill pattern during FIB milling process. (b) Perspective view of the fabricated micro-hemisphere. (c) Side view of device D214H146 with diameter D of 214 µm and height H of 146 µm. This micro-hemisphere is coated with 50 nm Au on the outer surface to improve optical reflectivity during measurement with the vibrometer. (d) Side view of device D184H144 having diameter D of 184 µm and height H of 144 µm. It is coated with 50 nm Pt on the outer surface.

6.2. Theoretical Analysis and Modeling

Theoretical and experimental analysis of the resonance frequencies of hemispherical shells have been studied extensively due to the advantages of vibrating hemispherical shells as high performance sensing elements [Fan91a, Fan91b, Hwa66, Cho11]. Based on Rayleigh's energy method, the natural frequency of the nth mode, f_n, of a perfect hemispherical shell in Hertz can be derived as [Ble79]:

$$f_n = \frac{\lambda_n}{2\pi(D/2)}\sqrt{\frac{E}{\rho}},\ n = 2, 3, 4 \ldots \tag{6.1}$$

$$\lambda_n^2 = \frac{(n^2-1)^2 n^2 h^2}{3(1+\nu)(D/2)^2}\frac{g_1(n,\phi_o)}{g_2(n,\phi_o)} \tag{6.2}$$

λ_n is a dimensionless parameter with $g_1(n,\phi_o)$ and $g_2(n,\phi_o)$ given by:

$$g_1(n,\phi_o) = \frac{1}{8}\left[\frac{(\tan(\phi_o/2))^{2n-2}}{n-1} + \frac{2(\tan(\phi_o/2))^{2n}}{n} + \frac{(\tan(\phi_o/2))^{2n+2}}{n+1}\right] \tag{6.3}$$

$$g_2(n,\phi_o)=\int_0^{\phi_o}(n^2+1+\sin^2\phi+2n\cos\phi)\cdot\sin\phi\cdot\tan^{2n}(\phi/2)d\phi \qquad (6.4)$$

In equations (6.1)-(6.4), n is the number of circumferential waves in the mode shape, E is the Young's Modulus of the shell material, ρ is the density of the shell material, and v is the Poisson's ratio of the material. E, ρ and v are assumed to be constant in a homogeneous shell. D is the diameter of the hemispherical shell, while h is the shell thickness, which is assumed to be constant. The term ϕ is the longitudinal angle measured from the pole based on the spherical coordinates shown in Figure 6.3(a), while θ is the circumferential angle. In this figure, z is the central axis and R is the radius of the hemispherical shell; the bottom angle, ϕ_F, is fixed, while the top angle, ϕ_o, is free. For a hemispherical shell, $\phi_o = \pi/2$ and $\tan(\phi_o/2) = 1$. Equation (6.2) becomes:

$$\lambda_n^2=\frac{1}{12(1+\nu)}\frac{h^2}{(D/2)^2}\frac{\left(n^3-n\right)\left(2n^2-1\right)}{g_2(n,\phi_o=\pi/2)},\ n=2,3,4\ldots \qquad (6.5)$$

To calculate the wine glass mode resonance frequency, n = 2 and $g_2(n, \phi_o = \pi/2)$ = 1.52961. From the equations, f_n increases when n increases, h increases, E increases, or D decreases.

Finite element analysis (COMSOL Multiphysics 4.2) is used to more precisely evaluate the wine glass mode resonance frequencies of two micro-hemispheres: D214H146 (hemisphere with diameter D = 214 μm and height H = 146 μm), and D184H144 (hemisphere with diameter D = 184 μm and height H = 144 μm). The shell is modeled as a composite layer consisting of the sodium borosilicate glass and metal layer, anchored at the bottom, with the rim free. The micro-hemispheres are assumed to have an ideal uniform shell thickness of 1.8 μm; the outer surface of device D214H146 is coated with a 50-nm-thick Au layer, while that of device D184H144 is coated with a 50-

nm-thick Pt layer. Eigenfrequency analysis reveals wine glass resonance frequencies of 331.5 kHz and 599.0 kHz for devices D214H146 and D184H144, respectively. The device parameters and material properties used in modeling are summarized in Table 6.1. These simulated frequency values are comparable to those obtained by theoretical calculations using equations (6.1)-(6.5). Figure 6.3(b) shows the actuated wine glass mode shape of a micro-hemisphere. The wine glass resonance frequencies of the micro-hemispheres are much smaller than those of the complete hollow spheres, which have frequencies above 20 MHz. Figure 6.4(a) shows, as a function of angle, the normalized difference in magnitude of the amplitude of the displacement in the fundamental wine glass mode. This is also representative of the maximum velocity of each point. The antinode corresponds to the highest amplitude displacement; the node corresponds to the lowest, but for the thin hemispherical shell, this is not necessarily a stationary point. The simulated results were obtained by modeling the frequency response in COMSOL.

Table 6.1: Device parameters and material properties used in modeling.

	Device D214H146	**Device D184H144**
Diameter of device (μm)	214	184
Height of device (μm)	146	144
Shell thickness (μm)	1.8	
Material of device	Sodium borosilicate glass	
Young's Modulus (GPa)	72.4	
Density (kg/m^3)	140	
Metal coating	Au	Pt
Young's Modulus of metal (GPa)	79	168
Density of metal (kg/m^3)	19300	21450
Metal thickness (nm)	50	
Simulated wine glass mode resonance frequency (kHz)	331.5	599.0

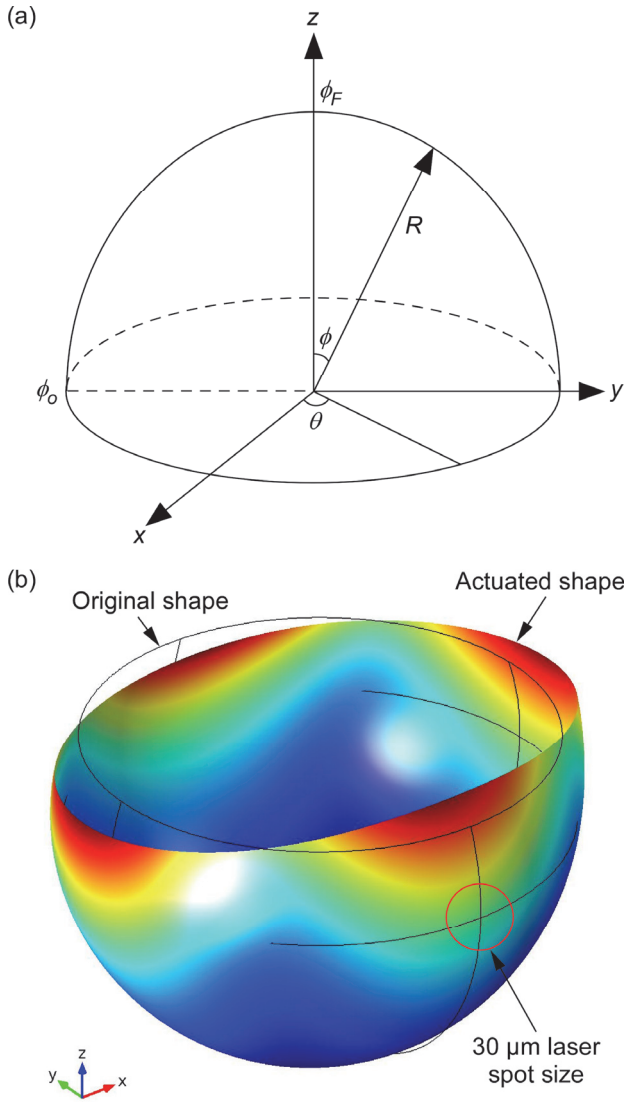

Figure 6.3: (a) Coordinate system and hemispherical shell model. (b) Original shape and actuated shape of the wine glass resonance mode shape of a micro-hemisphere as obtained by COMSOL Multiphysics 4.2. Simulations show that the wine glass resonance frequency of micro-hemisphere D214H146 is 331.5 kHz, while that of D184H144 is 599.0 kHz. Laser spot size of ≈30 μm from the vibrometer is also drawn.

6.3. Device Structure and Fabrication

The glass hemispheres are fabricated from sodium borosilicate cenospheres that are available commercially (Q-CEL 6014, Potters Industries LLC, Valley Forge, PA). They are made by heating solid glass particles [Goe93]; the gases within the glass act as blowing agents to expand the glass particles. The density of these glass spheres is

approximately 0.1–2.0 g/cm^3, and the sizes range from 5 μm to 200 μm. Microspheres of the desired sizes are obtained by filtering; antistatic solution (Amstat Industries Inc, Glenview, IL) is used to mitigate the static charge and permit filtration and subsequent attachment to a silicon substrate.

The micro-hemispheres are formed by FIB milling (Quanta 200 3D FIB, FEI, Hillsboro, OR). Figure 6.2 shows the fabrication steps of how the hemispheres are made starting with the original cenosphere in Figure 6.2(a). Prior to milling, the sample is brought to the eucentric position and tilted at 52° in the SEM/FIB chamber. A narrow rectangular mill pattern of height 400 nm is created as shown to cut the top of the sphere. The ion beam voltage and current are optimized during milling, and set at 10 kV and 26 nA, respectively, in order to successfully remove the top of the spheres without breaking the rest of the spheres. Figure 6.2(b) shows the perspective view of the final structure formed from the cenosphere in Figure 6.2(a). Figure 6.2(c) shows the side profile of device D214H146, having a diameter of 214 μm and height of 146 μm, while Figure 6.2(d) shows that of device D184H144 with a diameter of 184 μm and height of 144 μm. To improve the laser reflectivity for experimental observations, the outer surfaces of the micro-hemispheres are coated with a thin layer of metal. Device D214H146 is coated with 3 nm Ti / 50 nm Au, while device D184H144 is coated with 3 nm Ti / 50 nm Pt.

6.4. Experimental Evaluation

The silicon carrier substrates with the micro-hemispheres are attached to the surfaces of 5 × 5 × 2 mm^3 PZT stack actuators (Physik Instrumente GmbH & Co., Karlsruhe, Germany) using adhesive polymer. The PZT stack, in turn, is attached onto a

vertical rotary stage (Thorlabs, Newton, NJ) which is mounted on a high precision XY stage (Thorlabs, Newton, NJ). This measurement setup allows the micro-hemispheres to be centered at the axis of rotation of the rotary stage, and rotated for the measurement of the vibration velocities along the circumference of the micro-hemispheres to verify the wine glass resonance mode shape. The vibration velocities are measured by a laser vibrometer (OFV3001S, Polytec, Irvine, CA). The smallest spot size of the laser is 30 μm. As illustrated in Figure 6.3(b), this can provide substantial averaging over the surface that is only 200 μm in diameter. The PZT and micro-hemispheres are actuated by a network analyzer (HP4395A, Hewlett-Packard Company, Palo Alto, CA) through a power amplifier. The network analyzer sweeps the frequency supplied to the PZT, and receives the output from the laser vibrometer. All measurements are performed in air at atmospheric pressure.

The normalized measured velocities of device D214H146 at 332.5 kHz are plotted at every 10° rotational angle through a total rotation of 90° as shown in Figure 6.4(a). This confirms that 332.5 kHz is the wine glass mode resonance frequency. Figure 6.4(b) shows the plot of the wine glass mode resonance peak at rotation angle of 40°. Similarly, experimental evaluation of device D184H144 reveals that the wine glass resonance frequency is at 590 kHz (Figure 6.5). The normalized vibration velocities at 590 kHz are fitted to the function $|A_i \sin(2(\theta + \theta_i))|$ as represented by the (red) dashed line. The (blue) dashed line representing the response at 580 kHz is not fitted; it is drawn 45° apart from the fit at 590 kHz. The amplitude of this curve is the maximum normalized vibration velocity achieved at 580 kHz. The response at 580 kHz represents a structural non-ideality. The experimentally measured frequency mismatch, $\Delta f/f$, is 1.7% for device

D184H144. In air, the wine glass mode of micro-hemispheres D214H146 and D184H144 have measured quality factors of 130 and 105, respectively.

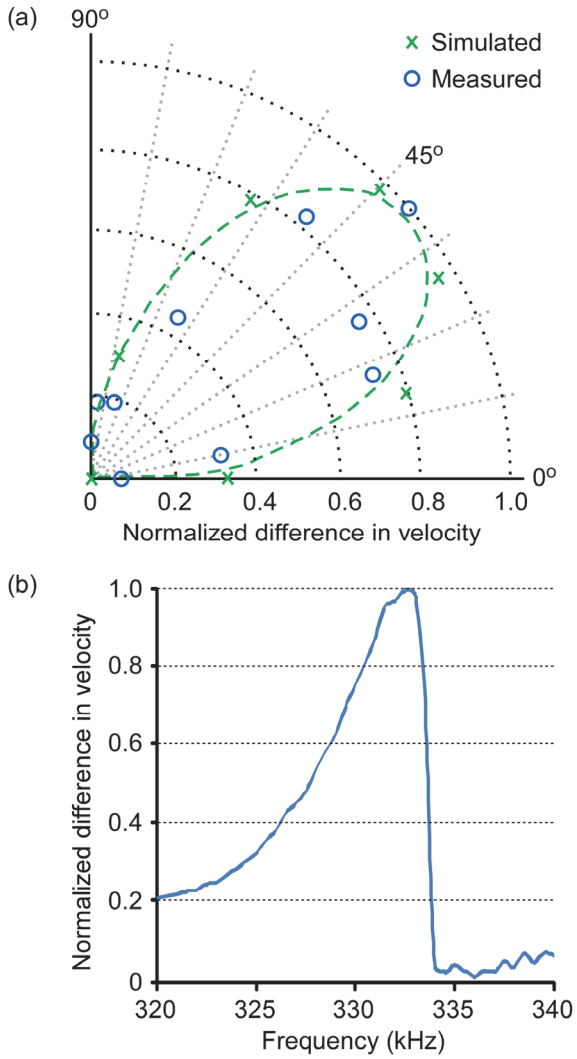

Figure 6.4: (a) Normalized variation in simulated amplitude and measured velocity in the fundamental wine glass resonance mode of device D214H146 at 332.5 kHz. The dashed line is a fit of simulated points to the function $|A_i \sin(2(\theta + \theta_i))|$. (b) Experimentally-obtained plot of the wine glass mode resonance peak measured at rotation angle of 40°. The measurements are performed in air at atmospheric pressure.

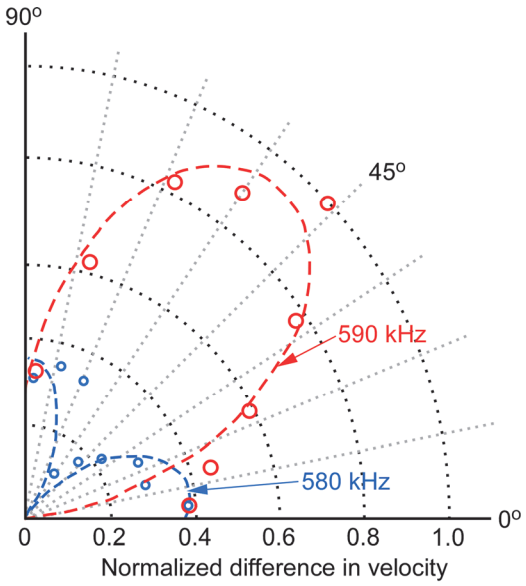

Figure 6.5: Experimentally measured response of micro-hemisphere D184H144 in wine glass mode at 590 kHz. The (red) dashed line is fitted to the data using function $|A_i \sin(2(\theta + \theta_i))|$. The response at 580 kHz represents a structural non-ideality.

6.5. Discussion and Conclusions

Cenosphere-derived borosilicate hemispherical shell resonators have characteristics that are well within the range of those for reported planar resonant sensors, and hence may be utilized in microsystems. The experimentally obtained resonance frequencies as well as normalized velocities match well with those obtained by simulations. The frequency mismatch of the resonators can be partly attributed to such non-idealities of the micro-hemispheres as non-uniformities in the shell thickness, structural asymmetry etc. This mismatch can be reduced by optimizing the ion beam voltage and current of the FIB in order to control the milling rate during the fabrication process, and ensure better device symmetry. The FIB milling technique is a micro-fabrication technique that is effective for making or modifying shell-type resonators. In this effort, the typical milling time was about 40 minutes per device. In the long term,

micromachining techniques such as plasma etching and laser cutting, together with assembly and integration methods, may offer higher throughput and parallelism.

Spheres made of materials with intrinsically higher quality factor such as fused silica and ultra low expansion glass can be utilized to produce devices with higher quality factor. The laser spot size of the vibrometer is undesirably large for the micro-hemispheres. This artifact is likely to be a source of velocity averaging that reduces the measured quality factor.

The attachment of spheres to the substrate by adhesive polymer may be a source of stress or damping, partly because this bonding method results in relatively large bonding surface areas. Alternatives such as frit glass may offer superior performance.

Finally, it is notable that spherical and hemispherical structures derived from cenospheres may also be useful as microsystems components that do not require mechanical resonance. These include, for example, radiofrequency antennae [Kis02], optical detectors [Vol02, Sch11], etc.

CHAPTER 7

Conclusions and future work

This chapter summarizes the contributions of the research efforts described in previous chapters, and recommends the directions of future work.

7.1. Major Contributions to the Field

Focusing on the questions raised in Chapter 1, this work has demonstrated the applications of Marangoni convection in actuating solid phase objects of a wide range of dimensions as well as of different geometries and densities. It is possible to localize sedimentations of suspension particles at desired locations on blank substrates, actuate millimeter-sized objects to make complete rotations, and sort spherical particles with a continuous distribution of diameters according to their sizes. The liquid used is only a few millimeters or less in depth; this facilitates the formation of high temperature gradients at the liquid surface, resulting in surface tension gradients which are the origins of Marangoni flows in the liquid. Thermocapillary flows can be generated by heating the liquid from above using millimeter-sized heaters. Alternatively, they can also be formed by heating the liquid from below as in the case of the Bénard experiment and evaporation of liquid droplets.

By creating localized temperature elevation at the liquid/air interface using millimeter-sized heaters suspended at close proximities above the liquid, Marangoni flows are generated in a liquid 1 mm deep; these flows can be used to direct the sedimentations of Φ = 25 μm suspension particles on a blank substrate. This is a contactless technique; there is no physical contact between the suspended heaters and the liquid surface. The main advantages are that contamination of liquid samples is avoided, and the reuse of the thermal elements for other applications is possible, reducing fabrication costs. The heat source employed in this work is a 16 × 8 heater array. Sedimentations of suspension particles occur directly below the active heater, and it is shown that the accumulations can be obtained at any desired locations on the blank substrate by simply activating any particular heater. The amount of accumulations can also be controlled by the activation of different numbers of heaters. Different liquids used also yield different sedimentation patterns.

As a first attempt, it has been shown in this work that thermocapillary flows may be utilized to actuate millimeter-sized object completely submerged in liquid. The same heater array is used to generate a spatially-defined temperature gradient at the liquid surface. By activating four heaters continuously in a particular configuration, a stainless steel rotary structure of diameter ≈4 mm mounted on a hub and completely submerged in silicone oil makes complete rotations. The speed of rotation depends on such factors as temperature gradient and viscosity of the liquid. The experimental results of this work are consistent with the modeling results in terms of the direction of rotation, as well as the varying torque experienced by the blades causing the structure to accelerate and decelerate as it makes a complete rotation.

To generate Marangoni flows in a liquid, the liquid may also be subjected to a heat source from below. When a liquid droplet evaporates on an unheated substrate, evaporation-induced radial flow is dominant due to the higher evaporation rates at the droplet edge. A stable Marangoni flow forms in an evaporating droplet when the substrate is heated. Depending on the type of particles, Marangoni flows may have to be suppressed to sort the particles of varying diameters according to size. For particles which have densities lower than the liquid, the presence of Marangoni flows is necessary for sorting. Cenospheres, a by-product of coal-burning power plants, float on most liquids, and they are once considered difficult waste. Today cenospheres are used as lightweight fillers in building materials, and also conducting fillers for electromagnetic interference shielding materials. Certainly new utilities of this by-product would help reduce disposal issues and environmental problems. Cenospheres are typically present in a continuous spectrum from 5 μm to 200 μm, and sorting them according to size on a large scale may be necessary for a variety of applications. This enables the different sizes to be compartmentalized, so that various uses can be systematically investigated for different size of cenospheres. The sorting of such hollow spheres using Marangoni flows is explored in this work. The cenospheres are mixed in IPA prior to sorting, and microliter droplets of such mixtures are deposited on the heated substrate. The result is larger spheres (100–150 μm) deposited at the center and smaller spheres (<50 μm) at the periphery of the droplet footprint. This enables the physical separation of large and small particles by the use of perforated metal plates. Cenospheres with sizes of ≈200 μm sorted by Marangoni flows in evaporating liquid droplets are physically isolated and the FIB is

used to form micro-hemispheres. The fundamental wine glass resonance mode of these structures is investigated, and methods to improve their performance are stated.

7.2. Suggested Future Work

Marangoni effect is a surface phenomenon that plays a vital role in microfluidics systems for biological, chemical and industrial applications. Further studies, theoretical and experimental, would enable better understanding of the physics in the micrometer scale and below, and lead to improvement of microfluidic systems designs as well as the discoveries of new applications.

One possible utility of Marangoni flows is in sorting blood samples for components that have characteristic sizes or flow behavior. Biomedical imaging, using techniques that involve ultrasound, non-ionizing electromagnetic radiation and X-ray among others, is currently widely used for early detection of various types of cancer [Fas08]. The trend is shifting to cancer detection when the tumor size is still small and highly localized in the body, and microfluidic technologies are attractive because very small sample volumes are needed, and processing times are relatively short. The use and development of microfluidic devices for cancer detection is relatively new, and intense research in the next few years is expected to ensue. Many fluidic techniques have been proposed for cancer cell detection, sorting and capture [Che12] – each with its own advantages and disadvantages. It is envisioned that multi-stage microfluidic devices can be designed and fabricated, integrating the different techniques to achieve optimum output and result for cell detection, sorting, capture and post-capture processing. Marangoni effect may play a pivotal role in this aspect. For example circulating tumor

cells (CTCs) are very rare, and it is challenging to isolate and characterize these cells. Marangoni flows may be used in sorting of CTCs since these cells are larger than other cells in blood. Micro-heaters are integrated in the microfluidic systems, for either contact or contactless operation, to achieve size-based sorting and separation. The size of the device channels and chambers are in the micrometer range, so Marangoni flows can be induced even at small temperature elevations. This prevents damage to cells sensitive to temperature rise. It is important to note that other than raising temperature, cooling also results in surface tension gradient and hence Marangoni forces [Bas07, Bas08b]. To increase the concentration of CTCs for post-sorting characterization, the sedimentation technique using Marangoni convection can be applied. At a later stage, the CTCs can be channeled to different compartments if necessary by either virtual channels created by different shapes of heat sources (parallel, annular and/or ring heat sources), or channel filtering for further processing and testing.

Monitoring the types of contaminants in water, soil and air is important in order to gain deeper understanding of the state of the environment so that necessary steps can be taken to mitigate risks to human health and the ecosystem. Microfluidic devices show great potential to feed the need for rapid, cost effective, portable and *in situ* systems in obtaining information about the environment. Tremendous progress has been made in the area of bio-sensors and analytical techniques for environmental monitoring [Rog06]. It has been shown that a wide range of airborne and waterborne bio-elements can be identified, but the detection and analysis of soil components by microfluidic devices remains a challenging problem [Mar05]. A research effort targeting the utility of

Marangoni convection in separating the complex components of soil materials for post-treatment and analysis is worthwhile.

It is difficult to mix various fluids in microfluidic systems due to the laminar nature of the liquid flows [Whi06]. The rotation of a microstructure by Marangoni convection can be used to mix samples and induce chemical reactions in microchambers, a necessary process in chemical and biological analyses. The mixing performance is measured by the mixing efficiency, which has to be enhanced because it determines the throughput of the microfluidic devices. The design of the rotary structure described in Chapter 4 can be improved so that rotation with higher angular velocities can be achieved. Instead of using microheaters, laser can be used to rotate the structure. There are many advantages of using laser as a heat source. Firstly, microheaters do not have to be fabricated, thus reducing costs. Secondly, the setup is also more versatile because lasers can be easily controlled to follow the blades of the structure as it makes rotations, hence the structure does not decelerate. Lastly, unnecessary joule heating is circumvented.

Since its observation and identification in the 19th Century, Marangoni effect has enticed many researchers to study the phenomenon and determine how it can be utilized or suppressed in industrial applications to achieve specific outcomes. As this phenomenon becomes dominant at small length scales, Marangoni effect cannot be neglected and it may play a significant role in microfluidic systems for various applications. The Marangoni technique presents a low-cost method for fluidic manipulations without the need to fabricate complex fluidic substrates, and can potentially complement and be integrated with other fluidic manipulation techniques in microfluidic systems for environmental monitoring, bioanalysis, clinical applications etc.

Possibilities are boundless when the different areas of nanotechnology, microfluidics and analytical systems are incorporated to produce Micro Total Analysis Systems (μTAS) or Lab-on-a-chip (LOC).

APPENDIX A

Boundary conditions to simulate thermocapillary actuation of rotary structures

This appendix contains the full details of the boundary conditions of the simulation work performed for the research effort described in Chapter 4. A 3D modeling is performed using COMSOL Multiphysics® 4.3. Four modules are utilized to perform this simulation: *Laminar Flow*, *Solid Mechanics*, *Heat Transfer in Fluids* and *Heat Transfer in Solids*. A quadrant of the setup is created as shown in Figure A1, with one blade and blade arm immersed in the liquid. The height of the liquid above the blade arm is 200 μm.

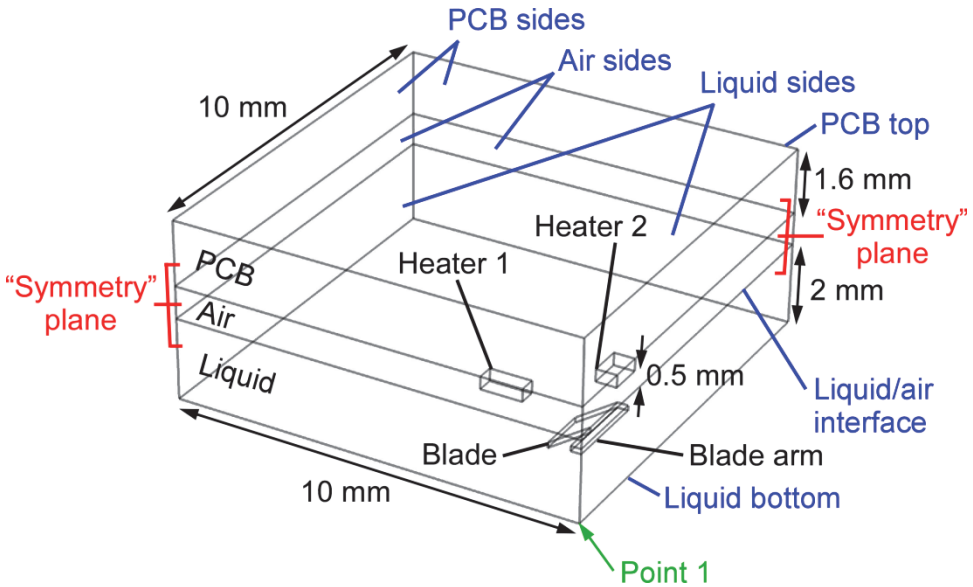

Figure A1: A quadrant of the setup is created to perform the simulation using COMSOL Multiphysics® 4.3.

Simulation result shows that when the liquid surface is subjected to heat sources suspended at close proximity, Marangoni flows are generated inside the liquid layer. The conditions set for the four modules are described below.

Module 1: LAMINAR FLOW (For liquid layer)

- The sides of the liquid, bottom of the liquid and the surfaces of the blade have "Wall" and "No slip" boundary conditions.
- The surface of the liquid in contact with air (liquid/air interface) has a "Wall" and "Slip" boundary condition. Equation (2.6) is imposed on the liquid surface using a *weak contribution* with the following *weak expression*: "test(u)*(gamma*Tx) + test(v)*(gamma*Ty)".
- The symmetry faces of the liquid have "Symmetry" boundaries. The entire blade and blade arm are within the liquid layer, and none of the blade surface has a "Symmetry" boundary.
- The pressure point constant is set to be zero at point 1.

Module 2: SOLID MECHANICS (For blade)

- The blade is "Free" to move.

Module 3: HEAT TRANSFER IN FLUIDS (For heat transfer in liquid)

- This module takes into account conduction and convection.
- The bottom and sides of the liquid are at room temperature of 300 K.
- The symmetry faces of the liquid are set as "Symmetry".

- The liquid/air surface is assigned the "Open boundary" condition (This is a boundary condition for modeling heat flux across an open boundary. The heat can flow out of the domain or into the domain).
- The blade surfaces are set as "Thermal insulation" (This is the default setting in COMSOL. It models a well insulated boundary with no heat flux across the boundary: $-\mathbf{n}\cdot(-k\nabla T)=0$).

Module 4: HEAT TRANSFER IN SOLIDS (For heat transfer in air, blade and PCB)

- This module takes into account conduction only.
- Air is treated like a solid because the air layer is thin, and heat transfer in air is assumed to be by conduction only. This simplifies the modeling as well.
- The symmetry faces of the air, heaters and PCB are set as "Symmetry".
- The heater surfaces facing the liquid are set as 446.5 K.
- The sides of the air and PCB, as well as top surface of PCB are set as 300 K.
- The liquid/air interface is set as "Open boundary".
- The blade surfaces are set as "Thermal insulation".

APPENDIX B

EDM code for machining rotary structures

This appendix contains the EDM code for machining the rotary structures for the effort described in Chapter 4, as well as releasing the structures.

- **Machining the rotary structure:**

```
'    MG-ED72 TEST PROGRAM
'       ( USMTOOL.BAS )
'
'      FOR MAKING FAN DESIGN 4
'      1 MAR 2011
'      USM tool with 0.300 mm dia
'
DECLARE SUB KAKO ()
DECLARE SUB OPUT (MCODE AS STRING)

DIM SHARED E AS STRING
DIM SHARED YPOS AS STRING
DIM SHARED ANSCODE AS STRING

'MAIN
        CLS
        ON ERROR GOTO PEND
        OPEN "COM1: 2400,N,8,1,ASC,LF" FOR RANDOM AS #1

        CALL KAKO

PEND:

        CALL OPUT("BUZ 2")
        CLOSE #1
        SYSTEM
        END

SUB KAKO

        CALL OPUT("BACK X 1")
        CALL OPUT("BACK Y 1")
```

```
        CALL OPUT("FSF X 12000")
        CALL OPUT("FSF Y 12000")
        CALL OPUT("FSF Z 200")
        CALL OPUT("SPN 0")

        CALL OPUT("FSM Z 10")
        CALL OPUT("VOL 2 80")
        CALL OPUT("CON 3")
        CALL OPUT("VOL 0")

        CALL OPUT("POS X")
        XORG = VAL(MID$(ANSCODE, 2))
        CALL OPUT("POS Y")
        YORG = VAL(MID$(ANSCODE, 2))


        D = 100/10
        D1 = 1100/11
        D2 = 1000/10
        D3 = 2500/25


hole1a:
'D2
        CALL OPUT("VOL 2 110")
        CALL OPUT("CON 1")
        X1 = XORG + 27000
        Y1 = YORG + 3000
                        CALL OPUT("ABS X" + STR$(X1))
                        CALL OPUT("ABS Y" + STR$(Y1))
                        CALL OPUT("MAC" + STR$(D2))

        CALL OPUT("INC Z -2000")

hole2a:
'SmoothenHole
        CALL OPUT("VOL 2 80")
        CALL OPUT("CON 3")
        X1 = XORG + 27000
        Y1 = YORG + 3000
                        CALL OPUT("ABS X" + STR$(X1))
                        CALL OPUT("ABS Y" + STR$(Y1))
                        CALL OPUT("MAC" + STR$(D))

        CALL OPUT("INC Z -2000")

'INPUT "CAUTION: RELEASING - ENTER  'Y' TO CONTINUE?"; E
        'IF E = "N" THEN GOTO JEND:

'Thinning
SLOT3a1:
'D1
        CALL OPUT("VOL 2 110")
        CALL OPUT("CON 1")

        X1 = XORG + 5000
```

```
        Y1 = YORG + 7500
                        CALL OPUT("ABS X" + STR$(X1))
                        CALL OPUT("ABS Y" + STR$(Y1))
                        CALL OPUT("MCV X 5000 5000" + STR$(D1))
        CALL OPUT("INC Z -2000")

SLOT3a2:
'D1
        CALL OPUT("VOL 2 110")
        CALL OPUT("CON 1")

        X1 = XORG + 15000
        Y1 = YORG + 7500
                        CALL OPUT("ABS X" + STR$(X1))
                        CALL OPUT("ABS Y" + STR$(Y1))
                        CALL OPUT("MCV X 5000 5000" + STR$(D1))
        CALL OPUT("INC Z -2000")

SLOT3b1:
'D1
        CALL OPUT("VOL 2 110")
        CALL OPUT("CON 1")

        X1 = XORG + 22500
        Y1 = YORG - 9000
                        CALL OPUT("ABS X" + STR$(X1))
                        CALL OPUT("ABS Y" + STR$(Y1))
                        CALL OPUT("MCV Y 5000 5000" + STR$(D1))
        CALL OPUT("INC Z -2000")

SLOT3b2:
'D1
        CALL OPUT("VOL 2 110")
        CALL OPUT("CON 1")

        X1 = XORG + 22500
        Y1 = YORG - 19000
                        CALL OPUT("ABS X" + STR$(X1))
                        CALL OPUT("ABS Y" + STR$(Y1))
                        CALL OPUT("MCV Y 5000 5000" + STR$(D1))
        CALL OPUT("INC Z -2000")

SLOT3c1:
'D1
        CALL OPUT("VOL 2 110")
        CALL OPUT("CON 1")

        X1 = XORG + 39000
        Y1 = YORG - 1500
                        CALL OPUT("ABS X" + STR$(X1))
                        CALL OPUT("ABS Y" + STR$(Y1))
                        CALL OPUT("MCV X 5000 5000" + STR$(D1))
        CALL OPUT("INC Z -2000")

SLOT3c2:
'D1
```

```
        CALL OPUT("VOL 2 110")
        CALL OPUT("CON 1")

        X1 = XORG + 49000
        Y1 = YORG - 1500
                        CALL OPUT("ABS X" + STR$(X1))
                        CALL OPUT("ABS Y" + STR$(Y1))
                        CALL OPUT("MCV X 5000 5000" + STR$(D1))
        CALL OPUT("INC Z -2000")

SLOT3d1:
'D1
        CALL OPUT("VOL 2 110")
        CALL OPUT("CON 1")

        X1 = XORG + 31500
        Y1 = YORG + 25000
                        CALL OPUT("ABS X" + STR$(X1))
                        CALL OPUT("ABS Y" + STR$(Y1))
                        CALL OPUT("MCV Y 5000 5000" + STR$(D1))
        CALL OPUT("INC Z -2000")

SLOT3d2:
'D1
        CALL OPUT("VOL 2 110")
        CALL OPUT("CON 1")

        X1 = XORG + 31500
        Y1 = YORG + 15000
                        CALL OPUT("ABS X" + STR$(X1))
                        CALL OPUT("ABS Y" + STR$(Y1))
                        CALL OPUT("MCV Y 5000 5000" + STR$(D1))
        CALL OPUT("INC Z -2000")

INPUT "CAUTION: RELEASING - ENTER  'Y' TO CONTINUE?"; E
        IF E = "N" THEN GOTO JEND:

'Cutting edges of fan
SLOT2a:
'D3
        CALL OPUT("VOL 2 110")
        CALL OPUT("CON 1")

        X1 = XORG - 1500
        Y1 = YORG + 4500
                        CALL OPUT("ABS X" + STR$(X1))
                        CALL OPUT("ABS Y" + STR$(Y1))
                        CALL OPUT("MCV Y 4500 5000" + STR$(D3))
        CALL OPUT("INC Z -2000")

SLOT2b1:
'D3
        CALL OPUT("VOL 2 110")
        CALL OPUT("CON 1")

        X1 = XORG + 6000
```

```
        Y1 = YORG - 1500
                        CALL OPUT("ABS X" + STR$(X1))
                        CALL OPUT("ABS Y" + STR$(Y1))
                        CALL OPUT("MCV X 6000 6000" + STR$(D3))
        CALL OPUT("INC Z -2000")

SLOT2b2:
'D3
        CALL OPUT("VOL 2 110")
        CALL OPUT("CON 1")

        X1 = XORG + 18000
        Y1 = YORG - 1500
                        CALL OPUT("ABS X" + STR$(X1))
                        CALL OPUT("ABS Y" + STR$(Y1))
                        CALL OPUT("MCV X 4500 6000" + STR$(D3))
        CALL OPUT("INC Z -2000")

SLOT2c:
'D3
        CALL OPUT("VOL 2 110")
        CALL OPUT("CON 1")

        X1 = XORG + 18000
        Y1 = YORG - 2500
                        CALL OPUT("ABS X" + STR$(X1))
                        CALL OPUT("ABS Y" + STR$(Y1))
                        CALL OPUT("MCV X 4500 7000" + STR$(D3))
        CALL OPUT("INC Z -2000")

SLOT2d1:
'D3
        CALL OPUT("VOL 2 110")
        CALL OPUT("CON 1")

        X1 = XORG + 9500
        Y1 = YORG - 9000
                        CALL OPUT("ABS X" + STR$(X1))
                        CALL OPUT("ABS Y" + STR$(Y1))
                        CALL OPUT("MCV Y 5000 5000" + STR$(D3))
        CALL OPUT("INC Z -2000")

SLOT2d2:
'D3
        CALL OPUT("VOL 2 110")
        CALL OPUT("CON 1")

        X1 = XORG + 9500
        Y1 = YORG - 19000
                        CALL OPUT("ABS X" + STR$(X1))
                        CALL OPUT("ABS Y" + STR$(Y1))
                        CALL OPUT("MCV Y 5000 5000" + STR$(D3))
        CALL OPUT("INC Z -2000")


SLOT2e:
```

```
'D3
        CALL OPUT("VOL 2 110")
        CALL OPUT("CON 1")

        X1 = XORG + 15000
        Y1 = YORG - 25500
                        CALL OPUT("ABS X" + STR$(X1))
                        CALL OPUT("ABS Y" + STR$(Y1))
                        CALL OPUT("MCV X 5000 3000" + STR$(D3))
        CALL OPUT("INC Z -2000")


SLOT2f:
'D3
        CALL OPUT("VOL 2 110")
        CALL OPUT("CON 1")

        X1 = XORG + 25000
        Y1 = YORG - 25500
                        CALL OPUT("ABS X" + STR$(X1))
                        CALL OPUT("ABS Y" + STR$(Y1))
                        CALL OPUT("MCV X 5000 5000" + STR$(D3))
        CALL OPUT("INC Z -2000")

SLOT2g1:
'D3
        CALL OPUT("VOL 2 110")
        CALL OPUT("CON 1")

        X1 = XORG + 31500
        Y1 = YORG - 18000
                        CALL OPUT("ABS X" + STR$(X1))
                        CALL OPUT("ABS Y" + STR$(Y1))
                        CALL OPUT("MCV Y 6000 6000" + STR$(D3))
        CALL OPUT("INC Z -2000")

SLOT2g2:
'D3
        CALL OPUT("VOL 2 110")
        CALL OPUT("CON 1")

        X1 = XORG + 31500
        Y1 = YORG - 6000
                        CALL OPUT("ABS X" + STR$(X1))
                        CALL OPUT("ABS Y" + STR$(Y1))
                        CALL OPUT("MCV Y 4500 6000" + STR$(D3))
        CALL OPUT("INC Z -2000")

SLOT2h:
'D3
        CALL OPUT("VOL 2 110")
        CALL OPUT("CON 1")

        X1 = XORG + 32500
        Y1 = YORG - 6500
                        CALL OPUT("ABS X" + STR$(X1))
```

```
                        CALL OPUT("ABS Y" + STR$(Y1))
                        CALL OPUT("MCV Y 5000 6500" + STR$(D3))
        CALL OPUT("INC Z -2000")

SLOT2i1:
'D3
        CALL OPUT("VOL 2 110")
        CALL OPUT("CON 1")

        X1 = XORG + 39000
        Y1 = YORG - 14500
                        CALL OPUT("ABS X" + STR$(X1))
                        CALL OPUT("ABS Y" + STR$(Y1))
                        CALL OPUT("MCV X 5000 5000" + STR$(D3))
        CALL OPUT("INC Z -2000")

SLOT2i2:
'D3
        CALL OPUT("VOL 2 110")
        CALL OPUT("CON 1")

        X1 = XORG + 49000
        Y1 = YORG - 14500
                        CALL OPUT("ABS X" + STR$(X1))
                        CALL OPUT("ABS Y" + STR$(Y1))
                        CALL OPUT("MCV X 3000 5000" + STR$(D3))
        CALL OPUT("INC Z -2000")

SLOT2j:
'D3
        CALL OPUT("VOL 2 110")
        CALL OPUT("CON 1")

        X1 = XORG + 55500
        Y1 = YORG - 8000
                        CALL OPUT("ABS X" + STR$(X1))
                        CALL OPUT("ABS Y" + STR$(Y1))
                        CALL OPUT("MCV Y 5000 5000" + STR$(D3))
        CALL OPUT("INC Z -2000")

SLOT2k:
'D3
        CALL OPUT("VOL 2 110")
        CALL OPUT("CON 1")

        X1 = XORG + 55500
        Y1 = YORG + 1000
                        CALL OPUT("ABS X" + STR$(X1))
                        CALL OPUT("ABS Y" + STR$(Y1))
                        CALL OPUT("MCV Y 5000 4000" + STR$(D3))
        CALL OPUT("INC Z -2000")

SLOT2l1:
'D3
        CALL OPUT("VOL 2 110")
        CALL OPUT("CON 1")
```

```
        X1 = XORG + 48000
        Y1 = YORG + 7500
                        CALL OPUT("ABS X" + STR$(X1))
                        CALL OPUT("ABS Y" + STR$(Y1))
                        CALL OPUT("MCV X 6000 6000" + STR$(D3))
        CALL OPUT("INC Z -2000")


SLOT2l2:
'D3
        CALL OPUT("VOL 2 110")
        CALL OPUT("CON 1")

        X1 = XORG + 36000
        Y1 = YORG + 7500
                        CALL OPUT("ABS X" + STR$(X1))
                        CALL OPUT("ABS Y" + STR$(Y1))
                        CALL OPUT("MCV X 6000 4500" + STR$(D3))
        CALL OPUT("INC Z -2000")


SLOT2m:
'D3
        CALL OPUT("VOL 2 110")
        CALL OPUT("CON 1")

        X1 = XORG + 37000
        Y1 = YORG + 8500
                        CALL OPUT("ABS X" + STR$(X1))
                        CALL OPUT("ABS Y" + STR$(Y1))
                        CALL OPUT("MCV X 6000 5500" + STR$(D3))
        CALL OPUT("INC Z -2000")

SLOT2n1:
'D3
        CALL OPUT("VOL 2 110")
        CALL OPUT("CON 1")

        X1 = XORG + 44500
        Y1 = YORG + 15000
                        CALL OPUT("ABS X" + STR$(X1))
                        CALL OPUT("ABS Y" + STR$(Y1))
                        CALL OPUT("MCV Y 5000 5000" + STR$(D3))
        CALL OPUT("INC Z -2000")

SLOT2n2:
'D3
        CALL OPUT("VOL 2 110")
        CALL OPUT("CON 1")

        X1 = XORG + 44500
        Y1 = YORG + 25000
                        CALL OPUT("ABS X" + STR$(X1))
                        CALL OPUT("ABS Y" + STR$(Y1))
                        CALL OPUT("MCV Y 5000 5000" + STR$(D3))
```

```
        CALL OPUT("INC Z -2000")

SLOT2o:
'D3
        CALL OPUT("VOL 2 110")
        CALL OPUT("CON 1")

        X1 = XORG + 38000
        Y1 = YORG + 31500
                        CALL OPUT("ABS X" + STR$(X1))
                        CALL OPUT("ABS Y" + STR$(Y1))
                        CALL OPUT("MCV X 3000 5000" + STR$(D3))
        CALL OPUT("INC Z -2000")

SLOT2p:
'D3
        CALL OPUT("VOL 2 110")
        CALL OPUT("CON 1")

        X1 = XORG + 29000
        Y1 = YORG + 31500
                        CALL OPUT("ABS X" + STR$(X1))
                        CALL OPUT("ABS Y" + STR$(Y1))
                        CALL OPUT("MCV X 4000 5000" + STR$(D3))
        CALL OPUT("INC Z -2000")

SLOT2q1:
'D3
        CALL OPUT("VOL 2 110")
        CALL OPUT("CON 1")

        X1 = XORG + 22500
        Y1 = YORG + 24000
                        CALL OPUT("ABS X" + STR$(X1))
                        CALL OPUT("ABS Y" + STR$(Y1))
                        CALL OPUT("MCV Y 6000 6000" + STR$(D3))
        CALL OPUT("INC Z -2000")

SLOT2q2:
'D3
        CALL OPUT("VOL 2 110")
        CALL OPUT("CON 1")

        X1 = XORG + 22500
        Y1 = YORG + 12000
                        CALL OPUT("ABS X" + STR$(X1))
                        CALL OPUT("ABS Y" + STR$(Y1))
                        CALL OPUT("MCV Y 6000 4500" + STR$(D3))
        CALL OPUT("INC Z -2000")

SLOT2r:
'D3
        CALL OPUT("VOL 2 110")
        CALL OPUT("CON 1")

        X1 = XORG + 21500
```

```
        Y1 = YORG + 13000
                        CALL OPUT("ABS X" + STR$(X1))
                        CALL OPUT("ABS Y" + STR$(Y1))
                        CALL OPUT("MCV Y 6000 5500" + STR$(D3))
        CALL OPUT("INC Z -2000")

SLOT2s1:
'D3
        CALL OPUT("VOL 2 110")
        CALL OPUT("CON 1")

        X1 = XORG + 15000
        Y1 = YORG + 20500
                        CALL OPUT("ABS X" + STR$(X1))
                        CALL OPUT("ABS Y" + STR$(Y1))
                        CALL OPUT("MCV X 5000 5000" + STR$(D3))
        CALL OPUT("INC Z -2000")

SLOT2s2:
'D3
        CALL OPUT("VOL 2 110")
        CALL OPUT("CON 1")

        X1 = XORG + 5000
        Y1 = YORG + 20500
                        CALL OPUT("ABS X" + STR$(X1))
                        CALL OPUT("ABS Y" + STR$(Y1))
                        CALL OPUT("MCV X 5000 5000" + STR$(D3))
        CALL OPUT("INC Z -2000")

SLOT2t:
'D3
        CALL OPUT("VOL 2 110")
        CALL OPUT("CON 1")

        X1 = XORG - 1500
        Y1 = YORG + 13000
                        CALL OPUT("ABS X" + STR$(X1))
                        CALL OPUT("ABS Y" + STR$(Y1))
                        CALL OPUT("MCV Y 4000 4000" + STR$(D3))
        CALL OPUT("INC Z -2000")


        CALL OPUT("SPN 1")
INPUT "WARNING: moving to origin - REMOVE THE MAGNET/OBSTACLES"; E
        IF E = "N" THEN GOTO JEND:
     CALL OPUT("SPN 0")


JEND:
        CALL OPUT("SPN 0")
        CALL OPUT("ABS X" + STR$(XORG))
        CALL OPUT("ABS Y" + STR$(YORG))
        CALL OPUT("INC Z -2000")

        CALL OPUT("SPN 1")
```

```
END SUB

SUB OPUT (MCODE AS STRING)

        a = 0
AGIN:
        PRINT MCODE
        PRINT #1, MCODE
        INPUT #1, ANSCODE
        PRINT ANSCODE
        a = a + 1
        IF a = 5 THEN
                ERROR 200
        END IF
        IF MID$(ANSCODE, 1, 1) <> "N" THEN
                GOTO AGIN:
        END IF
END SUB
```

- **Releasing the rotary structure:**

```
SUB MACHINING

        CALL OPUT("BACK X 1")
        CALL OPUT("BACK Y 1")
        CALL OPUT("FSF X 15000")
        CALL OPUT("FSF Y 15000")
        CALL OPUT("FSF Z 200")
        CALL OPUT("SPN 0")
        CALL OPUT("VOL 2 110")
        CALL OPUT("CON 1")
        CALL OPUT("VOL 0")

        CALL OPUT("POS X")
        XPOS = MID$(ANSCODE, 2)
        XORG = VAL(MID$(ANSCODE, 2))
        CALL OPUT("POS Y")
        YORG = VAL(MID$(ANSCODE, 2))

' *****300um Diameter Tool*****

' VERT *********************************

'       CALL OPUT("FSF Z 200")

'       CALL OPUT("FSM Z 3")
'       CALL OPUT("MCV Y 5000 5000 450")

' HORIZ ********************************

'       CALL OPUT ("FSF Z 200")

'       CALL OPUT("FSM Z 3")
'       CALL OPUT("MCV X 4500 4500 500")
```

```
' DRILL ********************************

topleft:
        X1 = XORG - 1500
        Y1 = YORG + 18500

        CALL OPUT("FSF Z 10000")
        CALL OPUT("INC Z -50000")

                CALL OPUT("ABS X" + STR$(X1))
                CALL OPUT("ABS Y" + STR$(Y1))
                CALL OPUT("INC Z 50000")

                CALL OPUT("FSF Z 200")

                CALL OPUT("FSM Z 10")
                CALL OPUT("MAC 1400")

        CALL OPUT("INC Z -2000")
        CALL OPUT("FSF Z 10000")
        CALL OPUT("INC Z -50000")

topright:
        X1 = XORG + 43000
        Y1 = YORG + 31500

                CALL OPUT("ABS X" + STR$(X1))
                CALL OPUT("ABS Y" + STR$(Y1))
                CALL OPUT("INC Z 50000")

                CALL OPUT("FSF Z 200")

                CALL OPUT("FSM Z 10")
                CALL OPUT("MAC 1400")

        CALL OPUT("INC Z -2000")
        CALL OPUT("FSF Z 10000")
        CALL OPUT("INC Z -50000")

btmleft:
        X1 = XORG + 11000
        Y1 = YORG - 25500

                CALL OPUT("ABS X" + STR$(X1))
                CALL OPUT("ABS Y" + STR$(Y1))
                CALL OPUT("INC Z 50000")

                CALL OPUT("FSF Z 200")

                CALL OPUT("FSM Z 10")
                CALL OPUT("MAC 1400")

        CALL OPUT("INC Z -2000")
        CALL OPUT("FSF Z 10000")
        CALL OPUT("INC Z -50000")
```

```
btmright:
        X1 = XORG + 54000
        Y1 = YORG - 14500

                CALL OPUT("ABS X" + STR$(X1))
                CALL OPUT("ABS Y" + STR$(Y1))
                CALL OPUT("INC Z 50000")

                CALL OPUT("FSF Z 200")

                CALL OPUT("FSM Z 10")
                CALL OPUT("MAC 1400")

        CALL OPUT("INC Z -2000")
        CALL OPUT("FSF Z 10000")
        CALL OPUT("INC Z -50000")

'*****************************************************
'STORAGE
'       CALL OPUT("SPN 1")
'INPUT "ELECTRODE OK?"; E
'IF E = "N" THEN GOTO JEND:
'       CALL OPUT("SPN 0")
'
'
'       CALL OPUT("FSF Z 25000")
'       CALL OPUT("INC Z -250000")
'       CALL OPUT("SPN 1")
'INPUT "NEXT IS HOLE CUT FOR PINCHING. ELECTRODE OK?"; E
'IF E = "N" THEN GOTO JEND:
'       CALL OPUT("SPN 0")
'       CALL OPUT("INC Z 250000")
'       CALL OPUT("FSF Z 200")
'*****************************************************
```

REFERENCES

[3M01] Product information on Fluorinert™ Electronic Fluid FC-3283, 3M Specialty Materials, St. Paul, MN, 2001.

[Ahn98] S.H. Ahn, Y.K. Kim, "Fabrication and experiment of a planar micro ion drag pump," *Sensors and Actuators A (Physical)*, vol. 70, no. 1-2, pp. 1-5, Oct. 1998.

[Aja05] V.S. Ajaev, "Spreading of thin volatile liquid droplets on uniformly heated surfaces," *Journal of Fluid Mechanics*, vol. 528, pp. 279-296, Apr. 2005.

[Ald10] Product information on P9770 – Weed pollens from *Kochia Scoparia* (firebush), Sigma-Aldrich, St. Louis, MO, 2010.

[And89] J.L. Anderson, "Colloid transport by interfacial forces," *Annual Review of Fluid Mechanics*, vol. 21, pp. 61-99, 1989.

[And95] D.M. Anderson, S.H. Davis, "The spreading of volatile liquid droplets on heated surfaces," *Physics of Fluids*, vol. 7, no. 2, pp. 248-265, Feb. 1995.

[Aub05] A. D'Aubeterre, R. Da Silva, M.E. Aguilera, "Experimental study on Marangoni effect induced by heat and mass transfer," *International Communications in Heat and Mass Transfer*, vol. 32, no. 5, pp. 677-684, Apr. 2005.

[Bar07a] C.N. Baroud, M.R. de Saint Vincent, J.-P. Delville, "An optical toolbox for total control of droplet microfluidics," *Lab on a Chip*, vol. 7, no. 8, pp. 1029-1033, Aug. 2007.

[Bar07b] C.N. Baroud, J.-P. Delville, F. Gallaire, R. Wunenburger, "Thermocapillary valve for droplet production and sorting," *Physical Review E*, vol. 75, no. 4, pp. 046302-1-5, Apr. 2007.

[Bas07] A.S. Basu, Y.B. Gianchandani, "Shaping high-speed Marangoni flow in liquid films by microscale perturbations in surface temperature," *Applied Physics Letters*, vol. 90, no. 3, pp. 034102-1-3, Jan. 2007.

[Bas08a] A.S. Basu, Y.B. Gianchandani, "Virtual microfluidic traps, filters, channels and pumps using Marangoni flows," *Journal of Micromechanics and Microengineering*, vol. 18, no. 11, pp. 115031 (11 pages), Nov. 2008.

[Bas08b] A.S. Basu, *Microthermal devices for fluidic actuation by modulation of surface tension,* Ph.D dissertation, Department of Electrical Engineering and Computer Science, University of Michigan, Ann Arbor, MI, 2008.

[Bas09] A.S. Basu, Y.B. Gianchandani, "A programmable array for contact-free manipulation of floating droplets on featureless substrates by the modulation of surface tension," *Journal of Microelectromechanical Systems*, vol. 18, no. 6, pp. 1163-1172, Dec. 2009.

[Ben00] H. Bénard, "Les tourbillons cellulaires dans une nappe liquid," *Revue Gén. Sci. Pure Appl*, 11, pp. 1261-1271, 1309-1328, 1900.

[Ber08] J. Berthier, *Microdrops and digital microfluidics*, New York: William Andrew Inc., 2008, pp. 138.

[Ber65] J.C. Berg, A. Acrivos, "The effect of surface active agents on convection cells induced by surface tension," *Chemical Engineering Science*, vol. 20, no. 8, pp. 737-745, Aug. 1965.

[Bha09] R. Bhardwaj, X. Fang, D. Attinger, "Pattern formation during the evaporation of a colloidal nanoliter drop: A numerical and experimental study," *New Journal of Physics*, vol. 11, no. 7, pp. 075020 (33 pages), Jul. 2009.

[Big06] T.P. Bigioni, X.-M. Lin, T.T Nguyen, E.I. Corwin, T.A. Witten, H.M. Jaeger, "Kinetically driven self assembly of highly ordered nanoparticle monolayers," *Nature Materials*, vol. 5, no. 4, pp. 265-270, Apr. 2006.

[Bla00] F. Blanco, P. Garcia, P. Mateos, J. Ayala, "Characteristics and properties of lightweight concrete manufactured with cenospheres," *Cement and Concrete Research*, vol. 30, no. 11, pp. 1715-1722, Nov. 2000.

[Ble79] R.D. Blevins, *Formulas for natural frequency and mode shape*, New York: Van Nostrand Reinhold Company Inc., 1979, pp. 291-336.

[Blo56] M.J. Block, "Surface tension as the cause of Bénard cells and surface deformation in a liquid film," *Nature*, 178, pp. 650-651, Sep. 1956.

[Bru08] H. Bruus, *Theoretical microfluidics*, New York: Oxford University Press Inc., 2008, pp. 1-18.

[Cha06] Y.-H. Chang, G.-B. Lee, F.-C. Huang, Y.-Y. Chen, J.-L. Lin, "Integrated polymerase chain reaction chips utilizing digital microfluidics," *Biomedical Microdevices*, vol. 8, no. 3, pp. 215-225, Sep. 2006.

[Cha12] M. L. Chan, P. Fonda, C. Reyes, J. Xie, H. Najar, L. Lin, K. Yamazaki, D. A. Horsley, "Micromachining 3D hemispherical features in silicon via micro-EDM," *IEEE 25th International Conference on Micro Electro Mechanical Systems (MEMS 2012)*, Paris, France, Jan. 29 – Feb. 2, 2012, pp. 289-292.

[Che02] C.-H. Chen, J.G. Santiago, "A planar electroosmotic micropump," *Journal of Microelectromechanical Systems*, vol. 11, no. 6, pp. 672-683, Dec. 2002.

[Che12] J. Chen, J. Li, Y. Sun, "Microfluidic approaches for cancer cell detection, characterization, and separation," *Lab on a Chip*, vol. 12, no. 10, pp. 1753-1767, Feb. 2012.

[Cho11] S.-Y. Choi, J.-H. Kim, "Natural frequency split estimation for inextensional vibration of imperfect hemispherical shell," *Journal of Sound and Vibration*, vol. 330, no. 9, pp. 2094-2106, Apr. 2011.

[Chu79] C.-H. Chun, W. Wuest, "Experiments on the transition from the steady to the oscillatory Marangoni-convection of a floating zone under reduced gravity effect," *Acta Astronautica*, vol. 6, pp. 1073-1082, Jan. 1979.

[Chu80] C.-H. Chun, "Marangoni convection in a floating zone under reduced gravity," *Journal of Crystal Growth*, vol. 48, no. 4, pp. 600-610, Apr. 1980.

[Chu81] C.-H. Chun, W. Wuest, "Suppression of temperature oscillations of thermal Marangoni convection in a floating zone by superimposing of rotating flows," *Acta Astronautica*, vol. 9, no. 4, pp. 225-230, Apr. 1981.

[Com11] *Marangoni Convection*, COMSOL Inc, Burlington, MA, 2011, pp. 1-14.

[Dar03a] A.A. Darhuber, J.P. Valentino, J.M. Davis, S.M. Troian, S. Wagner, "Microfluidic actuation by modulation of surface stresses," *Applied Physics Letters*, vol. 82, no. 4, pp. 657-659, Jan. 2003.

[Dar03b] A.A. Darhuber, J.P. Valentino, S.M. Troian, S. Wagner, "Thermocapillary actuation of droplets on chemically patterned surfaces by programmable microheater arrays," *Journal of Microelectromechanical Systems*, vol. 12, no. 6, pp. 873-879, Dec. 2003.

[Dar05] A.A. Darhuber, S.M. Troian, "Principles of microfluidics actuation by modulation of surface stresses," *Annual Review of Fluid Mechanics*, vol. 37, pp. 425-455, Jan. 2005.

[Dar10] A.A. Darhuber, J.P. Valentino, S.M. Troian, "Planar digital nanoliter dispensing system based on thermocapillary actuation," *Lab on a Chip*, vol. 10, no. 8, pp. 1061-1071, Apr. 2010.

[Dee00a] R.D. Deegan, "Pattern formation in drying drops," *Physical Review E*, vol. 61, no. 1, pp. 475-485, Jan. 2000.

[Dee00b] R.D. Deegan, O. Bakajin, T.F. Dupont, G. Huber, S.R. Nagel, T.A. Witten, "Contact line deposits in an evaporating drop," *Physical Review E*, vol. 62, no. 1, pp. 756-765, Jul. 2000.

[Dee97] R.D. Deegan, O. Bakajin, T.F. Dupont, G. Huber, S.R. Nagel, T.A. Witten, "Capillary flow as the cause of ring stains from dried liquid drops," *Nature*, vol. 389, no. 6653, pp. 827-829, Oct. 1997.

[Dhu11] R.K. Dhull, L. Fuller, P.-C. Kao, Y.-C. Liao, Y.-W. Lu, "Two degree-of-freedom micromirror actuation using thermocapillary effect in liquid droplets," *Sensors and Actuators A: Physical*, vol. 168, no. 1, pp. 162-167, Jul. 2011.

[Dow98a] Product information on Dow Corning 702, 704, 705 fluids, Dow Corning Corporation, Midland, MI, 1998.

[Dow98b] Product information on Dow Corning 550 fluid, Dow Corning Corporation, Midland, MI, 1998.

[Duh04] S. Duhr, S. Arduini, D. Braun, "Thermophoresis of DNA determined by microfluidic fluorescence," *European Physical Journal E*, vol. 15, no. 3, pp. 277-286, Nov. 2004.

[Duh05] S. Duhr, D. Braun, "Two-dimensional colloidal crystals formed by thermophoresis and convection," *Applied Physics Letters*, vol. 86, no. 13, pp. 131921-1-3, Mar. 2005.

[Eot86] R. Eötvös, "Ueber den Zusammenhang der Oberflächenspannung der Flüssigkeiten mit ihrem Molecularvolumen," *Annalen der Physik*, vol. 263, no. 3, pp. 448-459, 1886.

[Eye85] A. Eyer, H. Leiste, R. Nitsche, "Floating zone growth of silicon under microgravity in a sounding rocket," *Journal of Crystal Growth*, vol. 71, no. 1, pp. 173-182, Jan.-Feb. 1985.

[Fan04] F. Fan, K.J. Stebe, "Assembly of colloidal particles by evaporation on surfaces with patterned hydrophobicity," *Langmuir*, vol. 20, no. 8, pp. 3062-3067, Apr. 2004.

[Fan91a] S.-C. Fan, G.-Y. Liu, Z.-J. Wang, "On flexural vibration of hemispherical shell," *Applied Mathematics and Mechanics*, vol. 12, no. 10, pp. 1023-1030, Oct. 1991.

[Fan91b] S.-C. Fan, G.-Y. Liu, Z.-J. Wang, "On vibration of hemispherical shell by using finite element method," *Applied Mathematics and Mechanics*, vol. 12, no. 12, pp. 1169-1175, Dec. 1991.

[Far04] R.H. Farahi, A. Passian, T.L. Ferrell, T. Thundat, "Microfluidic manipulation via Marangoni forces," *Applied Physics Letters*, vol. 85, no. 18, pp. 4237-4239, Nov. 2004.

[Far06] R.H. Farahi, A. Passian, S. Zahrai, A.L. Lereu, T.L. Ferrell, T. Thundat, "Microscale Marangoni actuation: All-optical and all-electrical method," *Ultramicroscopy*, vol. 106, no. 8-9, pp. 815-821, Jun.-Jul. 2006.

[Fas08] L. Fass, "Imaging and cancer: A review," *Molecular Oncology*, vol. 2, no. 2, pp. 115-152, May 2008.

[Fis02] B.J. Fischer, "Particle convection in an evaporating colloidal droplet," *Langmuir*, vol. 18, no. 1, pp. 60-67, Jan. 2002.

[Gas02] P.R.C. Gascoyne, J. Vykoukal, "Particle separation by dielectrophoresis," *Electrophoresis*, vol. 23, no. 13, pp. 1973-83, Jul. 2002.

[Gio95] F. Di-Giovanni, P.G. Kevan, M.E. Nasr, "The variability in settling velocities of some pollen and spores," *Grana*, vol. 34, no. 1, pp. 39-44, 1995.

[Gir06] F. Girard, M. Antoni, S. Faure, A. Steinchen, "Evaporation and Marangoni driven convection in small heated water droplets," *Langmuir,* vol. 22, no. 26, pp. 11085-11091, Dec. 2006.

[Gir08] F. Girard, M. Antoni, "Influence of substrate heating on the evaporation dynamics of pinned water droplets," *Langmuir*, vol. 24, no. 20, pp. 11342-11345, Oct. 2008.

[God07] M. Godin, A. K. Bryan, T. P. Burg, K. Babcock, S. R. Manalis, "Measuring the mass, density, and size of particles and cells using a suspended microchannel resonator," *Applied Physics Letters*, vol. 91, no. 12, pp. 123121-1-3, Sep. 2007.

[Goe93] K. E. Goetz, J. A. Hagarman, J. P. Giovene, "Hollow glass spheres," U.S. Patent 5,217,928, Jun. 8, 1993.

[Gug45] E.A. Guggenheim, "The principle of corresponding states," *Journal of Chemical Physics*, vol. 13, no. 7, pp. 253-261, Jul. 1945.

[Han11] W. Han, M. Byun, Z. Lin, "Assembling and positioning latex nanoparticles via controlled evaporative self-assembly," *Journal of Materials Chemistry*, vol. 21, no. 42, pp. 16968-16972, Nov. 2011.

[Han12] W. Han, Z. Lin, "Learning from 'coffee rings': Ordered structures enabled by controlled evaporative self-assembly," *Angewandte Chemie International Edition*, vol. 51, no. 7, pp. 1534-1546, Feb. 2012.

[Hen10] E. Hendarto, Y.B. Gianchandani, "Directed precipitation of suspension particles onto blank substrates using Marangoni cells," in *the 14th International Conference on Miniaturized Systems for Chemistry and Life Sciences (MicroTAS 2010),* Groningen, The Netherlands, Oct. 2010, pp. 1100-1102.

[Hen11a] E. Hendarto, Y.B. Gianchandani, "A non-contact method for spatially localized sedimentation of particles from liquid suspensions using Marangoni forces," *Journal of Micromechanics and Microengineering*, vol. 21, no. 11, pp. 115028 (7 pages), Nov. 2011.

[Hen11b] E. Hendarto, Y.B. Gianchandani, "Marangoni-driven micromotor in liquid medium," in *16th International Conference on Solid-State Sensors, Actuators and Microsystems (Transducers 2011)*, Beijing, China, Jun. 2011, pp. 246-249.

[Hen13a] E. Hendarto, Y.B. Gianchandani, "Thermocapillary actuation of millimeter-scale rotary structures," *Journal of Microelectromechanical Systems*, (in review).

[Hen13b] E. Hendarto, T. Li, Y.B. Gianchandani, "Investigation of wine glass mode resonance in 200-μm-diameter cenosphere-derived borosilicate hemispherical shells," *Journal of Micromechanics and Microengineering*, vol. 23, no. 5, pp. 055013 (6 pages), Apr. 2013.

[Hen13c] E. Hendarto, Y.B. Gianchandani, "Size sorting of floating spheres based on Marangoni forces in evaporating droplets," *Journal of Micromechanics and Microengineering*, (in review).

[Hig00] F.J. Higuera, "Steady thermocapillary-buoyant flow in an unbounded liquid layer heated uniformly from above," *Physics of Fluids*, vol. 12, no. 9, pp. 2186-2197, Sep. 2000.

[Hoi09] S.-K. Hoi, C. Udalagama, C.-H. Sow, F. Watt, A.A. Bettiol, "Microfluidic sorting system based on optical force switching," *Applied Physics B: Lasers and Optics*, vol. 97, no. 4, pp. 859-865, Dec. 2009.

[Hu02] H. Hu, R.G. Larson, "Evaporation of a sessile droplet on a substrate," *Journal of Physical Chemistry B*, vol. 106, no. 6, pp. 1334-1344, Feb. 2002.

[Hu05a] H. Hu, R.G. Larson, "Analysis of the effects of Marangoni stresses on the microflow in an evaporating sessile droplet," *Langmuir*, vol. 21, no. 9, pp. 3972-3980, Apr. 2005.

[Hu05b] H. Hu, R.G. Larson, "Analysis of the microfluid flow in an evaporating sessile droplet," *Langmuir*, vol. 21, no. 9, pp. 3963-3971, Apr. 2005.

[Hu06] H. Hu, R.G. Larson, "Marangoni effect reverses coffee-ring depositions," *Journal of Physical Chemistry B,* vol. 110, no. 14, pp. 7090-7094, Apr. 2006.

[Hua03] Y. Huang, J.M. Yang, P.J. Hopkins, S. Kassegne, M. Tirado, A.H. Forster, H. Reese, "Separation of simulants of biological warfare agents from blood by a miniaturized dielectrophoresis device", *Biomedical Microdevices*, vol. 5, no. 3, pp. 217-225, Sep. 2003.

[Huh03] D. Huh, A.H. Tkaczyk, J.H. Bahng, Y. Chang, H.-H. Wei, J.B. Grotberg, C.-J. Kim, K. Kurabayashi, S. Takayama, "Reversible switching of high-speed air-liquid two-phase flows using electrowetting-assisted flow-pattern change," *Journal of the American Chemical Society*, vol. 125, no. 48, pp. 14678-14679, Dec. 2003.

[Hwa66] C. Hwang, "Some experiments on the vibration of a hemispherical shell," *Journal of Applied Mechanics*, vol. 33, no. 4, pp. 817-824, Dec. 1966.

[Jin98] J. Jing, J. Reed, J. Huang, X. Hu, V. Clarke, J. Edington, D. Housman, T.S. Anantharaman, E.J. Huff, B. Mishra, B. Porter, A. Shenker, E. Wolfson, C. Hiort, R. Kantor, C. Aston, D.C. Schwartz, "Automated high resolution optical mapping using arrayed, fluid-fixed DNA molecules," *Proceedings of the National Academy of Science of the United States of America*, vol. 95, no. 14, pp. 8046-8051, Jul. 1998.

[Kam98] V.A. Kaminsky, A.V. Vyaz'min, N.N. Kulov, V.V. Dil'man, "Marangoni effect in the presence of bulk turbulence," *Chemical Engineering Science*, vol. 53, no. 19, pp. 3347-3353, Oct. 1998.

[Kao09] P. Kao, S. Doerner, T. Schneider, D. Allara, P. Hauptmann, S. Tadigadapa, "A micromachined quartz resonator array for biosensing applications," *Journal of Microelectromechanical Systems*, vol. 18, no. 3, pp. 522-530, Jun. 2009.

[Kis02] A. A. Kishk, Y. Yin, A. W. Glisson, "Conical dielectric resonator antennas for wide-band applications," *IEEE Transactions on Antennas and Propagation*, vol. 50, no. 4, pp. 469-474, Apr. 2002.

[Koh08] D. Kohlheyer, J.C.T. Eijkel, A. van den Berg, R.B.M. Schasfoort, "Miniaturizing free-flow electrophoresis – a critical review," *Electrophoresis*, vol. 29, no. 5, pp. 977-993, Mar. 2008.

[Kot04] K.T. Kotz, K.A. Noble, G.W. Faris, "Optical microfluidics," *Applied Physics Letters*, vol. 85, no. 13, pp. 2658-2660, Sep. 2004.

[Kri09] J.N. Krishnan, C. Kim, H.J. Park, J.Y. Kang, T.S. Kim, S.K. Kim, "Rapid microfluidic separation of magnetic beads through dielectrophoresis and magnetophoresis," *Electrophoresis*, vol. 30, no. 9, pp. 1457-1463, May 2009.

[Lai86] C.-L. Lai, A.-T. Chai, "Surface temperature distribution along a thin liquid layer due to thermocapillary convection," *Acta Astronautica*, vol. 13, no. 11-12, pp. 655-659, Nov.-Dec. 1986.

[Lap05] M. Lappa, "Review: Possible strategies for the control and stabilization of Marangoni flow in laterally heated floating zones," *Tech Science Press*, vol. 1, no. 2, pp. 171-187, 2005.

[Law98] A. Lawrence, *Modern inertial technology: navigation, guidance and control*. New York: Springer-Verlag, 1998, pp. 152-168.

[Lee90] A.F.M. Leenaars, J.A.M Huethorst, J.J. van Oekel, "Marangoni drying: A new extremely clean drying process," *Langmuir*, vol. 6, no. 11, pp. 1701-1703, Nov. 1990.

[Leu05] K.W. Leung, H.K. Ng, "The slot-coupled hemispherical dielectric resonator antenna with a parasitic patch: Applications to the circularly polarized antenna and wide-band antenna," *IEEE Transactions on Antennas and Propagation*, vol. 53, no. 5, pp. 1762- 1769, May 2005.

[Leu93] K.W. Leung, K.M. Luk, K.Y.A. Lai, D. Lin, "Theory and experiment of a coaxial probe fed hemispherical dielectric resonator antenna," *IEEE Transactions on Antennas and Propagation*, vol. 41, no. 10, pp. 1390-1398, Oct. 1993.

[Li08] D. Li, *Encyclopedia of microfluidics and nanofluidics*, New York: Springer Science + Business Media LLC, 2008, pp. 2032-2034.

[Li93] J. Li, J. Sun, Z. Saghir, "Buoyant and thermocapillary flow in liquid encapsulated floating zone," *Journal of Crystal Growth*, vol. 131, no. 1-2, pp. 83-96, Jul. 1993.

[Lip75] G. Lippmann, "Relations entre les phenomenes electriques et capillaires," *Ann. Chim. Phys.*, 5, pp. 494, 1875.

[Lon99] J.P. Longtin, K. Hijikata, K. Ogawa, "Laser-induced surface-tension-driven flows in liquid," *International Journal of Heat and Mass Transfer*, vol. 42, no. 1, pp. 85-93, Jan. 1999.

[Lou10] Y. Lou, L.M. Lunardi, J.F. Muth, "Fabrication of nanoshell arrays using directed assembly of nanospheres," *IEEE Sensors Journal*, vol. 10, no. 3, pp. 617-620, Mar. 2010.

[Lu96] H.-H. Lu, Y.-M. Yang, J.-R. Maa, "Effect of artificially provoked Marangoni convection at a gas/liquid interface on absorption," *Industrial and Engineering Chemistry Research*, vol. 35, no. 6, pp. 1921-1928, Jun. 1996.

[Maj12] M. Majumder, C.S. Rendall, J.A. Eukel, J.Y.L Wang, N. Behabtu, C.L. Pint, T.-Y. Liu, A.W. Orbaek, F. Mirri, J. Nam, A.R. Barron, R.H. Hauge, H.K. Schmidt, M. Pasquali, "Overcoming the 'coffee-stain' effect by compositional Marangoni-flow-assisted drop-drying," *Journal of Physical Chemistry B*, vol. 116, no. 22, pp. 6536-6542, Jun. 2012.

[Mar05] L. Marle, G.M. Greenway, "Microfluidic devices for environmental monitoring," *Trends in Analytical Chemistry*, vol. 24, no. 9, pp. 795-802, Oct. 2005.

[Mar65] C. Marangoni, "Sull' espansione delle gocce liquide," Pavia, 1865.

[Mar89] M. di Marzo, D.D. Evans, "Evaporation of a water droplet deposited on a hot high thermal conductivity surface," *Journal of Heat Transfer*, vol. 111, no. 1, pp. 210-213, Feb 1989.

[Mat11] M. Matsuda, M. Yamada, M. Seki, "Blood cell classification utilizing hydrodynamic filtration," *Electronics and Communications in Japan*, vol. 94, no. 1, pp. 1-6, Jan. 2011.

[McA84] M.W. McAllister, S.A. Long, "Resonant hemispherical dielectric antenna," *Electronics Letters*, vol. 20, no. 16, pp. 657-659, Aug. 1984.

[McB02] S.P. McBride, A. Shukla, A. Bose, "Processing and characterization of a lightweight concrete using cenospheres," *Journal of Materials Science*, vol. 37, no. 19, pp. 4217-4225, Oct. 2002.

[Mon94] R.K. Mongia, P. Bhartia, "Dielectric resonator antennas – A review and general design relations for resonant frequency and bandwidth," *International Journal of Microwave and Millimeter-Wave Computer-Aided Engineering*, vol. 4, no. 3, pp. 230-247, Jul. 1994.

[Moo09] H.-S. Moon, Y.-W. Nam, J.C. Park, H.-I. Jung, "Dielectrophoretic separation of airborne microbes and dust particles using a microfluidic channel for real-time bioaerosol monitoring," *Environmental Science and Technology*, vol. 43, no. 15, pp. 5857-5863, Aug. 2009.

[Ngu02] V.X. Nguyen, K.J. Stebe, "Patterning of small particles by a surfactant-enhanced Marangoni-Bénard instability," *Physical Review Letters*, vol. 88, no. 16, pp. 164501-1-4, Apr. 2002.

[Nik02] A.D. Nikolov, D.T. Wasan, A. Chengara, K. Koczo, G.A. Policello, I. Kolossvary, "Superspreading driven by Marangoni flow," *Advances in Colloid and Interface Science*, vol. 96, no. 1-3, pp. 325-338, Feb. 2002.

[Pam06] N. Pamme, C. Wilhelm, "Continuous sorting of magnetic cells via on-chip free-flow magnetophoresis," *Lab on a Chip*, vol. 6, no. 8, pp. 974-980, Aug. 2006.

[Pam07] N. Pamme, "Continuous flow separation in microfluidic devices," *Lab on a Chip*, vol. 7, no. 12, pp. 1644-1659, Dec. 2007.

[Par10] S.-Y. Park, M.A. Teitell, E.P.Y. Chiou, "Single-sided continuous optoelectrowetting (SCOEW) for droplet manipulation with light patterns," *Lab on a Chip*, vol. 10, no. 13, pp. 1655-1661, May 2010.

[Pea58] J.R.A. Pearson, "On convection cells induced by surface tension," *Journal of Fluid Mechanics*, vol. 4, no. 5, pp. 489-500, Sep. 1958.

[Pet10a] R. Pethig, "Review article – Dielectrophoresis: Status of the theory, technology, and applications," *Biomicrofluidics*, vol. 4, no. 2, pp. 022811-1-35, Jun. 2010.

[Pet10b] R. Pethig, A. Menachery, S. Pells, P. De Sousa, "Dielectrophoresis: A review of applications for stem cell research," *Journal of Biomedicine and Biotechnology*, vol. 2010, article 182581, 7 pages, Feb. 2010.

[Pet10c] A. Petosa, A. Ittipiboon, "Dielectric resonator antennas: A historical review and the current state of the art," *IEEE Antennas and Propagation Magazine*, vol. 52, no. 5, pp. 91-116, Oct. 2010.

[Pol00] M.G. Pollack, R.B. Fair, A.D. Shenderov, "Electrowetting-based actuation of liquid droplets for microfluidic applications," *Applied Physics Letters*, vol. 77, no. 11, pp. 1725-1726, Sep. 2000.

[Pol02] M.G. Pollack, A.D. Shenderov, R.B. Fair, "Electrowetting-based actuation of droplets for integrated microfluidics," *Lab on a Chip*, vol. 2, no. 2, pp. 96-101, May 2002.

[Pol11] M.G. Pollack, V.K. Pamula, V. Srinivasan, A.E. Eckhardt, "Applications of electrowetting-based digital microfluidics in clinical diagnostics," *Expert Review of Molecular Diagnostics*, vol. 11, no. 4, pp. 393-407, May 2011.

[Pri11] I. P. Prikhodko, S. A. Zotov, A. A. Trusov, A. M. Shkel, "Microscale glass-blown three-dimensional spherical shell resonators," *Journal of Microelectromechanical Systems*, vol. 20, no. 3, pp. 691-701, Jun. 2011.

[Ray16] L. Rayleigh, "On convection currents in a horizontal layer of fluid, when the higher temperature is on the under side," *Philosophical Magazine Series 6*, vol. 32, no. 192, pp. 529-546, Dec. 1916.

[Ric08] M.T. Richardson, Y.B. Gianchandani, "Achieving precision in high density batch mode micro-electro-discharge machining," *Journal of Micromechanics and Microengineering*, vol. 18, no. 1, pp. 015002 (12 pages), Jan. 2008.

[Ril98] R.J. Riley, G.P. Neitzel, "Instability of thermocapillary-buoyancy convection in shallow layers. Part I. Characterization of steady and oscillatory instabilities," *Journal of Fluid Mechanics*, vol. 359, pp. 143-164, Mar. 1998.

[Rog06] K.R. Rogers, "Recent advances in biosensor techniques for environmental monitoring," *Analytica Chimica Acta*, vol. 568, no. 1-2, pp. 222-231, May 2006.

[Ron07] L. Rongy, A. De Wit, "Marangoni flow around chemical fronts traveling in thin solution layers: Influence of the liquid depth," *Journal of Engineering Mathematics*, vol. 59, no. 2, pp. 221-227, Oct. 2007.

[Roz09] D. M. Rozelle, "The hemispherical resonator gyro: From wineglass to the planets," *Proceedings of the 19th AAS/AIAA Space Flight Mechanics Meeting*, Savannah, GA, Feb. 8–12, 2009, vol. 134, pp. 1157-1178.

[Rui02] O.E. Ruiz, W.Z. Black, "Evaporation of water droplets placed on a heated horizontal surface," *Journal of Heat Transfer*, vol. 124, no. 5, pp. 854-863, Oct. 2002.

[Rup89] R. Rupp, G. Müller, G. Neumann, "Three-dimensional time dependent modeling of the Marangoni convection in zone melting configurations for GaAs," *Journal of Crystal Growth*, vol. 97, no. 1, pp. 34-41, Sep. 1989.

[Sav02] R. Savino, D. Paterna, N. Favaloro, "Buoyancy and Marangoni effects in an evaporating drop," *Journal of Thermophysics and Heat Transfer*, vol. 16, no. 4, pp. 562-574 , Dec. 2002.

[Sch01] M.F. Schatz, G.P. Neitzel, "Experiments on thermocapillary instabilities," *Annual Review of Fluid Mechanics*, vol. 33, pp. 93-127, Jan. 2001.

[Sch11] K. Scholten, X. Fan, E.T. Zellers, "Microfabricated optofluidic ring resonator structures," *Applied Physics Letters*, vol. 99, no. 14, pp. 141108 (3 pages), Oct. 2011.

[Scr60] L.E. Scriven, C.V. Sternling, "The Marangoni effects," *Nature*, vol. 187, no. 4733, pp. 186-188, Jul. 1960.

[Sel09] B. Selva, J. Marchalot, M.-C. Jullien, "An optimized resistor pattern for temperature gradient control in microfluidics," *Journal of Micromechanics and Microengineering*, vol. 19, no. 6, pp. 065002 (10 pages), Jun. 2009.

[Sel10] B. Selva, V. Miralles, I. Cantat, M.-C. Jullien, "Thermocapillary actuation by optimized resistor pattern: Bubbles and droplets displacing, switching and trapping," *Lab on a Chip*, vol. 10, no. 14, pp. 1835-1840, Jul. 2010.

[Shi09] J. Shi, H. Huang, Z. Stratton, Y. Huang, T.J. Huang, "Continuous particle separation in a microfluidic channel via standing surface acoustic waves (SSAW)," *Lab on a Chip*, vol. 9, no. 23, pp. 3354-3359, Dec. 2009.

[Shu01] S. Shukla, S. Seal, J. Akesson, R. Oder, R. Carter, Z. Rahman, "Study of mechanism of electroless copper coating of fly-ash cenosphere particles," *Applied Surface Sciences,* vol. 181, no. 1-2, pp. 35-50, Sep. 2001.

[Shu02] S. Shukla, S. Seal, Z. Rahaman, K. Scammon, "Electroless copper coating of cenospheres using silver nitrate activator," *Materials Letters*, vol. 57, no. 1, pp. 151-156, Nov. 2002.

[Sod08] C. Sodtke, V.S. Ajaev, P. Stephan, "Dynamics of volatile liquid droplets on heated surfaces: theory versus experiment," *Journal of Fluid Mechanics*, vol. 610, pp. 343-362, Sep. 2008.

[Sor12] L. D. Sorenson, X. Gao, F. Ayazi, "3-D micromachined hemispherical shell resonators with integrated capacitive transducers," *IEEE 25th International Conference on Micro Electro Mechanical Systems (MEMS 2012)*, Paris, France, Jan. 29 – Feb. 2, 2012, pp. 168-171.

[Sos09] L.M. Sosnoskie, T.M. Webster, D. Dales, G.C. Rains, T.L. Grey, A.S. Culpepper, "Pollen grain size, density and settling velocity for Palmer Amaranth (*Amaranthus palmeri*)," *Weed Science*, vol. 57, no. 4, pp. 404-409, Jul. 2009.

[Tad09] R. Tadmor, "Marangoni flow revisited," *Journal of Colloid and Interface Science*, vol. 332, no. 2, pp. 451-454, Apr. 2009.

[Tak02] K. Takahata, Y.B. Gianchandani, "Batch mode micro-electro-discharge machining," *Journal of Microelectromechanical Systems*, vol. 11, no. 2, pp. 102-110, Apr. 2002.

[Tak10] A. Takei, K. Matsumoto, I. Shomoyama, "Capillary motor driven by electrowetting," *Lab on a Chip*, vol. 10, no. 14, pp. 1781-1786, Jul. 2010.

[Tho55] J. Thomson, "On certain curious motions observable on the surfaces of wine and other alcoholic liquors, *Philosophical Magazine*, vol. 10, pp. 330-333, 1855.

[Vel09] E. Vela, M. Hafez, S. Regnier, "Laser-induced thermocapillary convection for mesoscale manipulation," *International Journal of Optomechatronics*, vol. 3, no. 4, pp. 289-302, Oct. 2009.

[Vis11] K. Visvanathan, T. Li, Y. B. Gianchandani, "3D-SOULE: A fabrication process for large scale integration and micromachining of spherical structures," *IEEE 24th*

International Conference on Micro Electro Mechanical Systems (MEMS 2011), Cancun, Mexico, Jan. 23–27, 2011, pp. 45-48.

[Vol02] F. Vollmer, D. Braun, A. Libchaber, M. Khoshsima, I. Teraoka, S. Arnold, "Protein detection by optical shift of a resonant microcavity, " *Applied Physics Letters*, vol. 80, no. 21, pp. 4057-4059, May 2002.

[Vol06] J. Voldman, "Electrical forces for microscale cell manipulation," *Annual Review of Biomedical Engineering*, vol. 8, pp. 425-454, Mar. 2006.

[Wan96] T. Wandell, "Cenospheres: From waste to profits," *American Ceramic Society Bulletin*, vol. 75, no. 6, pp. 79-84, Jun. 1996.

[Wan97] X.-B. Wang, Y. Huang, P.R.C. Gascoyne, F.F. Becker, "Dielectrophoretic manipulation of particles," *IEEE Transactions on Industry Applications*, vol. 33, no. 3, pp. 660-669, May-Jun. 1997.

[Whi06] G.M. Whitesides, "The origins and the future of microfluidics," *Nature*, vol. 442, no. 7101, pp. 368-373, Jul. 2006.

[Won93] K.-L. Wong, N.-C. Chen, H.-T Chen, "Analysis of a hemispherical dielectric resonator antenna with an airgap," *IEEE Microwave and Guided Wave Letters*, vol. 3, no. 10, pp. 355-357, Oct. 1993.

[Wur07] A. Würger, "Thermophoresis in colloidal suspensions driven by Marangoni forces," *Physical Review Letters*, vol. 98, no. 13, pp. 138301-1-4, Mar. 2007.

[Xia09] Product information on Xiameter® PMX-200 silicone fluid: 5-20 cSt, Xiameter, Dow Corning Corporation, Midland, MI, 2009.

[Xu11] W. Xu, X. Zhang, S. Choi, J. Chae, "A high-quality-factor film bulk acoustic resonator in liquid for biosensing applications," *Journal of Microelectromechanical Systems*, vol. 20, no. 1, pp. 213-220, Feb. 2011.

[Yag06] P. Yager, T. Edwards, E. Fu, K. Helton, K. Nelson, M.R. Tam, B.H. Weigl, "Microfluidic diagnostic technologies for global public health," *Nature*, vol. 442, no. 7101, pp. 412-418, Jul. 2006.

[Yun11] P.J. Yunker, T. Still, M.A. Lohr, A.G. Yodh, "Suppression of the coffee-ring effect by shape-dependent capillary interactions," *Nature*, vol. 476, no. 7360, pp. 308-311, Aug. 2011.

[Zha01] B. Zhao, J.S. Moore, D.J. Beebe, "Surface-directed liquid flow inside microchannels," *Science*, vol. 291, no. 5506, pp. 1023-1026, Feb. 2001.

[Zha10] C. Zhang, K. Khoshmanesh, A. Mitchell, K. Kalantar-Zadeh, “Dielectrophoresis for manipulation of micro/nano particles in microfluidic systems,” *Analytical and Bioanalytical Chemistry*, vol. 396, no. 1, pp. 401-420, Jan. 2010.

[Zot12] S. A. Zotov, A. A. Trusov, A. M. Shkel, “Three-dimensional spherical shell resonator gyroscope fabricated using wafer-scale glassblowing,” *Journal of Microelectromechanical Systems*, vol. 21, no. 3, pp. 509-510, Jun. 2012.